Phase Separation of EARLY FLOWERING 3 and Plant Thermoresponse

Aleksandra Mironova

THÈSE

Pour obtenir le grade de

DOCTEUR DE L'UNIVERSITÉ GRENOBLE ALPES

École doctorale : CSV- Chimie et Sciences du Vivant
Spécialité : Biotechnologie
Unité de recherche : LPCV - Laboratoire de Physiologie Cellulaire Végétale

Séparation de phase de la protéine EARLY FLOWERING 3 et réponse aux températures chez les plantes

Phase Separation of EARLY FLOWERING 3 and Plant Thermoresponse

Présentée par :

Aleksandra MIRONOVA

Direction de thèse :

Chloé ZUBIETA CNRS Alpes	Directrice de thèse
Mark TULLY ESRF	Co-encadrant de thèse

Rapporteurs :

Mohammed BENDAHMANE
DIRECTEUR DE RECHERCHE, INRAE
Yvonne STAHL
PROFESSEURE, Goethe University

Thèse soutenue publiquement le **9 décembre 2024**, devant le jury composé de :

Chloe ZUBIETA, DIRECTRICE DE RECHERCHE, CNRS Alpes	Directrice de thèse
Mohammed BENDAHMANE, DIRECTEUR DE RECHERCHE, INRAE	Rapporteur
Yvonne STAHL, PROFESSEURE, Goethe University	Rapporteure
Marc JAMIN, PROFESSEUR DES UNIVERSITES, Université Grenoble Alpes	Président
Judit SZECSI, INGENIEURE DE RECHERCHE, ENS Lyon	Examinatrice
Juliette SALVAING, CHARGEE DE RECHERCHE, INRAE	Examinatrice

Invités :

Mark Tully
DOCTEUR EN SCIENCES, European Synchrotron Radiation Facility, BM 29

Acknowledgments

I would like to express my sincere gratitude to my thesis supervisor, Dr. Chloe Zubieta. Her guidance throughout the project has been instrumental at every stage of my research. Her expertise and support not only shaped the direction of this work, but also inspired me to develop as a researcher. I am grateful for her work, which has given me the confidence and knowledge I needed to overcome the challenges on my path to a PhD.

I am also deeply grateful to my co-supervisor, Dr. Mark Tully, whose invaluable assistance in implementing the project and organizing the workflow using different approaches was crucial to the success of this work. Dr. Tully played a key role in bringing together the different methodologies and ensuring a coherent research process, for which I am deeply grateful.

I would like to express my deepest gratitude to my daily supervisor, Dr. Stephanie Hutin, for her invaluable guidance, support, and patience throughout this journey. Her insightful feedback and continuous encouragement have greatly contributed to the successful completion of this thesis. I am also thankful to my thesis committee, Dr. Gabrielle Tichtinsky, Dr. Renaud Dumas, and Dr. Jean-Luc Pellequer, for their thoughtful feedback and invaluable suggestions during key stages of my PhD.

A special thanks to my labmates and colleagues, especially Sara Pullara, Aline Janeau, for the warm atmosphere and interesting discussions, and for always being there to offer both academic and moral support. I learned a lot from each of you, and your camaraderie made the experience not only productive but enjoyable.

To my husband, Valentin Foissac, I am forever grateful for your unwavering belief in me, your constant support, and for being my source of strength during difficult moments. To my friends, especially Anastasia Zaigraeva, thank you for your encouragement, your patience, and for always being there when I needed it most, even if you live on the other side of this globally warming planet.

I am deeply grateful to Labex GRAL for its financial support and to Anne-Mathilde Thierry for her personal engagement and dedication to the students. My PhD journey started by meeting you and I am sincerely grateful for your involvement. My thanks also go to ESRF, CEA, and the LPCV staff for their resources and for creating a favorable environment for my research.

Completing this PhD has been a transformative journey, and I am thankful to everyone who contributed both academically and personally. Your support has been invaluable, and I am forever grateful.

Table of contents

Résume

L'augmentation des températures moyennes due au réchauffement climatique a déjà modifié la phénologie des plantes, tant pour les espèces sauvages que pour les espèces domestiques. Les plantes sont capables de percevoir la température et de reprogrammer leur croissance et leur développement pour une reproduction et une survie optimales dans des conditions climatiques plus chaudes. La protéine végétale conservée EARLY FLOWERING 3 (ELF3) joue un rôle central dans les voies de signalisation de la croissance régulée par le rythme circadien et de la réponse environnementale. ELF3 agit comme un échafaudage pour la formation de complexes avec des facteurs de transcription tels que LUX ARRYTHMO, EARLY FLOWERING 4 et PHYTOCHROME INTERACTING FACTOR 4, tous connus pour jouer un rôle dans la croissance régulée par le rythme circadien et la réponse à la température. Chez la plante *Arabidopsis thaliana* et d'autres Brassicaceae, ELF3 possède un domaine de type prion (PrD) peu complexe.

Des études récentes ont montré que le domaine Prion-like (PrD) de ELF3 induit une séparation de phase liquide-liquide (LLPS) à la fois *in vitro* et *in vivo*, ce processus étant sensible au pH et à la température. La séparation de phase liquide-liquide est essentielle pour la thermosensibilité des plantes, mais les mécanismes moléculaires à l'origine de la séparation de phase ne sont pas encore clairs. Cette thèse de doctorat étudie le comportement structurel et fonctionnel des mutants ELF3 PrD en utilisant une combinaison d'essais biochimiques et de diffusion des rayons X aux petits angles (SAXS), en corrélant ces résultats avec les fonctions *in planta*. Les principaux résultats révèlent que les mutants ELF3^{PrDR597A}, ELF3$^{PrD2xR/A}$, ELF3$^{PrDΔ486-496}$ et ELF3$^{PrD12xY/Q}$ présentent une LLPS réduite ou inexistante *in vitro,* seul le mutant ELF3PrD9xH/R présentant un comportement propice à la séparation de phase.

Les expériences SAXS ont révélé que la plupart des mutants ELF3 PrD forment de grands oligomères, à l'exception du mutant ELF3$^{12xY/Q}$, qui reste un monomère désordonné, ce qui indique un comportement structurel différent. D'autres expériences, telles que les essais de déplacement de mobilité électrophorétique (EMSA), ont montré que les mutations de la PrD d'ELF3 peuvent influencer sa capacité à lier l'ADN dans le complexe du soir (Evening Complex), un régulateur clé des réponses photopériodiques. Plus précisément, le ELF3$^{12xY/Q}$, qui ne subit pas de LLPS, présente une liaison plus forte de l'ADN dans le complexe du soir à une température plus élevée, ce qui indique un comportement insensible à la température.

In vivo, le mutant R597A complète partiellement la fonction de ELF3, tandis que le mutant ELF3$^{12xY/Q}$ présente un phénotype de perte de fonction, et les western blots confirment que la protéine mutante est indétectable, probablement parce que sa forme monomérique est plus sujette à la dégradation. Cela suggère que l'oligomérisation est cruciale pour la stabilité et la fonction d'ELF3 dans les plantes. Ces résultats mettent en évidence la relation complexe entre les propriétés structurelles d'ELF3, le comportement des LLPS et son rôle régulateur dans la perception de la température. De futures études seront nécessaires pour disséquer davantage les mécanismes moléculaires et confirmer le rôle de l'oligomérisation dans le maintien de la stabilité d'ELF3.

Cette thèse de doctorat met en évidence l'importance de résidus d'acides aminés spécifiques dans la séparation des phases de l'ELF3. Des mutations systématiques ont montré que les résidus arginine et tyrosine jouent un rôle clé dans la promotion de la séparation des

phases, les interactions cation-π entre l'arginine et la tyrosine stabilisant la LLPS. La perturbation de ces interactions diminue la LLPS, tandis que l'ajout d'arginine augmente la LLPS dans certaines conditions, ce qui permet de mieux comprendre les effets de ces résidus sur le comportement d'ELF3. À long terme, ces résultats jettent les bases de la manipulation du comportement de phase d'ELF3 afin d'optimiser les réponses des plantes à la température dans des conditions climatiques changeantes.

Abstract

Increased average temperatures due to global warming have already altered plant phenology for both wild and domesticated species. Plants are able to perceive temperature and subsequently reprogram their growth and development for optimal reproduction and survival under warmer climatic conditions. The conserved plant protein, EARLY FLOWERING 3 (ELF3), plays a central role in both the circadian regulated growth and environmental response signalling pathways. ELF3 acts as a scaffold for complex formation with transcription factors such as LUX ARRYTHMO, EARLY FLOWERING 4 and PHYTOCHROME INTERACTING FACTOR 4, all known to play roles in circadian regulated growth and temperature response. In *Arabidopsis thaliana* and other *Brassicaceae*, ELF3 has a low complexity prion-like domain (PrD).

Recent studies have shown that the PrD of ELF3 induces liquid - liquid phase separation (LLPS) both *in vitro* and *in vivo*, with this process being sensitive to pH and temperature. LLPS is essential for plant thermoresponsiveness, but the molecular mechanisms driving phase separation remain unclear. This PhD thesis investigates the structural and functional behavior of ELF3 PrD mutants using a combination of biochemical assays and small-angle X-ray scattering (SAXS), correlating these findings with *in planta* functions. Key findings reveal that the ELF3^{PrDR597A}, ELF3$^{PrD2xR/A}$, ELF3$^{PrDΔ486-496}$, and ELF3$^{PrD12xY/Q}$ mutants show reduced or no LLPS *in vitro*, with only the ELF3$^{PrD9xH/R}$ mutant displaying phase separation-prone behavior.

SAXS experiments revealed that most ELF3 PrD mutants form large oligomers, except for the ELF3$^{PrD12xY/Q}$ mutant, which remains a disordered monomer, indicating a different structural behavior. Further experiments, such as electrophoretic mobility shift assays (EMSA), showed that mutations in ELF3's PrD can influence its ability to bind DNA in the Evening Complex (EC), a key regulator of photoperiodic responses. Specifically, the ELF3$^{PrD12xY/Q}$, which does not undergo LLPS, exhibit stronger DNA binding in the Evening Complex at higher temperature, indicating temperature insensitive behavior.

In vivo, the R597A mutant partially complemented ELF3 function, while the ELF3$^{12xY/Q}$ mutant showed a loss-of-function phenotype, and western blots confirmed that the mutant protein was undetectable, likely due to its monomeric form being more prone to degradation. This suggests that oligomerization is crucial for ELF3's stability and function in plants. These findings highlight the complex relationship between ELF3's structural properties, LLPS behavior, and its regulatory role in temperature perception. Future studies will be needed to further dissect the molecular mechanisms and confirm the role of oligomerization in maintaining ELF3 stability.

This PhD thesis highlights the importance of specific amino acid residues in driving ELF3's phase separation. Systematic mutations showed that arginine and tyrosine residues play key roles in promoting phase separation, with cation-π interactions between arginine and tyrosine stabilizing LLPS. Disruption of these interactions decreased LLPS, whereas arginine addition increased LLPS under certain conditions, providing insight into the effects of these residues on ELF3 behavior. In the long term, these results lay the foundation for manipulating ELF3 phase behavior to optimize plant temperature responses under changing climatic conditions.

List of abbreviations

35S – Promoter of the Cauliflower Mosaic Virus

Å – Ångström

AHK2 – Histidine Kinase 2

AHK3 – Histidine Kinase 3

APX2 – L-ascorbate peroxidase 2

ARR – Type-A *Arabidopsis* (*Arabidopsis thaliana*) Response Regulators

AS – Alternative splicing

bHLH – Basic helix-loop-helix A basic helix-loop-helix

BOP – Blade-On-Petiole

Bp – Base pairs

BSA – Bovine Serum Albumin

BTP – 1,3-bis(tris(hydroxymethyl)methylamino)propane

CAPS – 3-(Cyclohexylamino)-1-Propanesulfonic acid

CBF – C-repeat Binding Factor

CBL – Calcineurin B-Like proteins

CIPK – CBL-Interacting Protein Kinases

CCA1 – Circadian Clock Associated 1

CHE – CCA1 Hiking Expedition

CJD – Creutzfeldt–Jakob disease

CO – Constans

Col-0 – Columbia

COP1 – Constitutive Photomorphogenic 1

COR – Cold-Regulated genes

CRY2 – Cryptochrome 2

Cy5 – Cyanine 5.18

DBD – DNA binding domain

D_{max} – Maximal Dimension

DNA – Deoxyribonucleic acid

dNTPs – Deoxynucleotide triphosphates

DREB2A – Dehydration-responsive element-binding protein 2A

EC – Evening Complex

EDTA – Ethylenediaminetetraacetic acid

ELF3 – Early Flowering 3

EMSA – Electrophoretic Mobility Shift Assay

FLC – Flowering Locus C

FLM – Flowering Locus M

FRI – Frigida

FT – Flowering Locus T

GFP – Green fluorescent protein

GI – Gigantea

GRN – Gene Regulatory Network

HATs – Histone acetyltransferases

HDACs – Histone Deacetylases

HPLC – High-Performance Liquid Chromatography

HSEs – Heat Shock Elements

HSFs – Heat Shock Factors

HSPs – Heat Shock Proteins

HY5 – Elongated Hypocotyl 5

ICE – Inducer of CBF Expression 1

IDP – Intrinsically Disordered Protein

IDR – Intrinsically Disordered Region

IPTG – Isopropyl β-d-1-thiogalactopyranoside

kDa – KiloDalton

LARKS – Low-complexity Aromatic-Rich Kinked Segments

LCST – Lower Critical Solution Temperature

LD – Long Day

LHY – Late Elongated Hypocotyl

LLPS – Liquid-Liquid Phase Separation

LRBs -– Light-Response Bric-a-Brack/Tramtrack/Broads

mRNA – Messenger RNA

MS – Murashige and Skoog medium

MW – Molecular Weight

NMR – Nuclear Magnetic Resonance

PCR – Polymerase Chain Reaction

Pfr – Physiologically-active form of the phytochrome B, induced by far-red light

PhyB – Phytochrome B

pI – Isoelectric point

PIF4 – Phytochrome-interacting factor 4

PIF7 – Phytochrome-interacting factor 7

pKa – Acid dissociation constant

PLAAC – Proin-Like Amino Acid Composition Algorithm

Pol II – RNA Polymerase II

PolyQ – Polyglutamine stretch

Pr – Physiologically-inactive form of the phytocrhome B, induced by red light

PrD – Prion-like Domain

PRRs – Pseudo-Response Regulators

R_g – Radius of gyration

RNA – Ribonucleic acid

ROS – Reactive Oxygen Species

SAR – Shade-Avoidance Response

SAXS – Small-Angle X-ray Scattering

SD – Short Day

SDS-PAGE – Sodium Dodecyl Sulfate–Polyacrylamide Gel Electrophoresis

SEC – Size-Exclusion Chromatography

SEC-MALS – Size-Exclusion Chromatography Multi-Angle Light Scattering

SEC-SAXS – Size-exclusion chromatography coupled with Small-Angle X-ray Scattering

SVP – Short Vegetative Phase

TAIR – The *Arabidopsis* Information Resource

TBE – Tris/Borate/EDTA

TCEP – Tris(2-carboxyethyl)phosphine

TEV – Tobacco Etch Virus cleavage site

TOC1 – Timing of CAB Expression

UCST – Upper Critical Solution Temperature

UV – Ultraviolet light

VIN3 – Vernalisation Insensitive 3

V_p – Excluded particle volume

VRN1 – Vernalisation 1

WRKYs – Plant-specific transcription factors with WRKY signature amino acid sequence

WT – Wild Type

YUCCA8 – Tryptophan aminotransferase of *Arabidopsis* (TAA), auxin biosynthetic enzyme

ZTL – Zeitlupe

List of figures

List of tables

CHAPTER 1 Introduction

1.1. Global Warming – an environmental challenge

Global warming represents one of the most significant challenges facing plant ecosystems worldwide. Defined as the long-term increase in Earth's average surface temperature, this phenomenon is primarily driven by human activities, particularly the burning of fossil fuels (Mitchell, 1989). The combustion of fossil fuels releases over 36 gigatons of carbon dioxide (CO_2) annually, along with other potent greenhouse gases such as methane (CH_4) and nitrous oxide (N_2O) (CO2 Emissions in 2022, 2023 IEA Report). These greenhouse gases act to trap heat within the Earth's atmosphere, leading to a progressive elevation of global temperatures (Ledley et al., 1999).

Beyond fossil fuel combustion, other human activities such as deforestation, livestock production, and various industrial processes further exacerbate global warming. Deforestation reduces the number of trees available to sequester CO_2, thereby reducing the planet's natural capacity to absorb this primary greenhouse gas (Lawrence et al., 2022). Moreover, the cleared land is frequently repurposed for intensive agricultural practices, such as livestock grazing, which contributes additional methane emissions (Lassey, 2007). A single cow, for example, is able to produce 100 kg of methane per year and ruminant livestock account for over 6% of anthropogenic greenhouse gas emissions yearly (Beauchemin et al., 2020). These practices not only diminish the Earth's carbon sequestration potential but also directly increase greenhouse gas emissions, thus accelerating the ongoing deleterious trend of global warming.

Over the past two centuries, the Earth's average annual temperature has risen by approximately 1.5 degrees Celsius (Thépaut, J-N., 2023). This upward trend has consistently broken yearly temperature records, with the warmest years recorded within the last decade, 2023 (The World Meteorological Organization (WMO), 2024). These changes in the average ambient will have profound implications for plant ecosystems worldwide.

1.1.1. The Impact of Rapid Climate Change on Plants

The consequences of global warming are not simply an increase in average temperatures, but also include unpredictable changes in climate patterns, which affect different regions of the world in varied ways. These changes include shifts in precipitation patterns, alterations in wind patterns, fluctuations in local temperature, and an increase in the frequency and severity of extreme weather events, including cold spells and heatwaves. Such shifts have far-reaching effects on plant and animal ecosystems, human communities and economic activities, with certain regions experiencing more dramatic alterations in weather and climate than others (Alkama et al., 2020; Clem et al., 2020; Rantanen et al., 2022) (Figure 1).

The speed of global warming poses a critical challenge for plant species, many of which are unable to adapt quickly enough to the rapidly changing conditions. Evolutionary adaptation mechanisms typically operate over much longer periods of time (thousands to millions of years as opposed to decades), allowing species to gradually adjust to environmental changes (Vogt, 2022). However, the current pace of climate change far outstrips the rate at which many plants can evolve (Abbass et al., 2022). As a result, numerous

plant species face the risk of habitat displacement or loss, population decline due to non-optimal reproductive conditions, or even extinction (Catford & Jones, 2019; Möhl et al., 2022).

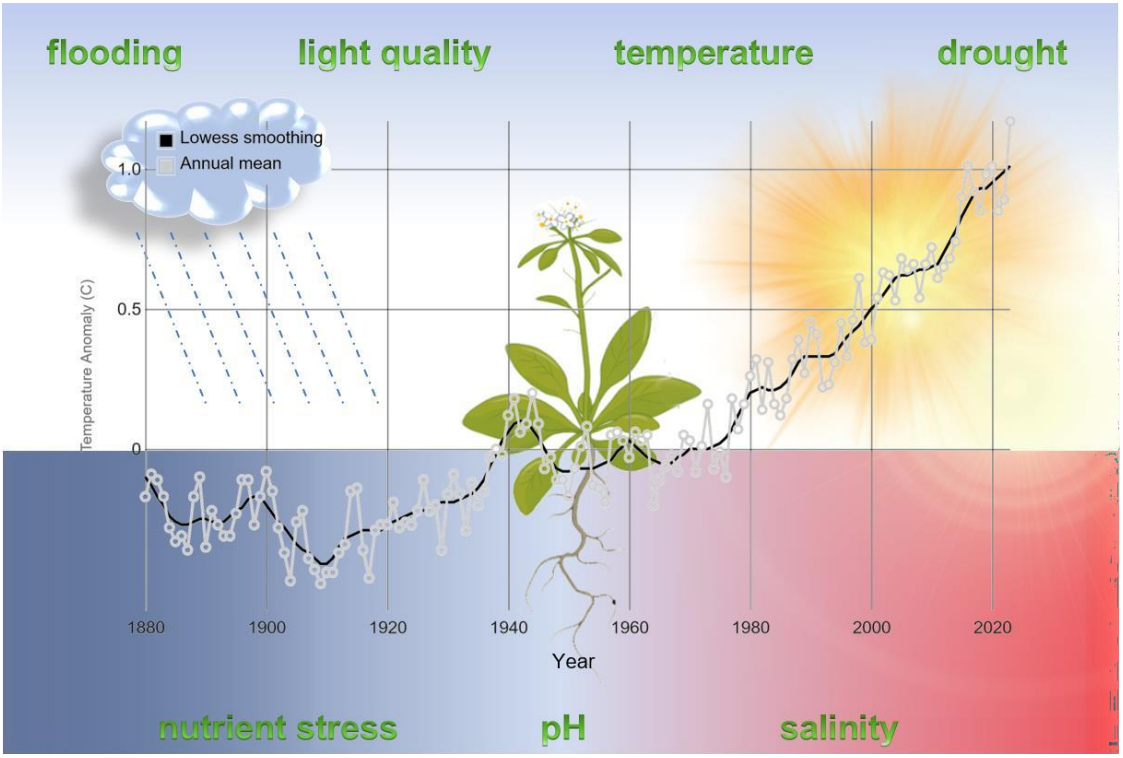

Figure 1. Environmental perception by plants. Plants as sessile organism are exposed to different environmental conditions like availability of water, light quality, temperature and soil conditions. The average annual anomalies in temperature have reached +1° C, (adapted from: climate.nasa.gov).

Recent studies have highlighted the vulnerability of specific ecosystems to these rapid climatic alterations. For instance, research conducted in the French Alps, a region characterized by multi-altitude landscapes, has shown that forest ecosystems are increasingly susceptible to fires, exacerbated by dry, warmer springs and rising temperatures (Dupire et al., 2019). Alpine grasslands, the high-altitude ecosystems found above the treeline, are particularly sensitive to climate change. These grasslands are characterized by low temperatures, short growing seasons, and unique flora and fauna adapted to these niche conditions (Korner, 2012; Paulsen & Körner, 2014; Körner, 2019). In contrast to negative effects of warmer climate to alpine forests, alpine grasslands have demonstrated a positive correlation between increased spring temperatures and enhanced grass biomass and changes in species distribution (Choler, 2015). Species distribution changes, in particular the invasion of species from lower altitudes that outcompete native alpine plants, is one likely scenario. This “homogenization” of plant communities will result in the loss of specialized alpine species. In addition, phenological shifts, such as earlier flowering and leaf-out times, have been observed in various plant species (Catford & Jones, 2019; Möhl et al., 2022). These shifts can disrupt the synchronization between plants and their pollinators, which is crucial for successful reproduction and will negatively affect plant populations.

Recent studies using the model plant, *Arabidopsis thaliana*, have demonstrated that native populations are out-competed by warm-temperature genotypes, further underscoring the likelihood for population and/or species loss due to adaptational lag (Exposito-Alonso et al., 2019; Wilczek et al., 2014). While short-lived species, such as *Arabidopsis thaliana*, may have extensive distinct local populations adapted to different climactic conditions, offering genetic potential for evolutionary rescue of native populations, for longer lived species this may be more difficult and require new conservation strategies to avoid species loss (Aitken et al., 2008; St Clair & Howe, 2007). While changing temperatures, and overall warming climates, result in alterations of species and population distributions, the effects of temperature on an individual plant are also observable from germination (Lippmann et al., 2019).

Arabidopsis thaliana was one of the first plants to have genetic loci identified for climate adaptation (Ågren et al., 2013; Hancock et al., 2011). Its large genetic variation enables local adaptability, with different populations displaying traits like drought tolerance, heat resistance, and changes in flowering time regulation (Valladares et al., 2014; Vidigal et al., 2016). Studying these genetic adaptations provides key insights into the molecular mechanisms that drive resilience, offering potential applications for improving crop species and agricultural sustainability under climate change (Exposito-Alonso et al., 2019; Scheepens et al., 2018; Tajima et al., 2007).

1.1.2. Temperature in Plant Development

Even modest increases in average temperatures of a degree within the growth-permissive range of a species can lead to substantial alterations in plant development, architecture, and vegetative to reproductive transitions, a phenomenon known as thermomorphogenesis (Quint et al., 2016). Thermomorphogenesis encompasses a suite of morphological and developmental adaptations that plants undergo in response to elevated ambient temperatures. These elevated temperature effects occur prior to heat stress conditions, in which the heat shock response is triggered. Thermomorphogenic changes include accelerated germination, hypocotyl elongation, earlier flowering, and elongated petioles and stems. Such adaptations represent a broad mechanism by which plants adjust their growth and development to cope with shifts in ambient temperature (Casal & Balasubramanian, 2019; Delker et al., 2022; S. Lee et al., 2021).

The effects of elevated temperatures are evident throughout the entire life cycle of a plant. During early development, warmer conditions can expedite seed germination, leading to quicker sprouting. Following germination, seedlings exposed to higher temperatures often exhibit elongated hypocotyls and cotyledon petioles, a reflection of their adaptation to the elevated temperatures. As the plant matures, the leaves formed during the rosette stage remain elongated compared to those grown under cooler ambient temperature conditions. Thermomorphogenesis also includes the upward movement of leaves, known as hyponasty, and the production of leaves with reduced blade size when plants are grown at temperatures above their optimal range (Quint et al., 2016; Casal & Balasubramanian, 2019).

These adaptations help plant species survive in the short term, however the long-term consequences of global warming on plant survival are difficult to predict. The accelerated pace of climate change may lead to mismatches between plant development and environmental conditions, resulting in reduced flowering, fruiting, seed production, and overall biomass, which for crop plants and human food security is a major challenge (Abbass et al., 2022; Al-

Khatib & Paulsen, 1984; Asseng et al., 2015; Dai, 2013; Gérard et al., 2020; He et al., 2015). Thus, global warming presents an unprecedented challenge to plant. The rapid pace of climate change, driven by human activities, outpaces the ability of many plant species to adapt through evolutionary mechanisms (Gil & Park, 2019; Tabas-Madrid et al., 2018). This mismatch threatens to cause significant shifts in habitat, reductions in reproductive success, and ultimately, the extinction of vulnerable species (Wang et al., 2024; Weiskopf et al., 2020). As global temperatures continue to rise, elevated temperatures will affect human food security.

1.1.3. Crop Plants and Climate Change

Crop plants, unlike their wild counterparts, have been selectively bred over generations to enhance specific agronomic traits such as yield, taste, and resistance to pests. However, this selective breeding process often comes at the cost of an increased sensitivity to abiotic stresses, particularly elevated temperatures (Snowdon et al., 2021). This reduction in stress tolerance is largely due to a decrease in allele diversity and the elimination of genes that could be crucial for adapting to changing environmental conditions (Dewitt et al., 1998; van Kleunen & Fischer, 2005). For example, the narrowing of genetic diversity during breeding can result in crops that are less tolerant to high temperatures during the growing season, which in turn affects their overall productivity (Cox et al., 1986). This has been studied in wheat, for example. High ambient temperatures, especially during critical growth phases like grain filling, reduce wheat's capacity to produce large, high-quality grains (Midmore et al., 1982). In the plant face a heat stress, it accelerates the plant's senescence, leading to smaller yields (Al-Khatib & Paulsen, 1984; Asseng et al., 2015).

Climate change has already had significant impacts on global food production, posing serious challenges to food security worldwide (Roser & Ritchie, 2022; Smith & Gregory, 2013). One of the primary effects of climate change on plants is the alteration of various physiological processes, leading to a cascade of growth and developmental disruptions. Over the past decade, rising temperatures have interfered with the delicate process of flowering, causing it to occur earlier in some crops or be delayed in others (He et al., 2015; Büntgen et al., 2022). For instance, in Japan, cherry trees have been observed to flower earlier in response to elevated temperatures, a phenomenon closely tied to rising global temperatures (Christidis et al., 2022) (Figure 2). Conversely, olive trees have shown delayed flowering under similar temperature increases, illustrating the diverse impacts of climate change on different plant species (Everingham et al., 2023).

The timing of flowering is, for example, critical for insect-pollinated plants, as it must align closely with the activity of pollinators. Disruptions in this synchrony due to climate-induced changes in flowering times can lead to ineffective pollination, which compromises fruit and seed development. This, in turn, results in reduced crop yields, presenting significant challenges for agriculture and food security (Lesk et al., 2016; Saini & Aspinall, 1982; Sheoran & Saini, 1996; Tito et al., 2018). The disruption of the balance between plants and their pollinators highlights the broader ecological impacts of climate change on both natural and managed ecosystems.

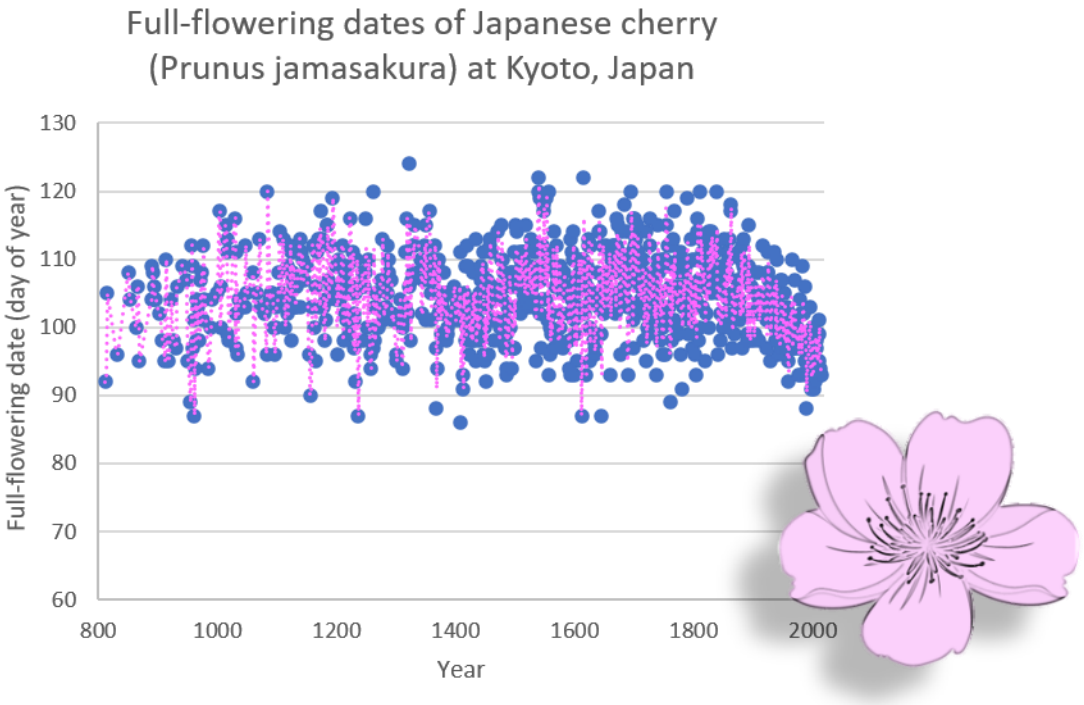

Figure 2. Time of cherry blossom in Kyoto 800-2012 years. Japanese cherry trees flower earlier due to rising temperature (adapted from Christidis et al., 2022).

Elevated temperatures can also accelerate the transition between phenological stages in many plants (Zhao et al., 2017). While this might appear beneficial at first glance, it often results in a mismatch between the plant's growth stages and the optimal environmental conditions required for each stage. For example, crops might reach their reproductive phase during unfavorable conditions in which they have fewer stored nutrients, or lower photosynthetic capacity for seed and fruit production, or less biomass to support larger fruits and seeds, which can reduce their overall productivity. These shifts can disrupt the synchronization between plants and environmental cues like temperature and moisture, which are critical for optimal growth. For instance, if a plant's flowering period is shifted to a hotter part of the season due to climate change, the increased heat can lead to flower drop and reduced fruit set (Guilioni et al., 1997; Lohani et al., 2022). Grains that mature too quickly under elevated temperatures might have reduced nutritional content, negatively impacting food quality and human nutrition. Similarly, fruits that develop under heat stress may be smaller, less flavorful, or have a poor texture, impacting their market value and consumer preference (Devi et al., 2023; Sehgal et al., 2018). Thus, accelerated development shortens the overall growing season, giving crops less time to mature fully and accumulate the necessary resources for optimal yield.

As climate change progresses, understanding the mechanisms of plant ambient temperature sensing and the genetic pathways involved becomes increasingly important. Advances in gene editing technologies offer the potential to modify temperature responses in crops predictably (Karavolias et al., 2021; Ndudzo et al., 2024). However, the development of new F1 hybrids and crop varieties is currently facing challenges due to the limited genetic diversity in breeding material. Consequently, there is a growing emphasis on the need to identify and incorporate new genes and alleles into the genetic pool to enhance crop

resilience with respect to climate change (Bay et al., 2018; Capblancq et al., 2020; Rellstab et al., 2021).

In summary, the increase in global temperatures due to climate change, even within non-stressful ranges, can cause significant disruptions in plant phenology. These shifts in flowering times and accelerated developmental stages can interfere with crucial processes like pollination, leading to reduced crop yields and quality. The shortened growing seasons and diminished crop productivity pose significant threats to global food production and food security, highlighting the urgent need for adaptation, new breeding methods, including genetic modification, and mitigation strategies in agricultural practices. In order to implement these, an understanding of temperature sensing mechanisms in plants is critical.

1.1.4. *Arabidopsis thaliana* as a Model system

Arabidopsis thaliana has emerged as an essential model organism for studying plant biology, particularly in the context of understanding temperature-sensing mechanisms. *A. thaliana* is genetically tractable due to its relatively small and well-annotated genome and the ease of Agrobacterium-mediated transformation (Zhang et al., 2006). Its genome was one of the first plant genomes to be fully sequenced, and forward and reverse genetic studies have been performed using *A. thaliana* for over 50 years (Provart et al., 2016). The wealth of genetic resources already available for *A. thaliana* further enhances its utility as a model organism (Alonso-Blanco et al., 2016; Lasky et al., 2012; Meinke & Scholl, 2003). Extensive libraries of mutants and genetic lines, available through community seed banks such as NAASC, RIKEN and ABRC and curated databases of genetic information such as TAIR have made *A. thaliana* the model dicot of choice for many plant biology studies (Seki, 2003; Meinke & Scholl, 2003; Koornneef & Meinke, 2010; Reiser et al., 2016). These resources are invaluable for investigating the functions of particular genes in response to temperature fluctuations, enabling detailed studies of how plants sense and react to heat and cold. In addition, advanced genetic tools and techniques, such as CRISPR/Cas9 gene editing, are also well established in *A. thaliana*, allowing for precise modifications of genes and/or *cis*-elements involved in temperature sensing and response. These tools facilitate the exploration of genetic pathways and mechanisms with a level of precision that is difficult to achieve in other plant species (W. Jiang et al., 2013). The short life cycle of *A. thaliana* — approximately nine weeks from germination to seed production — allows for “rapid” experimentation and transgenic studies. In addition to its genetic and life cycle advantages, *A. thaliana* is easy to cultivate under laboratory conditions, requiring minimal space and resources. Its small size and ease of growth enables experiments under controlled conditions, with specific light and temperature regimes, key considerations for investigating temperature sensing mechanisms and thermomorphogenesis (Quint et al., 2016).

Importantly, the significance of *A. thaliana* extends beyond its own species due to the conservation of many physiological and developmental pathways across plant taxa. Discoveries made in *A. thaliana* often have broad applicability, providing insights relevant to crop plants, especially concerning stress responses and adaptation mechanisms (Capblancq et al., 2020; Frachon et al., 2018; Hancock et al., 2011). Research in drought tolerance, water use efficiency, and the effects of elevated CO_2 levels and changing light conditions performed in *A. thaliana* are applicable to other species with conservation of many gene regulatory networks (Foyer & Noctor, 2020; Gupta et al., 2020; Ponnu & Hoecker, 2022). Many of the gene regulatory networks (GRN) and pathways important in temperature sensing have been

determined based on work in *A. thaliana*, including the heat and cold stress responses and ambient temperature sensing pathways, which will be briefly summarized below (Chinnusamy et al., 2007; Haider et al., 2021; Jeon et al., 2010; Jung et al., 2020; Nover et al., 2001; Vierling, 1991; Zarka et al., 2003).

1.2. General Temperature Sensing Mechanisms

Membrane fluidity is a fundamental property that enables both prokaryotic and eukaryotic cells to detect and respond to temperature changes. Both cold and elevated temperatures are likely directly sensed via the cell membrane and different ion channels. (Niu & Xiang, 2018; Cano-Ramirez et al., 2021). As temperature varies, the lipid bilayer of the membrane undergoes alterations. Elevated temperatures can increase membrane fluidity by promoting the accumulation of unsaturated fatty acids, which have kinked structures that prevent tight packing of the lipids (Figure 3) (Los & Murata, 2004).

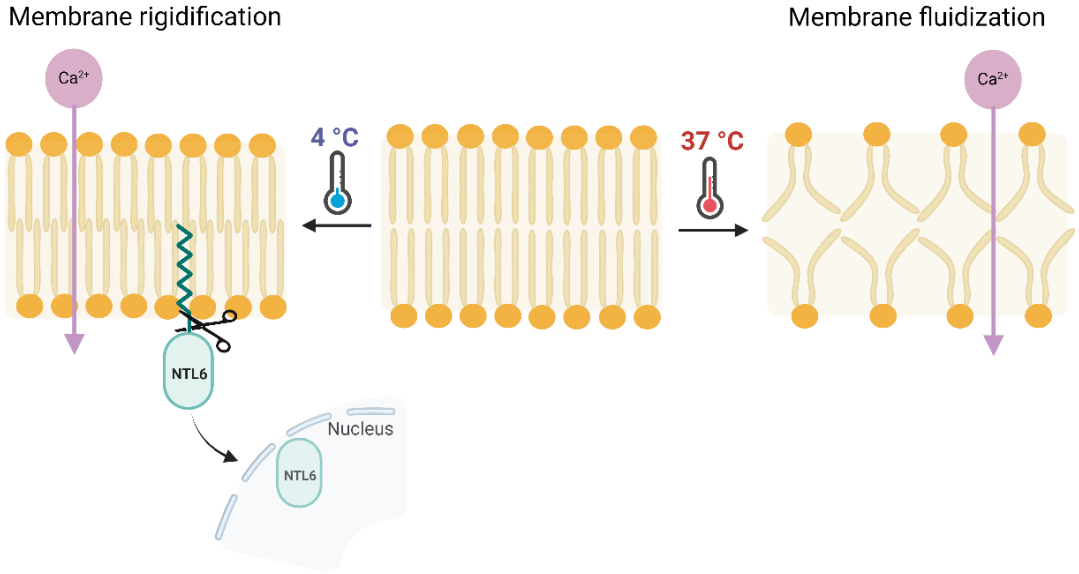

Figure 3. Scheme of membrane rearrangement due to temperature changes. At low temperatures membrane rigidify, leading to the cleavage of NTL6 protein and its nuclear localization, while at high temperature the fluidization of membrane increases, triggering calcium ion influx. Figure adapted from Jung et al., 2023.

In contrast, cold conditions lead to membrane rigidity, as the proportion of saturated fatty acids — lipids with straight chains that pack closely together — increases (Martz et al., 2006; Martinière et al., 2011). Changes in the lipid bilayer composition can influence the conformation and activity of membrane-integrated proteins. For instance, at optimal growth temperatures around 23°C, the NTL6 (NAC with transmembrane motif 1-like 6) transcription factor is inactive and anchored to the membrane. When temperatures drop to 4°C, cold-induced changes of a decrease in membrane fluidity, trigger the NTL6 cleavage through an unknown mechanism. Once released, NTL6 translocates to the nucleus, where it activates *Pathogenesis-Related* genes expression. This mechanism increases the plant's resilience to both cold stress and pathogen resistance (Seo et al., 2010; Seo & Park, 2010).

When the fluidity of the membrane is altered by temperature shifts, it triggers the opening of calcium channels, leading to an influx of Ca^{2+} ions into the cell. This calcium influx then initiates a series of downstream signaling cascades that result in various physiological

adjustments, helping the plant to respond appropriately to temperature changes (Puhakainen et al., 1999). Calcium-binding proteins, such as calmodulins and CBL-CIPK (Calcineurin B-like proteins and CBL-interacting protein kinases) complexes, detect these fluctuations in cytosolic calcium. CBL proteins bind to calcium and then interact with CIPKs, which are protein kinases that can phosphorylate target proteins (Guihur et al., 2022; Weinl & Kudla, 2009). The downstream effectors activated by calcium signaling play a vital role in modulating gene expression and metabolic pathways that are involved in temperature adaptation. For example, certain transcription factors may be activated to initiate the expression of genes that help the plant cope with temperature changes. For example, CBF (C-repeat binding factor) transcription factors, which are central TFs to cold stress responses, may be phosphorylated by CDPKs, enhancing their stability and activity (Pareek et al., 2017). Under heat sress, CDPKs phosphorylate HSFA1A and HSFA1B, enhancing their ability to activate the downstream HSFs and heat-responsive genes, activating a protective response against heat (Saidi et al., 2011).

The structural and physical changes in the membrane acts as a signaling mechanism to activate downstream cellular pathways, allowing the cell to respond to different temperature conditions. Heat and cold activate different gene regulatory networks and trigger different pathways in the cell as a response to significant temperature changes. These pathways have been well-studied in *A. thaliana* and are conserved in many other plant species. Below, a brief summary of the major networks important in heat and cold sensing are described.

1.3. Heat Stress Temperature Sensing Mechanisms

Heat stress in plants occurs when temperatures rise above their optimal physiological growth range, which for *A. thaliana* is between ~ 16 ° C and ~ 28 ° C (Faivre et al., 2024; Groot et al., 2017; Scheepens et al., 2018). Heat stress can be categorized into two main types: heat shock, which is a rapid increase in temperature, and chronic heat stress, which is characterized by a prolonged period of elevated temperatures (Zhang et al., 2020). Both types of heat stress can have severe consequences, including protein denaturation, disruption of cellular homeostasis, and, in extreme cases, cell death, which can ultimately lead to plant death (Ahuja et al., 2010; Vacca et al., 2004).

In *A. thaliana*, one of the best understood mechanisms describing heat stress response centers on a complex series of reactions involving the heat shock factors (HSFs) and their regulation by heat shock proteins (HSPs), which serve as molecular chaperones to proteins. (Vierling, 1991). When a cell receives a heat shock, HSP70, HSP90 release HSF1a, which becomes active, allowing it to translocate to the nucleus and bind its target genes (Hahn et al., 2011). This release is thought to be caused by an increase in misfolded cellular proteins due to heat stress (Kampinga & Craig, 2010; Kanzaki et al., 2003; Park et al., 2010). Once freed from these inactive complexes, HSF1a undergoes trimerization, to enable binding to heat shock elements (HSEs) in the promoters of genes which drives the expression of large amounts of HSPs, to protect the cell from further heat-induced damage (Figure 4) (Lee et al., 1995; Zhang et al., 2001; Wunderlich et al., 2003). Additionally, the activated, HSFA1a and other HSFs drive the expression of downstream heat response regulators such as the transcription factors WRKY25/26/33, DREB2A and the reactive oxygen species (ROS) scavenger, ASCORBATE PEROXIDASE 2 (APX2) (He et al., 2016; Jung et al., 2013; Li et al., 2010; Yoshida et al., 2011).

Once the HSPs accumulate and stress conditions return to normal, the HSPs are

then able to reassociate with the HSFs, thereby returning HSFs to their inactive state and conserving cellular resources once normal temperatures are restored (Scharf et al., 2012; Kotak et al., 2007; Yoshida & Maruyama, 2015).

1.4. Cold Sensing Mechanisms

The susceptibility of plants to cold stress varies significantly among species, depending on their evolutionary adaptation to native environments. When temperate plants, such as *A. thaliana*, are exposed to chilling temperatures, an acclimation process is initiated, including initial sensing of cold via changes in membrane fluidity, calcium signaling and the

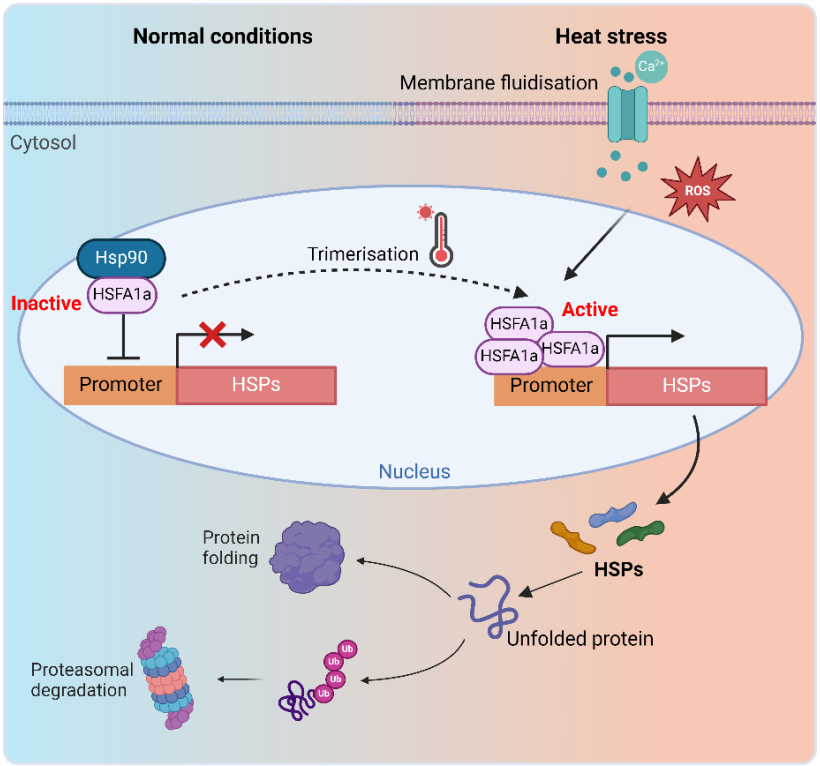

Figure 4. Scheme of main heat stress sensing mechanisms. Under non-stress conditions, HSPs like HSP70 and HSP90 maintain HSFs in an inactive state. In stress conditions, HSFs are released, which leads to their trimerization and binding to Heat Shock Elements (HSEs) in target genes, driving the expression of HSPs. These HSPs prevent protein aggregation and aid in cellular recovery (Adapted from Yoshida et al., 2011).

accumulation of compatible solutes, such as proline and sugars, which protect cellular structures. These changes collectively lead to increased tolerance to freezing temperatures, even if the initial exposure was to non-freezing cold (Juurakko et al., 2021).

A key mechanism underlying this acclimation process is the ICE-CBF-COR (Inducer of CBF Expression - C-repeat Binding Factors - Cold-Regulated genes) cascade (Figure 5). Upon exposure to chilling temperatures, plants perceive the cold signal via changes in membrane structure and fluidity (as previously described) which induces calcium channel signalling, resulting in the activation of ICE (Inducer of CBF Expression) transcription factors (Carpaneto et al., 2007; Yuan et al., 2018).

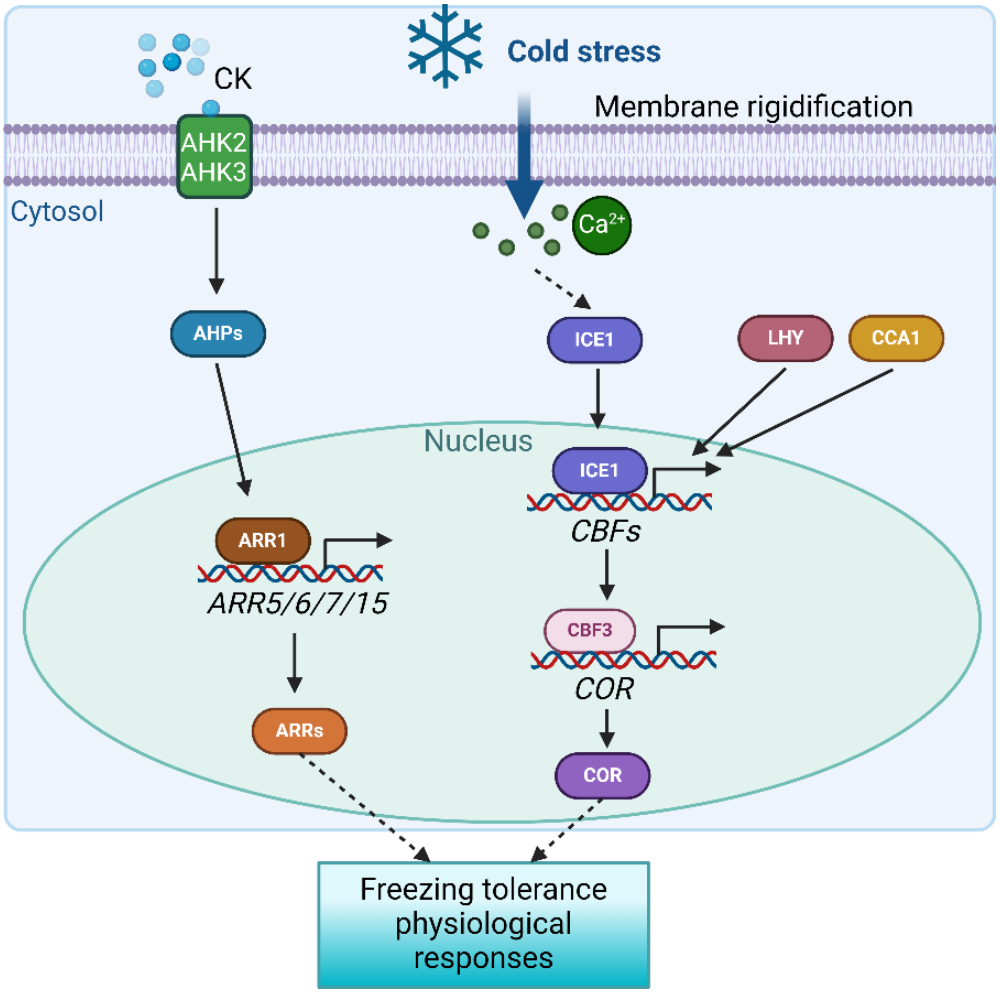

Figure 5. Scheme of main cold sensing mechanisms. Upon exposure to cold stress, in *Arabidopsis* is activated the ICE-CBF-COR cascade. Cold triggers membrane fluidity changes and calcium signaling, activating ICE transcription factors. ICE1 binds to CBF gene promoters, driving CBF3 expression. CBF3 upregulates *COR* genes, enhancing cold tolerance through physiological adjustments. Additionally, histidine kinases AHK2 and AHK3 detect cold signals and induce *ARR* gene expression, contributing to cold-stress adaptation. Adapted from Chinnusamy et al., 2007 and Jeon & Kim, 2013.

Once activated, ICE binds to the promoters of CBF (C-repeat Binding Factors) genes, initiating their expression. For example, the MYC-type basic helix-loop-helix (bHLH) transcription factor ICE1 specifically controls the expression of *CBF3*, a member of the APETALA2/ETHYLENE RESPONSE FACTOR (AP2/ERF) family. Once CBF3 is activated, it binds to specific DNA sequences, upregulating the expression of *COR* genes. These *COR* genes are crucial for enhancing cold tolerance, as they trigger protective responses that help the plant

withstand low temperatures by reducing water loss, slowing plant growth, and adjusting to shorter photoperiods (Zarka et al., 2003; Chinnusamy et al., 2007; Wang et al., 2018; Lata & Prasad, 2011; Jia et al., 2016; Shi et al., 2018). The expression of CBFs (also known as DREB1A-C) is further upregulated by circadian clock genes, such as LHY and CCA1, which entrain the temperature signal within the circadian clock (Dong et al., 2011; Fowler et al., 2005).

In addition to the ICE-CBF-COR cascade, another pathway involves histidine kinases that mediate cold-stress responses. When a plant is exposed to short periods of cold treatment, typically between 1 – 4 °C, the transcription of *A-type ARABIDOPSIS RESPONSE REGULATOR (ARR)* genes is upregulated. This upregulation is part of the plant's adaptive response to cold stress, where histidine kinases AHK2 and AHK3 play central roles (Figure 5). These kinases detect the cold signal and initiate a cascade of reactions leading to the activation of ARR genes, thereby enabling the plant to mount an effective response to low temperatures and improving its chances of survival under cold stress conditions (Jeon et al., 2010; Jeon & Kim, 2013).

For many biennials, winter annuals, certain perennials, brassicas, some flowering plants, and certain grass species, seasonal exposure to cold also needs to be sensed and this information incorporated into plant development in order to ensure flowering in the spring in a process called vernalization (Amasino, 2004). In regions with winters characterized by low temperatures, plants repress flowering during the winter season to protect buds and flowers from suboptimal conditions. This phenomenon is regulated by the genes *FRIGIDA (FRI)* and *FLOWERING LOCUS C (FLC)*. While the primary function of FRIGIDA is to regulate the timing of flowering, it also plays a role in helping plants adapt to cold conditions through phase separation. FRI can undergo liquid-liquid phase separation (LLPS), which may contribute to its ability to form protein assemblies that facilitate transcriptional regulation under varying temperatures (Zhang et al., 2023). FRI promotes the expression of *FLC*, which acts as a repressor of flowering by inhibiting the expression of *FLOWERING LOCUS T (FT)*, a gene crucial for the initiation of flowering. During vernalization, prolonged exposure to cold leads to the epigenetic silencing of *FLC* through chromatin modifications, such as histone methylation. This silencing is facilitated by a group of proteins including VERNALIZATION INSENSITIVE 3 (VIN3), VERNALIZATION 1 (VRN1), and VERNALIZATION 2 (VRN2), which form a complex that modifies the chromatin structure around the *FLC* locus, stably repressing its expression (Figure 6). As a result, once the cold period has passed, the repression of *FLC* allows the activation of *FT*, leading to flowering when temperatures rise. These regulatory layers through LLPS and epigenetic regulation ensure precise flowering control in response to seasonal temperature shifts (Choi et al., 2011; Johanson et al., 2000; Zhang et al., 2023).

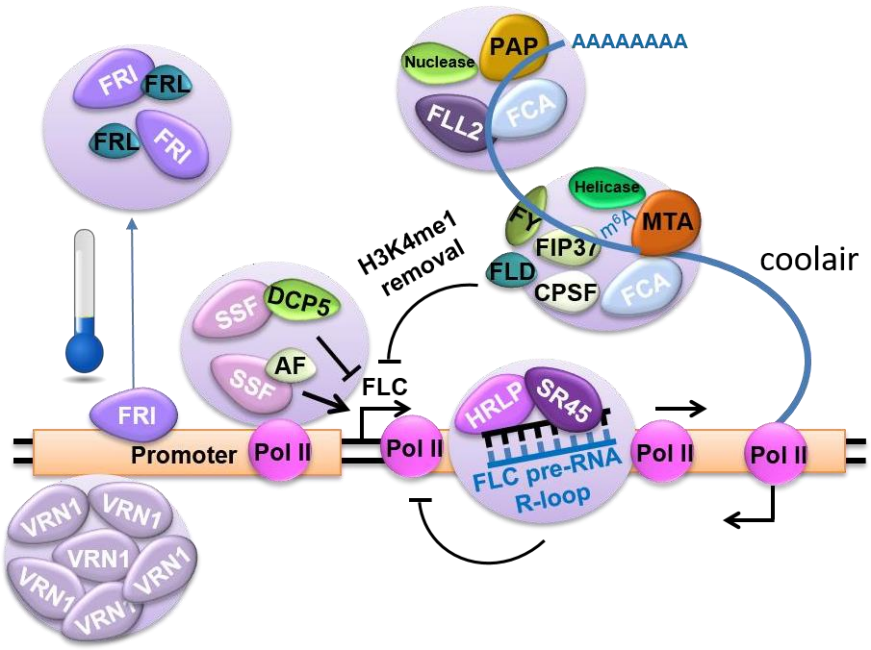

Figure 6. Biomolecular condensates regulate FLC transcription through various mechanisms. FLL2-driven phase separation forms condensates that promote COOLAIR polyadenylation. Similarly, droplets formed by FCA phase separation contain the m6A methyltransferase complex, which deposits m6A on COOLAIR and includes 3′-end processing factors that recruit FLD to remove H3K4me1 from FLC-associated chromatin, leading to FLC silencing. Phase separation of HRLP and SR45 forms condensates that promote R-loop formation, repressing Pol II-mediated FLC transcription. Cold-induced FRI forms condensates with FRL, preventing FRI localization to FLC's transcriptional activation site, thereby inhibiting transcription. Additionally, VRN1 phase separation forms droplets that inhibit FLC transcription, while SSF undergoes LLPS at the FLC genomic region, acting as a scaffold to interact with activating factors to promote transcription or with DCP5 to repress it. Adapted from Eljebbawi et al., 2024.

1.5. Ambient Temperature Sensing of Plants

While heat and cold stress pathways are relatively well studied in model plant species such as *A. thaliana*, the perception of small, non-stress ambient temperature changes are much less well described. The capacity to perceive and react to small growth permissive and non-stress temperature changes is crucial for optimizing various developmental processes, such as seed germination, flowering, and fruit ripening (Ausin et al., 2005; Bangerth et al., 2012; del Olmo et al., 2019; Piskurewicz et al., 2023). Thus, understanding the mechanisms of ambient temperature perception in plants may help optimize crop development and yield in the face of global warming. Here, some of the important factors for ambient temperature sensing will be briefly summarized in a general overview. The mechanism under study, and the subject of this thesis, temperature sensing via liquid-liquid phase separation of the protein EARLY FLOWERING 3, will be presented in more detail.

1.5.1. Histone modifications, RNA structure and light receptor conformational changes as ambient temperature sensors

Different mechanisms such as chromatin/histone modification, nucleosome positioning and alternative splicing have been postulated to play roles in plant temperature sensing and response (Lämke & Bäurle, 2017; Niu & Xiang, 2018; Shen et al., 2019). One example of histone modification involved in temperature response is histone acetylation and deacetylation. In warmer temperatures, there is often an increase in histone acetylation, facilitated by enzymes known as histone acetyltransferases (HATs) (Ha et al., 2017; Hu et al., 2015). This modification reduces the positive charge on histones, weakening their interaction with the negatively charged DNA. As a result, the chromatin becomes more relaxed or "open," making the DNA more accessible to transcription factors and other regulatory proteins, which enhances gene expression. Conversely, histone deacetylases (HDACs) can remove these acetyl groups, leading to a more compact or "closed" chromatin state, which can repress gene expression. The dynamic interplay between HATs and HDACs is crucial for finely regulating gene expression in response to temperature fluctuations. Temperature changes can increase or decrease the expression or activate specific HATs or HDACs through signal transduction pathways, resulting in targeted histone modifications at genes that are critical for responding to these changes. In addition, as with any enzymatic activity, temperature will alter the reaction rate of the acetylation/deacetylation reaction and specific HATs and HDACs will also have an optimum temperature for their activity, putatively providing a direct temperature read-out (Daniel et al., 2008). These histone modifications are often reversible and precisely controlled, allowing plants to adapt to fluctuating temperatures by selectively activating or repressing specific genes as necessary (Figure 7). Modifications such as histone methylation, ubiquitination and phosphorylation have also been implicated in temperature response pathways (Luo et al., 2012). In addition to histone modifications, nucleosome structure can be tuned via the incorporation of histone variants. For example, H2A.Z incorporation decreases with increasing temperature, resulting in differential gene expression as a function of temperature. H2A.Z-containing nucleosomes wrap DNA more tightly, which affects RNA polymerase (Pol) II access to the transcriptional start site of different genes and thus provides a mechanism for thermal regulation of the transcriptome (Cortijo et al., 2017; Olmo et al., 2019; Kumar, 2018; Kumar & Wigge, 2010).

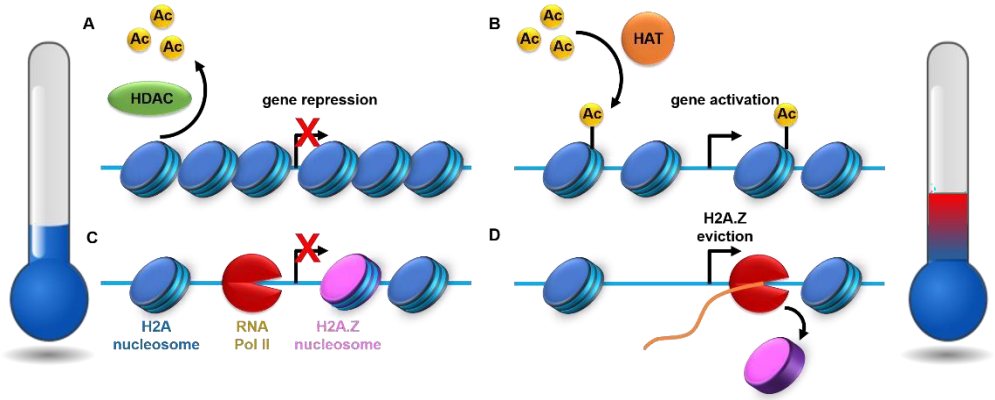

Figure 7. Histone modifications due to temperature. (A) In lower temperature condition histone deacetylases (HDACs) can remove acetyl groups, leading to a more compact or "closed" chromatin state, while at higher temperatures, **(B)** histone acetyltransferases (HATs) acetylates histones leading to a open chromatin form, making the DNA more accessible to transcription factors and other regulatory proteins. **(C)** At lower temperature, H2A.Z nucleosomes prevent transcription. **(D)** At higher temperature, H2A.Z nucleosome occupancy declines, leading to increased expression (adapted from Kumar & Wigge, 2010).

Additional direct read-outs of temperature include RNA structure. For example, the PIF7 mRNA has been shown to form a hairpin at its 5'UTR, which partially unfolds as the temperature increases, allowing for increased translation of PIF7 with higher temperatures (Chung et al., 2020). PIF7 is a transcription factor that directly regulates genes including *YUCCA8*, a gene involved in auxin biosynthesis and major component of the thermomorphogenic pathway. Other changes at the RNA level include alternative splicing (AS). As with any enzymatic reaction, AS will be affected by temperature. This has been well-established for the *FLOWERING LOCUS M (FLM*) gene, which undergoes AS, with the beta form produced at lower temperatures and the delta form at higher temperatures (Figure 8). This results in the formation of an active repressive complex of FLM-beta-SVP at lower temperatures and an inactive complex of FLM-delta-SVP at higher temperatures. The FLM-beta-SVP complex represses genes involved in the floral transition, such as *FT* (Posé et al., 2013).

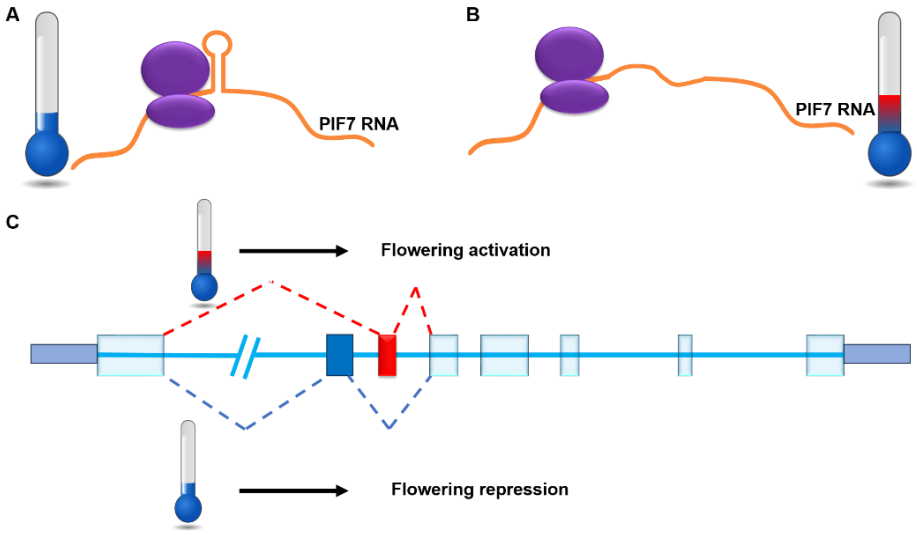

Figure 8. Temperature-dependent changes in mRNA folds and alternative splicing. (A) The PIF7 mRNA formations an RNA hairpin within its 5' UTR, which **(B)** adopts an alternative conformation at higher temperature, leading to increased protein synthesis. **(C)** FLOWERING LOCUS M (FLM) in *Arabidopsis thaliana* shows an alternative usage of exons 2 and 3, two mutually exclusive exons to act as a thermosensitive regulator in the flowering time pathway.

Light receptors in plants, such as cryptochromes and phytochromes, can also function as temperature sensors, playing a dual role in regulating plant responses to light and temperature. Cryptochromes detect blue light and are involved in controlling various growth processes. However, their activity and stability are also influenced by temperature changes.. For instance, cryptochrome 2 (CRY2) is sensitive to temperature fluctuations, which affect its stability and interactions with other proteins. At 16° C, CRY2 is less stable than at high ambient temperature due to Light-Response Bric-a-Brack/Tramtrack/Broads (LRBs) mediated proteasome degradation (Ma et al., 2021). In contrast, at low temperatures, such as 5 °C, CRY2 remains stable, avoiding degradation. This stability leads to the accumulation of ELONGATED HYPOCOTYL 5 (HY5), a transcription factor that plays a critical role in cold acclimation. By fluencing the levels of HY5, cryptochromes adjust plant growth and metabolic processes to cope with cold conditions (Ponnu & Hoecker, 2022).

Another light receptors, Phytochrome B (PhyB), is capable of sensing temperature through a process known as temperature-dependent or thermal reversion (Klose et al., 2020). In its inactive form, PhyB exists as dimers that absorb red light (Pr). Upon exposure to red light, PhyB undergoes a conformational change, transitioning to its active form (Pfr), which absorbs far-red light. This transformation is reversible, with the Pfr form reverting back to Pr through a light-independent process called dark reversion. Temperature plays a significant role in modulating these transitions. At elevated temperatures, such as 30 °C, the reversion from Pfr to Pr is accelerated (Sweere et al., 2001; Legris et al., 2016). Under reduced light and high ambient temperature conditions, dark reversion competes with the light-induced Pr to Pfr conversion, influencing the overall balance of active and inactive phytochrome forms (Figure 9). Furthermore, PhyB directly binds to the promoters of genes crucial for growth and development in a temperature-dependent manner, integrating light and temperature signals to regulate plant responses (Jung et al., 2016).

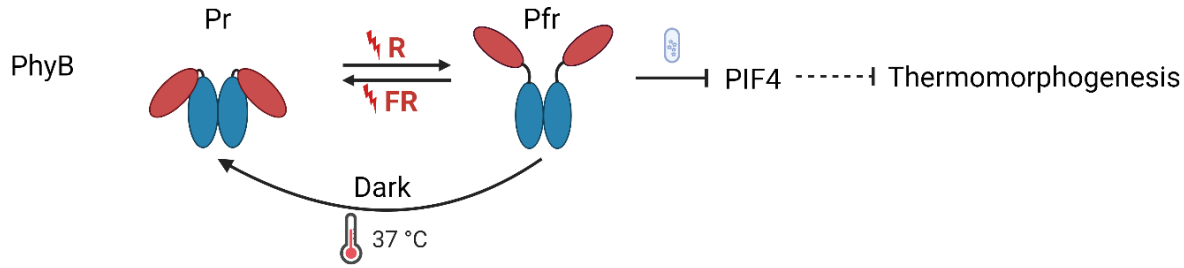

Figure 9. Scheme of Phytochrome B conversion under red and far-red light spectra and high ambient temperature conditions. Inactive form of PhyB (Pr) convert to an active form (Pfr) under red-light exposure, while Pfr form revert to Pr form at high temperature and dark. Figure is adapted from Jung et al., 2023.

In summary, temperature changes different genes in the plant and even small temperature changes trigger changes in transcription-translation outputs. Different mechanisms play a role in this, but there is a convergence in specific thermomorphogenic pathways, which will be described below.

1.5.2. Transcriptional regulators of thermomorphogenesis

Thermomorphogenesis, as previously described, is a form of plant response to high ambient temperature and results in morphological changes such as the elongation of hypocotyls, petioles, stems, and roots, as well as leaf bending, known as thermonasty (Figure 10). This process is primarily regulated by PHYTOCHROME INTERACTING FACTOR 4 (PIF4), a transcription factor that integrates temperature signals to control gene expression and

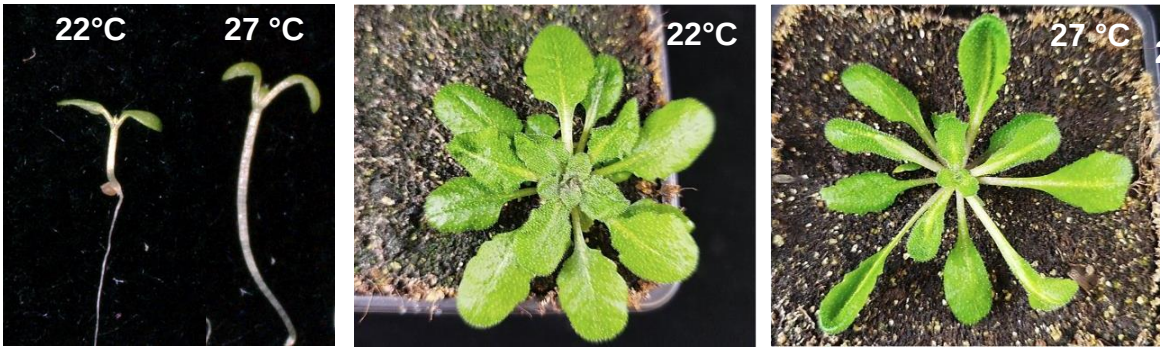

Figure 10. *Arabidopsis thaliana* plants Col-0 at 22° C and 27° C. At higher ambient temperature plants have adjusted morphology, such as elongated hypocotyls, leave petioles, and bend leaves upwards, **(A)** hypocotyls of *A. thaliana* at two different temperatures (22° C versus 27° C), **(B)** plants at juvenile stage grown at 22° C and 27° C.

developmental outcomes. Thermomorphogenic phenotypes are similar to those associated with shade avoidance response (SAR), an important adaptive strategy in which plants compete for light in crowded environments. SAR is triggered when plants detect a low ratio of red to far-red light (R), signaling the presence of neighboring plants that are absorbing more red light. In warmer conditions, this ratio suggests plants are shaded during the day (Franklin et al., 2003). Under these conditions, PhyB, becomes inactivated. This inactivation leads to the stabilization and accumulation of PIF4, which then promotes the expression of genes driving the elongation of stems and petioles, enabling the plant to outgrow its competitors and capture more light (Figure 11). Thus, PIF4 serves as a central regulator of the SAR and thermomorphogenesis as a key regulator responsible for the associated phenotypes.

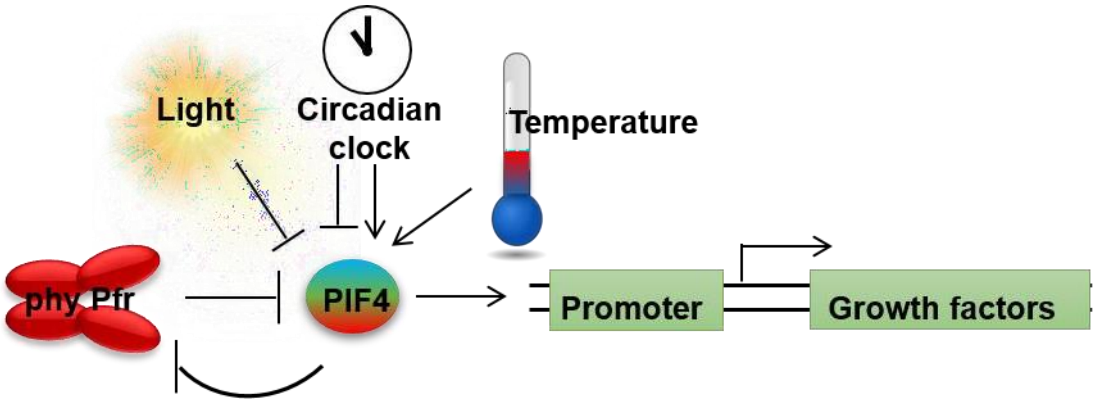

Figure 11. PIF4 constitute a developmental signaling hub downstream external cues such as light and temperature as well as the circadian clock and thereby affect multiple developmental processes including germination, vegetative growth and flowering.

Plants use light quality and temperature to respond to their surroundings. Warmer nighttime temperatures result in plants that undergo particularly pronounced thermomophogenesis as temperature signals dominate at night. Together, PhyB and PIF4 act as conduits for environmental signals, providing information about light and temperature into plant development. PIF4 is an important output of the circadian clock and is directly regulated

by clock factors. Interestingly, PIF4 can not sense temperature directly (Vu et al., 2019) but is regulated at the transcriptional level in a clock and temperature-dependent manner.

1.6. Circadian Clock and Plant Development

Temperature signaling in plants is integrated into a broad regulatory framework governed by the circadian clock. The circadian clock is a sophisticated system that allows plants to “anticipate” daily and seasonal changes, allowing them to adjust their metabolism, architecture, and development in a way that maximizes their chances of survival and growth. The plant circadian clock is an internal time-keeping mechanism that synchronizes with the Earth's day-night cycle, generating self-sustained oscillations with a period of about 24 hours (Dunlap, 1999). Similar to mammals, which also possess a circadian clock to regulate sleep-wake cycles and other bodily functions (Cameron et al., 2008; Eckel-Mahan & Storm, 2009; Green et al., 2008), the plant circadian clock comprises a series of interlocking negative transcription-translation feedback loops known as the morning loop, the central loop, and the evening loop (Bell-Pedersen et al., 2005; Pokhilko et al., 2010). The integration of these three loops ensures precise timing of gene expression, which in turn affects a wide array of physiological processes. For example, the circadian clock regulates photosynthesis, allowing plants to maximize light capture and energy production during daylight hours (Dodd et al., 2015). It also controls stomatal opening, which governs gas exchange and water loss in response to environmental conditions (Hubbard & Webb, 2015; Jurca et al., 2022). Additionally, the clock times the production and signaling of various hormones, such as auxins, gibberellins, and abscisic acid, coordinating growth and stress responses (Ezer et al., 2017). This intricate system ensures that plants can optimize their physiological functions and developmental processes in accordance with both daily and seasonal environmental cues, thereby enhancing their growth and survival. (Figure 12).

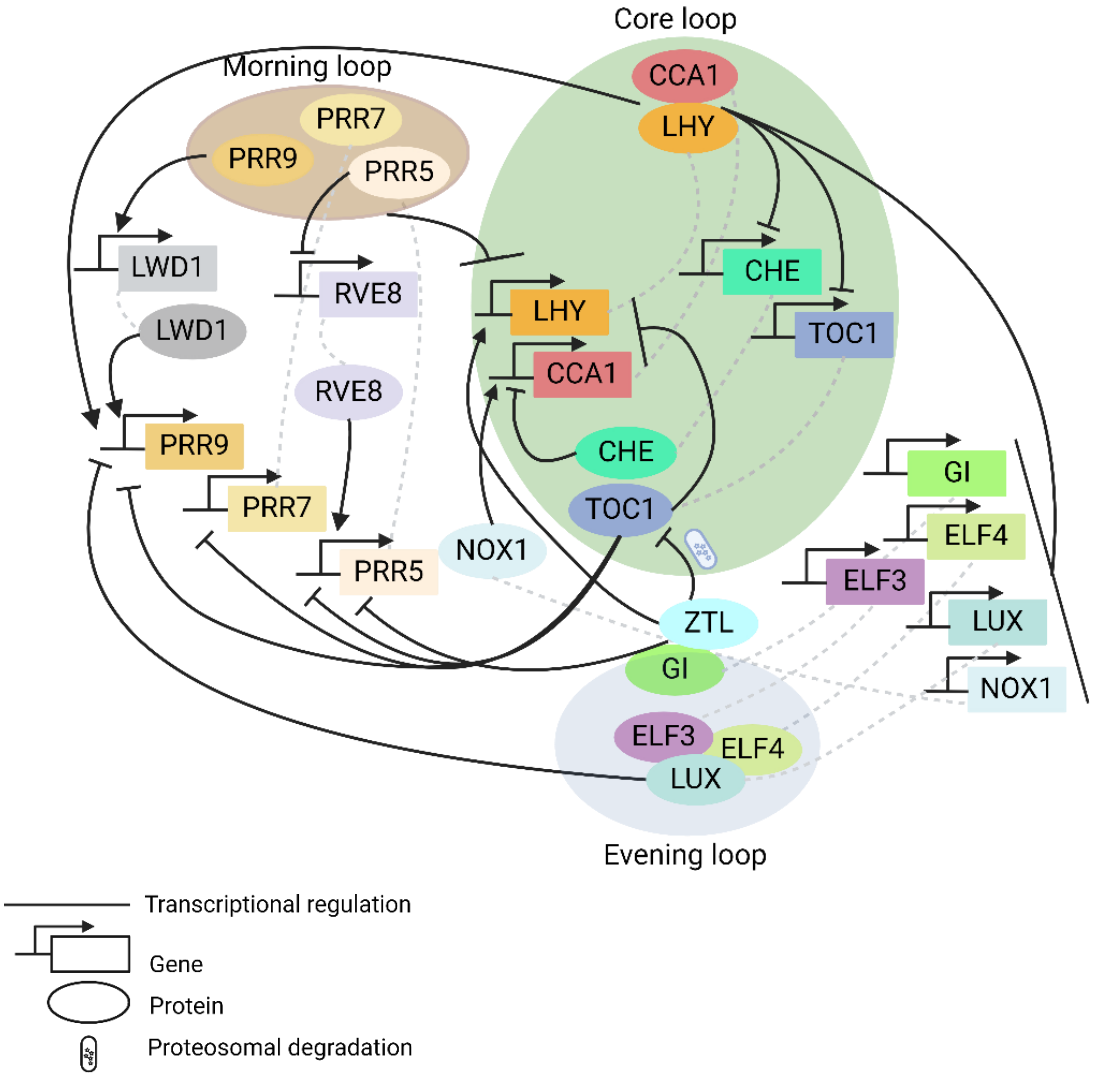

Figure 12. Simplified scheme of molecular regulation of circadian clock in *Arabidopsis thaliana*. Three negative feedback loops are formed: morning loop, containing PRR5, PRR7 and PRR9, a core loop with CCA1, LHY and TOC1 and evening loop, comprising of evening complex (ELF3, ELF4, LUX) and GI, ZTL. PRR7 and PRR9 repress core loop genes, CCA1 and LHY, which control evening gene expression. TOC1 (PRR1) represses CCA1/LHY in the afternoon, with ZEITLUPE (ZTL) regulating TOC1 degradation. The Evening Complex (ELF3, ELF4, LUX) represses morning loop genes and TOC1, ensuring proper timing of the circadian cycle. Figure adapted from Nagel & Kay, 2012.

The morning loop involves key genes such as *PSEUDO-RESPONSE REGULATOR 5, 7* and *9 (PRR5, PRR7* and *PRR9)*. These genes are expressed at dawn and repress the core loop genes such as *CCA1* and *LHY*. The core loop *CCA1 (CIRCADIAN CLOCK ASSOCIATED 1)* and *LHY (LATE ELONGATED HYPOCOTYL)* genes encode MYB-domain transcription factors and control evening genes by directly binding to evening gene promoters and repressing their expression in the morning. They also act as repressors of *PRR7* and *PRR9* (Farré et al., 2005; Nakamichi et al., 2005). Later in the day, PRR7 and PRR9 in turn repress *CCA1* and *LHY* (Nakamichi et al., 2010). CCA1 and LHY also inhibit their own expression creating a negative feedback loop that helps regulate their levels throughout the 24-hour cycle. LHY and CCA1 form a complex *in vivo*

(Lu et al., 2009). The core loop also features the gene *TIMING OF CAB EXPRESSION 1 (TOC1)*, also known as *PSEUDO RESPONSE REGULATOR 1 (PRR1)*. *TOC1* is expressed in the afternoon and plays a crucial role in repressing the expression of *CCA1* and *LHY*. As night falls and TOC1 levels decrease, the repression on *CCA1* and *LHY* is lifted, allowing their expression to rise again the following morning (Gendron et al., 2012). This feedback loop is essential for maintaining the oscillatory nature of the circadian clock. TOC1 directly interacts with CCA1 HIKING EXPEDITION (CHE). CHE also represses the expression of *CCA1* (Pruneda-Paz et al., 2009). The evening loop regulates genes and proteins in the morning, core and evening loops. ZEITLUPE (ZTL), a photoreceptor and E3 ligase, is part of the evening loop and binds TOC1 to trigger the degradation of TOC1 (Más et al., 2003). ZTL also regulates PRR5 degradation through direct binding (Kiba et al., 2007). ZTL is stabilized by direct interaction with GIGANTEA (GI) in blue light conditions (W.-Y. Kim et al., 2007). EARLY FLOWERING 3 (ELF3), together with LUX ARRYTHMO (LUX) and ELF4 forms the Evening Complex (EC), that acts in the evening loop of the circadian clock, directly repressing genes like *PRR7* and *PRR9* from the morning loop, and core loop (TOC1) (Brandoli et al., 2020; Gil & Park, 2019; McClung, 2006). By keeping TOC1 levels low during the night, the evening loop ensures that the central loop does not prematurely activate the morning loop, thereby maintaining the proper timing of the circadian cycle. In addition, the EC binds to non-circadian clock target genes, including PIF4, inhibiting their expression (Ezer et al., 2017). However, at high ambient temperatures, this binding is disrupted, leading to the de-repression of flowering genes (Figure 13) (Hutin et al., 2024; Jung et al., 2020; Silva et al., 2020). This precise temperature-responsive transcription regulation by the EC ultimately influences the timing of elongation and flowering. In addition to its role in the EC, ELF3 may acts independently of LUX and ELF4 to tune plant development.

1.6.1. ELF3-a key scaffold protein in different transcriptional complexes

ELF3 has been shown to give rise to altered thermal responsive growth not only in *Arabidopsis* but also in crop plants (Box et al., 2015; Gawroński et al., 2014; Raschke et al., 2015). ELF3, as part of the EC, represses GIGANTEA (GI) transcription, a protein that helps control the expression of CONSTANS (CO), a central regulator in the flowering process (Kubota et al., 2017). ELF3 permits the interaction of CONSTITUTIVE PHOTOMORPHOGENIC1 (COP1), an E3 ligase, with GI, triggering the degradation of GI and indirectly regulating CO expression (Brandoli et al., 2020). CO is stabilized by GI, and once stabilized, it activates the expression of FLOWERING LOCUS T (FT), a gene that triggers the floral transition, signaling the plant to begin flowering. The GI-CO-FT pathway serves as an important output of the circadian clock, linking the plant's internal timekeeping system to its flowering responses. The timing of CO expression is crucial for this process. In *Arabidopsis*, under short-day conditions, CO expression peaks at night, leading to CO protein degradation, which delays flowering. However, under long-day conditions, CO expression peaks during the day when ELF3 and GI concentrations are low. In daylight, CO is stabilized, allowing it to activate FT and promote flowering (Anwer et al., 2020; Valverde et al., 2004; Yanovsky & Kay, 2003; Yu et al., 2008a).

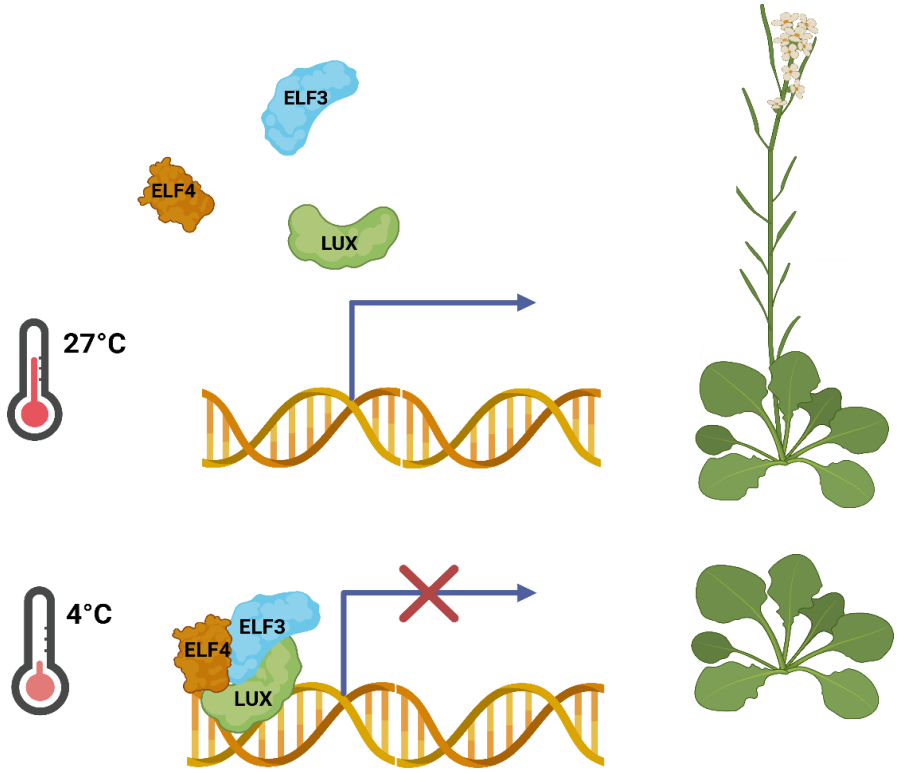

Figure 13. Scheme of evening complex DNA binding as a function of temperature. At lower temperature 4°C the evening complex binds to DNA, repressing target genes. At higher ambient temperature (27°C) the EC does not bind DNA, resulting in de-repression of genes and early flowering. Figure adapted from Silva et al., 2020.

ELF3 also plays a role in regulation of photoactive PHYTOCHROME B (PhyB), integrating light signals into the circadian clock. This interaction helps synchronize the internal clock with external light conditions. ELF3 and PhyB work together to regulate the expression of genes involved in light responses. For instance, under red light, PhyB promotes the degradation of ELF3, which in turn affects the expression of light-responsive genes (Nieto et al., 2015). This interaction can modulate the circadian clock's response to photoperiod changes, thus affecting flowering time and other light-dependent processes and ensuring that the plant's internal clock is synchronized with external light conditions.

Additionally, ELF3 interacts with ubiquitin E3 ligases, XBAT31 and XBAT35, that act redundantly, which mediate ELF3 proteasomal degradation at warm temperatures. This results in XBAT-mediated thermomorphogenesis, regulating hypocotyl elongation indirectly via increased PIF4 levels due to decreased ELF3 concentrations (Zhang et al., 2021, 2024). Interestingly, ELF3 degradation is regulated differently depending on the tome of day and environmental conditions. COP1 mediates ELF3 degradation at night, while XBAT31 facilitates its degradation during the day under light under warm temperature conditions.

Taken together, ELF3 serves as a scaffold for numerous protein interactions. ELF3 in complex with LUX and ELF4, is part of the core circadian clock component, the EC. ELF3 also acts independently of the EC, interacting with other proteins such as GI and COP1 to regulate growth and developmental processes. While ELF3 transcription is not temperature

dependent, its activity is (Ezer et al., 2017; Jung et al., 2020). The molecular mechanisms of these changes in ELF3 activity as a function of temperature are the subject of this thesis study.

1.7. ELF3 Protein Characteristics

ELF3 is a plant-specific protein with no domains of known function and acts as a scaffold as mentioned above (Huang et al., 2016a; Nieto et al., 2015). ELF3 is composed of 695 amino acids in *Arabidopsis thaliana* ecotype Columbia-0 (Figure 15). It contains an acidic region (206-320 residues), a proline-rich region (440-540), an aromatic-rich region (484-540) and a glutamine/threonine-rich region (544-653). There is very little secondary structure predicted for the protein apart from a long alpha helix (318-363) in the middle region and a short C-terminal alpha helix (669-693). In addition, a β-hairpin is predicted in the C-terminal region of the protein, comprising residues (470-487) based on Alphafold2 predictions (Figure 14). ELF3 possesses a C-terminal (388 to 625 residues) low-complexity intrinsically disordered region (IDR), in which is embedded a prion-like domain (PrD), located between 430 and 609 amino acid positions, has multiple repeats of poly-glutamines (polyQs, 7 to 29 glutamines across 181 natural *A. thaliana* accessions) (Hutin et al., 2023a; Tajima et al., 2007) with AtELF3 sequence shown in figure 15.

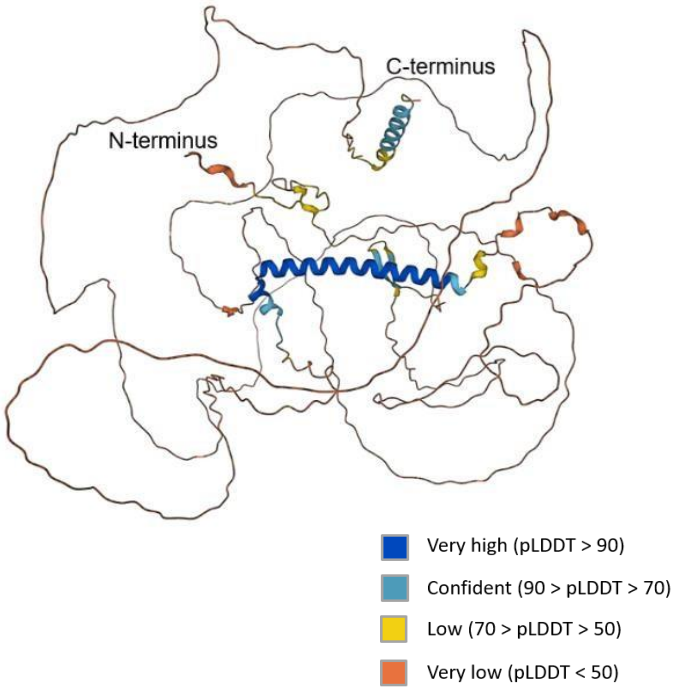

Figure 14. Predicted structure of ELF3 with Alphafold2. Scores of confidence are shown colored from blue to orange (high to low confidence). ELF3 is largely disordered with little secondary structure of two alpha helixes and small β-hairpin structure.

Intrinsically disordered proteins (IDPs) lack a well-defined secondary structure, however, they play crucial roles in cellular biology. This intrinsic disorder often allows IDPs to perform a wide range of biological functions and facilitates interactions between various molecules like proteins and nucleic acids (Van Der Lee et al., 2014). This makes them essential in processes like cellular signaling and regulation, where transient and versatile interactions are necessary. Because IDPs can easily change their conformations, they are often involved in

signaling pathways, acting as molecular switches or scaffolds that bring together various components of complex protein networks (Iakoucheva et al., 2002; Dunker et al., 2005; Galea et al., 2008; P. M. Kim et al., 2008).

Prion-like domains (PrDs) are specific sequences within proteins that can adopt multiple conformations, one of which may lead to self-propagating aggregation, similar to prions. Prion-like domains often exhibit repetitive sequences of aspartates or glutamates and are a subset of intrinsically disordered regions (IDRs) of proteins. These domains are typically enriched in polar and aromatic residues, sharing structural and functional similarities with prion proteins identified in yeast (Malinovska et al., 2015). While prions and prion-like proteins have been extensively studied in the context of human neurodegenerative diseases and regulatory mechanisms in yeasts, they are also prevalent across a wide range of organisms, including plants. In most organisms, PrDs are believed to play critical roles in processes such as signaling and scaffolding (Benkemoun & Saupe, 2006; Cortese et al., 2008; Uversky, 2015). Recent studies have identified PrDs in many plant proteins, suggesting that these domains are more widespread in the plant kingdom than previously recognized. For example, *A. thaliana* has approximately 500 PrD containing proteins and in rice, 60 proteins have been predicted to contain PrDs based on bioinformatics analyses (Chakrabortee et al., 2016; Garai et al., 2021). This finding suggests that PrDs may play significant and widespread roles in plant biology. A novel function recently attributed to PrDs in plants is their capacity to undergo liquid-liquid phase separation (LLPS) (Jung et al., 2020). LLPS is a thermodynamically driven process in which a macromolecular species, such as a protein, demixes into coexisting

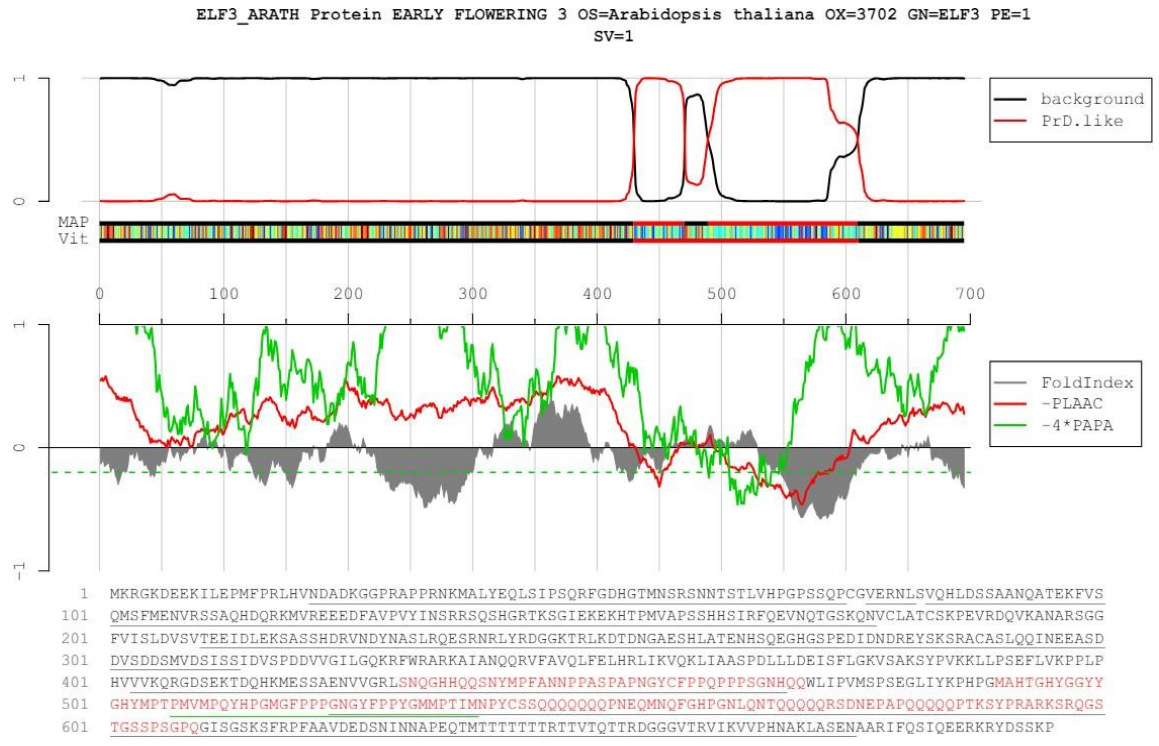

Figure 15. Prediction of prion-like domain in AtELF3 protein with PLAAC algorithm. ELF3 protein contains a PrD between 430 and 609 amino acid positions (Lancaster et al., 2014). At the top, the red color line indicate an enrichment of t log-likelihood ratio of the PrD, bottom – visualized prion-predicted scores such as PAPA, PLAAC and FoldIndex algorithms.

dilute and dense phases, leading to the formation of liquid-like compartments within cells, often referred to as biomolecular condensates. These condensates play crucial roles in organizing cellular processes without the need for membrane-bound organelles.

Research has shown that the temperature-sensitive function of the ELF3 protein in plants relies on its prion-like domain (Figure 15) (Lancaster et al., 2014). In addition, this domain acts as a driver of LLPS, with LLPS occurring in a temperature-dependent manner both *in vitro* and *in vivo* (Jung et al., 2020). Experiments swapping the ELF3 prion-like domain for the same region from *Brachypodium distachyon* that is not annotated as a PrD, revealed that the prion-like domain is crucial for temperature-sensitive flowering (Jung et al., 2020). Interestingly, different *A. thaliana* accessions, which are populations adapted to specific geographic regions, exhibit genetic variation in the ELF3 gene, particularly in the sequence of the PrD region (Alonso-Blanco et al., 2016). For example, the PrD contains a poly-glutamine (polyQ) tract, whose length varies across natural *Arabidopsis* accessions (Tajima et al., 2007), fine-tuning the temperature response of the protein and in consequence of the plant (Hutin et al., 2023; Jung et al., 2020).

These variations are thought to be the result of adaptation to local environmental conditions, reflecting the evolutionary pressures that shape plant responses to diverse climates. However, while this genetic diversity suggests that differences in ELF3 PrDs could potentially influence the protein's ability to undergo LLPS, experimental evidence confirming this connection is still lacking for most of *A. thaliana* accessions. Understanding how these natural variations impact ELF3 function and phase separation could provide deeper insights into the mechanisms by which plants adapt to their environments.

The main goals of this thesis were to biochemically and structurally characterize the ELF3 PrD and use this to information to rationally alter LLPS *in vitro* via point mutations. Based in this, mutants of interest were introduced into *elf3* loss-of-function *Arabidopsis* plants to robustly correlate *in vitro* activity with physiological function.

References

Abbass, K., Qasim, M. Z., Song, H., Murshed, M., Mahmood, H., & Younis, I. (2022). A review of the global climate change impacts, adaptation, and sustainable mitigation measures. Environmental Science and Pollution Research, 29(28), 42539–42559. https://doi.org/10.1007/s11356-022-19718-6

Ågren, J., Oakley, C. G., McKay, J. K., Lovell, J. T., & Schemske, D. W. (2013). Genetic mapping of adaptation reveals fitness tradeoffs in Arabidopsis thaliana. Proceedings of the National Academy of Sciences, 110(52), 21077–21082. https://doi.org/10.1073/pnas.1316773110

Ahuja, I., De Vos, R. C. H., Bones, A. M., & Hall, R. D. (2010). Plant molecular stress responses face climate change. Trends in Plant Science, 15(12), 664–674. https://doi.org/10.1016/j.tplants.2010.08.002

Aitken, S. N., Yeaman, S., Holliday, J. A., Wang, T., & Curtis-McLane, S. (2008). Adaptation, migration or extirpation: Climate change outcomes for tree populations. Evolutionary Applications, 1(1), 95–111. https://doi.org/10.1111/j.1752-4571.2007.00013.x

Alkama, R., Taylor, P. C., Garcia-San Martin, L., Douville, H., Duveiller, G., Forzieri, G., Swingedouw, D., & Cescatti, A. (2020). Clouds damp the radiative impacts of polar sea ice loss. The Cryosphere, 14(8), 2673–2686. https://doi.org/10.5194/tc-14-2673-2020

Al-Khatib, K., & Paulsen, G. M. (1984). Mode of high temperature injury to wheat during grain development. Physiologia Plantarum, 61(3), 363–368. https://doi.org/10.1111/j.1399-3054.1984.tb06341.x

Alonso-Blanco, C., Andrade, J., Becker, C., Bemm, F., Bergelson, J., Borgwardt, K. M., Cao, J., Chae, E., Dezwaan, T. M., Ding, W., Ecker, J. R., Exposito-Alonso, M., Farlow, A., Fitz, J., Gan, X., Grimm, D. G., Hancock, A. M., Henz, S. R., Holm, S., … Zhou, X. (2016). 1,135 Genomes Reveal the Global Pattern of Polymorphism in Arabidopsis thaliana. Cell, 166(2), 481–491. https://doi.org/10.1016/j.cell.2016.05.063

Amasino, R. (2004). Vernalization, Competence, and the Epigenetic Memory of Winter. The Plant Cell, 16(10), 2553–2559. https://doi.org/10.1105/tpc.104.161070

Asseng, S., Ewert, F., Martre, P., Rötter, R. P., Lobell, D. B., Cammarano, D., Kimball, B. A., Ottman, M. J., Wall, G. W., White, J. W., Reynolds, M. P., Alderman, P. D., Prasad, P. V. V., Aggarwal, P. K., Anothai, J., Basso, B., Biernath, C., Challinor, A. J., De Sanctis, G., … Zhu, Y. (2015). Rising temperatures reduce global wheat production. Nature Climate Change, 5(2), 143–147. https://doi.org/10.1038/nclimate2470

Ausin, I., Alonso-Blanco, C., & Martinez-Zapater, J.-M. (2005). Environmental regulation of flowering. The International Journal of Developmental Biology, 49(5–6), 689–705. https://doi.org/10.1387/ijdb.052022ia

Bangerth, F. K., Song, J., & Streif, J. (2012). Physiological Impacts of Fruit Ripening and Storage Conditions on Aroma Volatile Formation in Apple and Strawberry Fruit: A Review. HortScience, 47(1), 4–10. https://doi.org/10.21273/HORTSCI.47.1.4

Bay, R. A., Harrigan, R. J., Underwood, V. L., Gibbs, H. L., Smith, T. B., & Ruegg, K. (2018). Genomic signals of selection predict climate-driven population declines in a migratory bird. Science, 359(6371), 83–86. https://doi.org/10.1126/science.aan4380

Beauchemin, K. A., Ungerfeld, E. M., Eckard, R. J., & Wang, M. (2020). Review: Fifty years of research on rumen methanogenesis: lessons learned and future challenges for mitigation. Animal, 14, s2–s16. https://doi.org/10.1017/S1751731119003100

Bell-Pedersen, D., Cassone, V. M., Earnest, D. J., Golden, S. S., Hardin, P. E., Thomas, T. L., & Zoran, M. J. (2005). Circadian rhythms from multiple oscillators: Lessons from diverse organisms. Nature Reviews Genetics, 6(7), 544–556. https://doi.org/10.1038/nrg1633

Benkemoun, L., & Saupe, S. J. (2006). Prion proteins as genetic material in fungi. Fungal Genetics and Biology, 43(12), 789–803. https://doi.org/10.1016/j.fgb.2006.06.006

Bradley St Clair, J., & Howe, G. T. (2007). Genetic maladaptation of coastal Douglas-fir seedlings to future climates. Global Change Biology, 13(7), 1441–1454. https://doi.org/10.1111/j.1365-2486.2007.01385.x

Brandoli, C., Petri, C., Egea-Cortines, M., & Weiss, J. (2020). Gigantea: Uncovering New Functions in Flower Development. Genes, 11(10), 1142. https://doi.org/10.3390/genes11101142

Cameron, M. A., Barnard, A. R., & Lucas, R. J. (2008). The electroretinogram as a method for studying circadian rhythms in the mammalian retina. Journal of Genetics, 87(5), 459–466. https://doi.org/10.1007/s12041-008-0068-5

Cano-Ramirez, D. L., Carmona-Salazar, L., Morales-Cedillo, F., Ramírez-Salcedo, J., Cahoon, E. B., & Gavilanes-Ruíz, M. (2021). Plasma Membrane Fluidity: An Environment Thermal Detector in Plants. Cells, 10(10), 2778. https://doi.org/10.3390/cells10102778

Capblancq, T., Fitzpatrick, M. C., Bay, R. A., Exposito-Alonso, M., & Keller, S. R. (2020). Genomic Prediction of (Mal)Adaptation Across Current and Future Climatic Landscapes. Annual Review of Ecology, Evolution, and Systematics, 51(Volume 51, 2020), 245–269. https://doi.org/10.1146/annurev-ecolsys-020720-042553

Carpaneto, A., Ivashikina, N., Levchenko, V., Krol, E., Jeworutzki, E., Zhu, J.-K., & Hedrich, R. (2007). Cold Transiently Activates Calcium-Permeable Channels in Arabidopsis Mesophyll Cells. Plant Physiology, 143(1), 487–494. https://doi.org/10.1104/pp.106.090928

Casal, J. J., & Balasubramanian, S. (2019). Thermomorphogenesis. Annual Review of Plant Biology, 70(Volume 70, 2019), 321–346. https://doi.org/10.1146/annurev-arplant-050718-095919

Catford, J. A., & Jones, L. P. (2019). Grassland invasion in a changing climate. In D. J. Gibson & J. A. Newman (Eds.), Grasslands and Climate Change (1st ed., pp. 149–171). Cambridge University Press. https://doi.org/10.1017/9781108163941.011

Chakrabortee, S., Kayatekin, C., Newby, G. A., Mendillo, M. L., Lancaster, A., & Lindquist, S. (2016). Luminidependens (LD) is an Arabidopsis protein with prion behavior. Proceedings of the National Academy of Sciences, 113(21), 6065–6070. https://doi.org/10.1073/pnas.1604478113

Chinnusamy, V., Zhu, J., & Zhu, J.-K. (2007). Cold stress regulation of gene expression in plants. Trends in Plant Science, 12(10), 444–451. https://doi.org/10.1016/j.tplants.2007.07.002

Choi, K., Kim, J., Hwang, H.-J., Kim, S., Park, C., Kim, S. Y., & Lee, I. (2011). The FRIGIDA complex activates transcription of FLC, a strong flowering repressor in Arabidopsis, by recruiting chromatin modification factors. The Plant Cell, 23(1), 289–303. https://doi.org/10.1105/tpc.110.075911

Choler, P. (2015). Growth response of temperate mountain grasslands to inter-annual variations in snow cover duration. Biogeosciences, 12(12), 3885–3897. https://doi.org/10.5194/bg-12-3885-2015

Chung, B. Y. W., Balcerowicz, M., Di Antonio, M., Jaeger, K. E., Geng, F., Franaszek, K., Marriott, P., Brierley, I., Firth, A. E., & Wigge, P. A. (2020). An RNA thermoswitch regulates daytime growth in Arabidopsis. Nature Plants, 6(5), 522–532. https://doi.org/10.1038/s41477-020-0633-3

Clem, K. R., Fogt, R. L., Turner, J., Lintner, B. R., Marshall, G. J., Miller, J. R., & Renwick, J. A. (2020). Record warming at the South Pole during the past three decades. Nature Climate Change, 10(8), 762–770. https://doi.org/10.1038/s41558-020-0815-z

CO2 Emissions in 2022. (2023). IEA. https://www.iea.org/reports/co2-emissions-in-2022

Cortese, M. S., Uversky, V. N., & Dunker, A. K. (2008). Intrinsic disorder in scaffold proteins: Getting more from less. Progress in Biophysics and Molecular Biology, 98(1), 85–106. https://doi.org/10.1016/j.pbiomolbio.2008.05.007

Cortijo, S., Charoensawan, V., Brestovitsky, A., Buning, R., Ravarani, C., Rhodes, D., Noort, J. van, Jaeger, K. E., & Wigge, P. A. (2017). Transcriptional Regulation of the Ambient Temperature Response by H2A.Z Nucleosomes and HSF1 Transcription Factors in Arabidopsis. Molecular Plant, 10(10), 1258–1273. https://doi.org/10.1016/j.molp.2017.08.014

Dai, A. (2013). Increasing drought under global warming in observations and models. Nature Climate Change, 3(1), 52–58. https://doi.org/10.1038/nclimate1633

Daniel, R. M., Danson, M. J., Eisenthal, R., Lee, C. K., & Peterson, M. E. (2008). The effect of temperature on enzyme activity: New insights and their implications. Extremophiles, 12(1), 51–59. https://doi.org/10.1007/s00792-007-0089-7

del Olmo, I., Poza-Viejo, L., Piñeiro, M., Jarillo, J. A., & Crevillén, P. (2019). High ambient temperature leads to reduced expression and delayed flowering in Brassica rapa via a mechanism associated with H2A.Z dynamics. The Plant Journal, 100(2), 343–356. https://doi.org/10.1111/tpj.14446

Delker, C., Quint, M., & Wigge, P. A. (2022). Recent advances in understanding thermomorphogenesis signaling. Current Opinion in Plant Biology, 68, 102231. https://doi.org/10.1016/j.pbi.2022.102231

Devi, P., Awasthi, R., Jha, U., Sharma, K. D., Prasad, P. V. V., Siddique, K. H. M., Roorkiwal, M., & Nayyar, H. (2023). Understanding the effect of heat stress during seed filling on nutritional composition and seed yield in chickpea (Cicer arietinum L.). Scientific Reports, 13(1), 15450. https://doi.org/10.1038/s41598-023-42586-0

Dodd, A. N., Belbin, F. E., Frank, A., & Webb, A. A. R. (2015). Interactions between circadian clocks and photosynthesis for the temporal and spatial coordination of metabolism. Frontiers in Plant Science, 6. https://doi.org/10.3389/fpls.2015.00245

Dong, M. A., Farré, E. M., & Thomashow, M. F. (2011). CIRCADIAN CLOCK-ASSOCIATED 1 and LATE ELONGATED HYPOCOTYL regulate expression of the C-REPEAT BINDING FACTOR (CBF) pathway in Arabidopsis. Proceedings of the National Academy of Sciences, 108(17), 7241–7246. https://doi.org/10.1073/pnas.1103741108

Dunker, A. K., Cortese, M. S., Romero, P., Iakoucheva, L. M., & Uversky, V. N. (2005). Flexible nets: The roles of intrinsic disorder in protein interaction networks. The FEBS Journal, 272(20), 5129–5148. https://doi.org/10.1111/j.1742-4658.2005.04948.x

Dunlap, J. C. (1999). Molecular Bases for Circadian Clocks. Cell, 96(2), 271–290. https://doi.org/10.1016/S0092-8674(00)80566-8

Eckel-Mahan, K. L., & Storm, D. R. (2009). Circadian rhythms and memory: Not so simple as cogs and gears. EMBO Reports, 10(6), 584–591. https://doi.org/10.1038/embor.2009.123

Eljebbawi, A., Hutin, S., Zubieta, C., & Stahl, Y. (2024). Environmental signals driving liquid-liquid phase separation – a molecular memory in plants? Frontiers in Plant Science, 15, 1391043. https://doi.org/10.3389/fpls.2024.1391043

Exposito-Alonso, M., Burbano, H. A., Bossdorf, O., Nielsen, R., Weigel, D., & Weigel, D. (2019). Natural selection on the Arabidopsis thaliana genome in present and future climates. Nature, 573(7772), 126–129. https://doi.org/10.1038/s41586-019-1520-9

Ezer, D., Jung, J.-H., Lan, H., Biswas, S., Gregoire, L., Box, M. S., Charoensawan, V., Cortijo, S., Lai, X., Stöckle, D., Zubieta, C., Jaeger, K. E., & Wigge, P. A. (2017). The evening complex coordinates environmental and endogenous signals in Arabidopsis. Nature Plants, 3, 17087. https://doi.org/10.1038/nplants.2017.87

Faivre, L., Kinscher, N.-F., Kuhlmann, A. B., Xu, X., Kaufmann, K., & Schubert, D. (2024). Cold stress induces rapid gene-specific changes in the levels of H3K4me3 and H3K27me3 in Arabidopsis thaliana. Frontiers in Plant Science, 15, 1390144. https://doi.org/10.3389/fpls.2024.1390144

Farré, E. M., Harmer, S. L., Harmon, F. G., Yanovsky, M. J., & Kay, S. A. (2005). Overlapping and Distinct Roles of PRR7 and PRR9 in the Arabidopsis Circadian Clock. Current Biology, 15(1), 47–54. https://doi.org/10.1016/j.cub.2004.12.067

Fowler, S. G., Cook, D., & Thomashow, M. F. (2005). Low Temperature Induction of Arabidopsis CBF1 , 2 , and 3 Is Gated by the Circadian Clock. Plant Physiology, 137(3), 961–968. https://doi.org/10.1104/pp.104.058354

Frachon, L., Bartoli, C., Carrère, S., Bouchez, O., Chaubet, A., Gautier, M., Roby, D., & Roux, F. (2018). A Genomic Map of Climate Adaptation in Arabidopsis thaliana at a Micro-Geographic Scale. Frontiers in Plant Science, 9, 967. https://doi.org/10.3389/fpls.2018.00967

Franklin, K. A., Praekelt, U., Stoddart, W. M., Billingham, O. E., Halliday, K. J., & Whitelam, G. C. (2003). Phytochromes B, D, and E act redundantly to control multiple physiological responses in Arabidopsis. Plant Physiology, 131(3), 1340–1346. https://doi.org/10.1104/pp.102.015487

Galea, C. A., Wang, Y., Sivakolundu, S. G., & Kriwacki, R. W. (2008). Regulation of Cell Division by

Intrinsically Unstructured Proteins: Intrinsic Flexibility, Modularity, and Signaling Conduits. Biochemistry, 47(29), 7598–7609. https://doi.org/10.1021/bi8006803

Garai, S., Citu, Singla-Pareek, S. L., Sopory, S. K., Kaur, C., & Yadav, G. (2021). Complex Networks of Prion-Like Proteins Reveal Cross Talk Between Stress and Memory Pathways in Plants. Frontiers in Plant Science, 12. https://doi.org/10.3389/fpls.2021.707286

Gendron, J. M., Pruneda-Paz, J. L., Doherty, C. J., Gross, A. M., Kang, S. E., & Kay, S. A. (2012). Arabidopsis circadian clock protein, TOC1, is a DNA-binding transcription factor. Proceedings of the National Academy of Sciences, 109(8), 3167–3172. https://doi.org/10.1073/pnas.1200355109

Gérard, M., Vanderplanck, M., Wood, T., & Michez, D. (2020). Global warming and plant–pollinator mismatches. Emerging Topics in Life Sciences, 4(1), 77–86. https://doi.org/10.1042/ETLS20190139

Gil, K., & Park, C. (2019). Thermal adaptation and plasticity of the plant circadian clock. New Phytologist, 221(3), 1215–1229. https://doi.org/10.1111/nph.15518

Green, C. B., Takahashi, J. S., & Bass, J. (2008). The Meter of Metabolism. Cell, 134(5), 728–742. https://doi.org/10.1016/j.cell.2008.08.022

Groot, M. P., Kubisch, A., Ouborg, N. J., Pagel, J., Schmid, K. J., Vergeer, P., & Lampei, C. (2017). Transgenerational effects of mild heat in Arabidopsis thaliana show strong genotype specificity that is explained by climate at origin. New Phytologist, 215(3), 1221–1234. https://doi.org/10.1111/nph.14642

Guihur, A., Rebeaud, M. E., Bourgine, B., & Goloubinoff, P. (2022). How do humans and plants feel the heat? Trends in Plant Science, 27(7), 630–632. https://doi.org/10.1016/j.tplants.2022.03.006

Guilioni, L., Wery, J., & Tardieu, F. (1997). Heat Stress-induced Abortion of Buds and Flowers in Pea: Is Sensitivity Linked to Organ Age or to Relations between Reproductive Organs? Annals of Botany, 80(2), 159–168. https://doi.org/10.1006/anbo.1997.0425

Ha, J.-H., Lee, H.-J., Jung, J.-H., & Park, C.-M. (2017). Thermo-Induced Maintenance of Photo-oxidoreductases Underlies Plant Autotrophic Development. Developmental Cell, 41(2), 170-179.e4. https://doi.org/10.1016/j.devcel.2017.03.005

Hahn, A., Bublak, D., Schleiff, E., & Scharf, K.-D. (2011). Crosstalk between Hsp90 and Hsp70 chaperones and heat stress transcription factors in tomato. The Plant Cell, 23(2), 741–755. https://doi.org/10.1105/tpc.110.076018

Haider, S., Iqbal, J., Naseer, S., Yaseen, T., Shaukat, M., Bibi, H., Ahmad, Y., Daud, H., Abbasi, N. L., & Mahmood, T. (2021). Molecular mechanisms of plant tolerance to heat stress: Current landscape and future perspectives. Plant Cell Reports, 40(12), 2247–2271. https://doi.org/10.1007/s00299-021-02696-3

Hancock, A. M., Brachi, B., Faure, N., Horton, M. W., Jarymowycz, L. B., Sperone, F. G., Toomajian, C., Roux, F., & Bergelson, J. (2011). Adaptation to Climate Across the Arabidopsis thaliana Genome. Science, 334(6052), 83–86. https://doi.org/10.1126/science.1209244

He, G.-H., Xu, J.-Y., Wang, Y.-X., Liu, J.-M., Li, P.-S., Chen, M., Ma, Y.-Z., & Xu, Z.-S. (2016). Drought-responsive WRKY transcription factor genes TaWRKY1 and TaWRKY33 from wheat confer

drought and/or heat resistance in Arabidopsis. BMC Plant Biology, 16(1), 116. https://doi.org/10.1186/s12870-016-0806-4

He, L., Asseng, S., Zhao, G., Wu, D., Yang, X., Zhuang, W., Jin, N., & Yu, Q. (2015). Impacts of recent climate warming, cultivar changes, and crop management on winter wheat phenology across the Loess Plateau of China. Agricultural and Forest Meteorology, 200, 135–143. https://doi.org/10.1016/j.agrformet.2014.09.011

Hu, Z., Song, N., Zheng, M., Liu, X., Liu, Z., Xing, J., Ma, J., Guo, W., Yao, Y., Peng, H., Xin, M., Zhou, D., Ni, Z., & Sun, Q. (2015). Histone acetyltransferase GCN 5 is essential for heat stress-responsive gene activation and thermotolerance in Arabidopsis. The Plant Journal, 84(6), 1178–1191. https://doi.org/10.1111/tpj.13076

Huang, H., Alvarez, S., Bindbeutel, R., Shen, Z., Naldrett, M. J., Evans, B. S., Briggs, S. P., Hicks, L. M., Kay, S. A., & Nusinow, D. A. (2016). Identification of Evening Complex Associated Proteins in Arabidopsis by Affinity Purification and Mass Spectrometry. Molecular & Cellular Proteomics : MCP, 15(1), 201–217. https://doi.org/10.1074/mcp.M115.054064

Hubbard, K. E., & Webb, A. A. R. (2015). Circadian Rhythms in Stomata: Physiological and Molecular Aspects. In S. Mancuso & S. Shabala (Eds.), Rhythms in Plants (pp. 231–255). Springer International Publishing. https://doi.org/10.1007/978-3-319-20517-5_9

Hutin, S., Kumita, J. R., Strotmann, V. I., Dolata, A., Ling, W. L., Louafi, N., Popov, A., Milhiet, P.-E., Blackledge, M., Nanao, M. H., Wigge, P. A., Stahl, Y., Costa, L., Tully, M. D., & Zubieta, C. (2023). Phase separation and molecular ordering of the prion-like domain of the Arabidopsis thermosensory protein EARLY FLOWERING 3. Proceedings of the National Academy of Sciences, 120(28), e2304714120. https://doi.org/10.1073/pnas.2304714120

Hutin, S., Wigge, P. A., & Zubieta, C. (2024). In Vitro Determination of Temperature-Dependent DNA Binding of the Evening Complex Using Electrophoretic Mobility Shift Assays. In M. Chen (Ed.), Thermomorphogenesis: Methods and Protocols (pp. 135–147). Springer US. https://doi.org/10.1007/978-1-0716-3814-9_14

Iakoucheva, L. M., Brown, C. J., Lawson, J. D., Obradović, Z., & Dunker, A. K. (2002). Intrinsic Disorder in Cell-signaling and Cancer-associated Proteins. Journal of Molecular Biology, 323(3), 573–584. https://doi.org/10.1016/S0022-2836(02)00969-5

Jeon, J., & Kim, J. (2013). Arabidopsis Response Regulator1 and Arabidopsis Histidine Phosphotransfer Protein2 (AHP2), AHP3, and AHP5 Function in Cold Signaling1[W][OA]. Plant Physiology, 161(1), 408–424. https://doi.org/10.1104/pp.112.207621

Jeon, J., Kim, N. Y., Kim, S., Kang, N. Y., Novák, O., Ku, S.-J., Cho, C., Lee, D. J., Lee, E.-J., Strnad, M., & Kim, J. (2010). A Subset of Cytokinin Two-component Signaling System Plays a Role in Cold Temperature Stress Response in Arabidopsis*. Journal of Biological Chemistry, 285(30), 23371–23386. https://doi.org/10.1074/jbc.M109.096644

Jiang, W., Zhou, H., Bi, H., Fromm, M., Yang, B., & Weeks, D. P. (2013). Demonstration of CRISPR/Cas9/sgRNA-mediated targeted gene modification in Arabidopsis, tobacco, sorghum and rice. Nucleic Acids Research, 41(20), e188–e188. https://doi.org/10.1093/nar/gkt780

Johanson, U., West, J., Lister, C., Michaels, S., Amasino, R., & Dean, C. (2000). Molecular analysis of FRIGIDA, a major determinant of natural variation in Arabidopsis flowering time. Science (New

York, N.Y.), 290(5490), 344–347. https://doi.org/10.1126/science.290.5490.344

Jung, H.-S., Crisp, P. A., Estavillo, G. M., Cole, B., Hong, F., Mockler, T. C., Pogson, B. J., & Chory, J. (2013). Subset of heat-shock transcription factors required for the early response of Arabidopsis to excess light. Proceedings of the National Academy of Sciences of the United States of America, 110(35), 14474–14479.

Jung, J.-H., Barbosa, A. D., Hutin, S., Kumita, J. R., Gao, M., Derwort, D., Silva, C. S., Lai, X., Pierre, E., Geng, F., Kim, S.-B., Baek, S., Zubieta, C., Jaeger, K. E., & Wigge, P. A. (2020a). A prion-like domain in ELF3 functions as a thermosensor in Arabidopsis. Nature, 585(7824), 256–260. https://doi.org/10.1038/s41586-020-2644-7

Jung, J.-H., Domijan, M., Klose, C., Biswas, S., Ezer, D., Gao, M., Khattak, A. K., Box, M. S., Charoensawan, V., Cortijo, S., Kumar, M., Grant, A., Locke, J. C. W., Schäfer, E., Jaeger, K. E., & Wigge, P. A. (2016). Phytochromes function as thermosensors in Arabidopsis. Science (New York, N.Y.), 354(6314), 886–889. https://doi.org/10.1126/science.aaf6005

Jurca, M., Sjölander, J., Ibáñez, C., Matrosova, A., Johansson, M., Kozarewa, I., Takata, N., Bakó, L., Webb, A. A. R., Israelsson-Nordström, M., & Eriksson, M. E. (2022). ZEITLUPE Promotes ABA-Induced Stomatal Closure in Arabidopsis and Populus. Frontiers in Plant Science, 13, 829121. https://doi.org/10.3389/fpls.2022.829121

Juurakko, C. L., diCenzo, G. C., & Walker, V. K. (2021). Cold acclimation and prospects for cold-resilient crops. Plant Stress, 2, 100028. https://doi.org/10.1016/j.stress.2021.100028

Kampinga, H. H., & Craig, E. A. (2010). The HSP70 chaperone machinery: J proteins as drivers of functional specificity. Nature Reviews. Molecular Cell Biology, 11(8), 579–592. https://doi.org/10.1038/nrm2941

Kanzaki, H., Saitoh, H., Ito, A., Fujisawa, S., Kamoun, S., Katou, S., Yoshioka, H., & Terauchi, R. (2003). Cytosolic HSP90 and HSP70 are essential components of INF1-mediated hypersensitive response and non-host resistance to Pseudomonas cichorii in Nicotiana benthamiana. Molecular Plant Pathology, 4(5), 383–391. https://doi.org/10.1046/j.1364-3703.2003.00186.x

Karavolias, N. G., Horner, W., Abugu, M. N., & Evanega, S. N. (2021). Application of Gene Editing for Climate Change in Agriculture. Frontiers in Sustainable Food Systems, 5, 685801. https://doi.org/10.3389/fsufs.2021.685801

Kiba, T., Henriques, R., Sakakibara, H., & Chua, N.-H. (2007). Targeted Degradation of PSEUDO-RESPONSE REGULATOR5 by an SCF ZTL Complex Regulates Clock Function and Photomorphogenesis in Arabidopsis thaliana. The Plant Cell, 19(8), 2516–2530. https://doi.org/10.1105/tpc.107.053033

Kim, P. M., Sboner, A., Xia, Y., & Gerstein, M. (2008). The role of disorder in interaction networks: A structural analysis. Molecular Systems Biology, 4(1), 179. https://doi.org/10.1038/msb.2008.16

Kim, W.-Y., Fujiwara, S., Suh, S.-S., Kim, J., Kim, Y., Han, L., David, K., Putterill, J., Nam, H. G., & Somers, D. E. (2007). ZEITLUPE is a circadian photoreceptor stabilized by GIGANTEA in blue light. Nature, 449(7160), 356–360. https://doi.org/10.1038/nature06132

Klose, C., Nagy, F., & Schäfer, E. (2020). Thermal Reversion of Plant Phytochromes. Molecular Plant, 13(3), 386–397. https://doi.org/10.1016/j.molp.2019.12.004

Koornneef, M., & Meinke, D. (2010). The development of Arabidopsis as a model plant. The Plant Journal, 61(6), 909–921. https://doi.org/10.1111/j.1365-313X.2009.04086.x

Korner, C. (2012). Alpine treelines. Springer.

Körner, C. (2019). Mountain Biodiversity, its Causes and Function: An Overview. In Ch. Körner & E. M. Spehn (Eds.), Mountain Biodiversity (1st ed., pp. 3–20). Routledge. https://doi.org/10.4324/9780429342585-1

Kumar, S. V. (2018). H2A.Z at the Core of Transcriptional Regulation in Plants. Molecular Plant, 11(9), 1112–1114. https://doi.org/10.1016/j.molp.2018.07.002

Kumar, S. V., & Wigge, P. A. (2010). H2A.Z-Containing Nucleosomes Mediate the Thermosensory Response in Arabidopsis. Cell, 140(1), 136–147. https://doi.org/10.1016/j.cell.2009.11.006

Lämke, J., & Bäurle, I. (2017). Epigenetic and chromatin-based mechanisms in environmental stress adaptation and stress memory in plants. Genome Biology, 18(1), 124. https://doi.org/10.1186/s13059-017-1263-6

Lancaster, A. K., Nutter-Upham, A., Lindquist, S., & King, O. D. (2014). PLAAC: A web and command-line application to identify proteins with prion-like amino acid composition. Bioinformatics, 30(17), 2501–2502. https://doi.org/10.1093/bioinformatics/btu310

Lasky, J. R., Des Marais, D. L., McKAY, J. K., Richards, J. H., Juenger, T. E., & Keitt, T. H. (2012). Characterizing genomic variation of Arabidopsis thaliana: The roles of geography and climate: GEOGRAPHY, CLIMATE AND ARABIDOPSIS GENOMICS. Molecular Ecology, 21(22), 5512–5529. https://doi.org/10.1111/j.1365-294X.2012.05709.x

Lassey, K. R. (2007). Livestock methane emission: From the individual grazing animal through national inventories to the global methane cycle. Agricultural and Forest Meteorology, 142(2–4), 120–132. https://doi.org/10.1016/j.agrformet.2006.03.028

Lawrence, D., Coe, M., Walker, W., Verchot, L., & Vandecar, K. (2022). The Unseen Effects of Deforestation: Biophysical Effects on Climate. Frontiers in Forests and Global Change, 5, 756115. https://doi.org/10.3389/ffgc.2022.756115

Ledley, T. S., Sundquist, E. T., Schwartz, S. E., Hall, D. K., Fellows, J. D., & Killeen, T. L. (1999). Climate change and greenhouse gases. Eos, Transactions American Geophysical Union, 80(39), 453–458. https://doi.org/10.1029/99EO00325

Lee, J. H., Hübel, A., & Schöffl, F. (1995). Derepression of the activity of genetically engineered heat shock factor causes constitutive synthesis of heat shock proteins and increased thermotolerance in transgenic Arabidopsis. The Plant Journal: For Cell and Molecular Biology, 8(4), 603–612. https://doi.org/10.1046/j.1365-313x.1995.8040603.x

Lee, S., Zhu, L., & Huq, E. (2021). An autoregulatory negative feedback loop controls thermomorphogenesis in Arabidopsis. PLOS Genetics, 17(6), e1009595. https://doi.org/10.1371/journal.pgen.1009595

Legris, M., Klose, C., Burgie, E. S., Rojas, C. C. R., Neme, M., Hiltbrunner, A., Wigge, P. A., Schäfer, E., Vierstra, R. D., & Casal, J. J. (2016). Phytochrome B integrates light and temperature signals in

Arabidopsis. Science (New York, N.Y.), 354(6314), 897–900. https://doi.org/10.1126/science.aaf5656

Li, M., Berendzen, K. W., & Schöffl, F. (2010). Promoter specificity and interactions between early and late Arabidopsis heat shock factors. Plant Molecular Biology, 73(4–5), 559–567. https://doi.org/10.1007/s11103-010-9643-2

Lippmann, R., Babben, S., Menger, A., Delker, C., & Quint, M. (2019). Development of Wild and Cultivated Plants under Global Warming Conditions. Current Biology, 29(24), R1326–R1338. https://doi.org/10.1016/j.cub.2019.10.016

Lohani, N., Singh, M. B., & Bhalla, P. L. (2022). Short-term heat stress during flowering results in a decline in Canola seed productivity. Journal of Agronomy and Crop Science, 208(4), 486–496. https://doi.org/10.1111/jac.12534

Los, D. A., & Murata, N. (2004). Membrane fluidity and its roles in the perception of environmental signals. Biochimica et Biophysica Acta (BBA) - Biomembranes, 1666(1–2), 142–157. https://doi.org/10.1016/j.bbamem.2004.08.002

Lu, S. X., Knowles, S. M., Andronis, C., Ong, M. S., & Tobin, E. M. (2009). CIRCADIAN CLOCK ASSOCIATED1 and LATE ELONGATED HYPOCOTYL Function Synergistically in the Circadian Clock of Arabidopsis. Plant Physiology, 150(2), 834–843. https://doi.org/10.1104/pp.108.133272

Luo, M., Liu, X., Singh, P., Cui, Y., Zimmerli, L., & Wu, K. (2012). Chromatin modifications and remodeling in plant abiotic stress responses. Biochimica et Biophysica Acta (BBA) - Gene Regulatory Mechanisms, 1819(2), 129–136. https://doi.org/10.1016/j.bbagrm.2011.06.008

Ma, L., Li, X., Zhao, Z., Hao, Y., Shang, R., Zeng, D., & Liu, H. (2021). Light-Response Bric-A-Brack/Tramtrack/Broad proteins mediate cryptochrome 2 degradation in response to low ambient temperature. The Plant Cell, 33(12), 3610–3620. https://doi.org/10.1093/plcell/koab219

Malinovska, L., Palm, S., Gibson, K., Verbavatz, J.-M., & Alberti, S. (2015). Dictyostelium discoideum has a highly Q/N-rich proteome and shows an unusual resilience to protein aggregation. Proceedings of the National Academy of Sciences, 112(20), E2620–E2629. https://doi.org/10.1073/pnas.1504459112

Martinière, A., Shvedunova, M., Thomson, A. J. W., Evans, N. H., Penfield, S., Runions, J., & McWatters, H. G. (2011). Homeostasis of plasma membrane viscosity in fluctuating temperatures. New Phytologist, 192(2), 328–337. https://doi.org/10.1111/j.1469-8137.2011.03821.x

Martz, F., Sutinen, M.-L., Kiviniemi, S., & Palta, J. P. (2006). Changes in freezing tolerance, plasma membrane H+-ATPase activity and fatty acid composition in Pinus resinosa needles during cold acclimation and de-acclimation. Tree Physiology, 26(6), 783–790. https://doi.org/10.1093/treephys/26.6.783

Más, P., Kim, W.-Y., Somers, D. E., & Kay, S. A. (2003). Targeted degradation of TOC1 by ZTL modulates circadian function in Arabidopsis thaliana. Nature, 426(6966), 567–570. https://doi.org/10.1038/nature02163

McClung, C. R. (2006). Plant Circadian Rhythms. The Plant Cell, 18(4), 792–803. https://doi.org/10.1105/tpc.106.040980

Meinke, D., & Scholl, R. (2003). The Preservation of Plant Genetic Resources. Experiences with Arabidopsis. Plant Physiology, 133(3), 1046–1050. https://doi.org/10.1104/pp.103.024877

Midmore, D. J., Cartwright, P. M., & Fischer, R. A. (1982). Wheat in tropical environments. I. Phasic development and spike size. Field Crops Research, 5, 185–200. https://doi.org/10.1016/0378-4290(82)90022-3

Mitchell, J. F. B. (1989). The "Greenhouse" effect and climate change. Reviews of Geophysics, 27(1), 115–139. https://doi.org/10.1029/RG027i001p00115

Möhl, P., Von Büren, R. S., & Hiltbrunner, E. (2022). Growth of alpine grassland will start and stop earlier under climate warming. Nature Communications, 13(1), 7398. https://doi.org/10.1038/s41467-022-35194-5

Nagel, D. H., & Kay, S. A. (2012). Complexity in the Wiring and Regulation of Plant Circadian Networks. Current Biology, 22(16), R648–R657. https://doi.org/10.1016/j.cub.2012.07.025

Nakamichi, N., Kiba, T., Henriques, R., Mizuno, T., Chua, N.-H., & Sakakibara, H. (2010). PSEUDO-RESPONSE REGULATORS 9, 7, and 5 Are Transcriptional Repressors in the Arabidopsis Circadian Clock. The Plant Cell, 22(3), 594–605. https://doi.org/10.1105/tpc.109.072892

Nakamichi, N., Kita, M., Ito, S., Yamashino, T., & Mizuno, T. (2005). PSEUDO-RESPONSE REGULATORS, PRR9, PRR7 and PRR5, Together Play Essential Roles Close to the Circadian Clock of Arabidopsis thaliana. Plant and Cell Physiology, 46(5), 686–698. https://doi.org/10.1093/pcp/pci086

Ndudzo, A., Sibanda Makuvise, A., Moyo, S., & Bobo, E. D. (2024). CRISPR-Cas9 genome editing in crop breeding for climate change resilience: Implications for smallholder farmers in Africa. Journal of Agriculture and Food Research, 16, 101132. https://doi.org/10.1016/j.jafr.2024.101132

Nieto, C., López-Salmerón, V., Davière, J.-M., & Prat, S. (2015). ELF3-PIF4 Interaction Regulates Plant Growth Independently of the Evening Complex. Current Biology, 25(2), 187–193. https://doi.org/10.1016/j.cub.2014.10.070

Niu, Y., & Xiang, Y. (2018). An Overview of Biomembrane Functions in Plant Responses to High-Temperature Stress. Frontiers in Plant Science, 9, 915. https://doi.org/10.3389/fpls.2018.00915

Nover, L., Bharti, K., Döring, P., Mishra, S. K., Ganguli, A., & Scharf, K. D. (2001). Arabidopsis and the heat stress transcription factor world: How many heat stress transcription factors do we need? Cell Stress & Chaperones, 6(3), 177–189. https://doi.org/10.1379/1466-1268(2001)006<0177:aathst>2.0.co;2

Pareek, A., Khurana, A., Sharma, A. K., & Kumar, R. (2017). An Overview of Signaling Regulons During Cold Stress Tolerance in Plants. Current Genomics, 18(6). https://doi.org/10.2174/1389202918666170228141345

Park, C.-J., Bart, R., Chern, M., Canlas, P. E., Bai, W., & Ronald, P. C. (2010). Overexpression of the endoplasmic reticulum chaperone BiP3 regulates XA21-mediated innate immunity in rice. PloS One, 5(2), e9262. https://doi.org/10.1371/journal.pone.0009262

Paulsen, J., & Körner, C. (2014). A climate-based model to predict potential treeline position around the globe. Alpine Botany, 124(1), 1–12. https://doi.org/10.1007/s00035-014-0124-0

Piskurewicz, U., Sentandreu, M., Iwasaki, M., Glauser, G., & Lopez-Molina, L. (2023). The Arabidopsis endosperm is a temperature-sensing tissue that implements seed thermoinhibition through phyB. Nature Communications, 14(1), 1202. https://doi.org/10.1038/s41467-023-36903-4

Pokhilko, A., Hodge, S. K., Stratford, K., Knox, K., Edwards, K. D., Thomson, A. W., Mizuno, T., & Millar, A. J. (2010). Data assimilation constrains new connections and components in a complex, eukaryotic circadian clock model. Molecular Systems Biology, 6(1), 416. https://doi.org/10.1038/msb.2010.69

Ponnu, J., & Hoecker, U. (2022). Signaling Mechanisms by Arabidopsis Cryptochromes. Frontiers in Plant Science, 13. https://doi.org/10.3389/fpls.2022.844714

Posé, D., Verhage, L., Ott, F., Yant, L., Mathieu, J., Angenent, G. C., Immink, R. G. H., & Schmid, M. (2013). Temperature-dependent regulation of flowering by antagonistic FLM variants. Nature, 503(7476), 414–417. https://doi.org/10.1038/nature12633

Provart, N. J., Alonso, J., Assmann, S. M., Bergmann, D., Brady, S. M., Brkljacic, J., Browse, J., Chapple, C., Colot, V., Cutler, S., Dangl, J., Ehrhardt, D., Friesner, J. D., Frommer, W. B., Grotewold, E., Meyerowitz, E., Nemhauser, J., Nordborg, M., Pikaard, C., … McCourt, P. (2016). 50 years of Arabidopsis research: Highlights and future directions. New Phytologist, 209(3), 921–944. https://doi.org/10.1111/nph.13687

Pruneda-Paz, J. L., Breton, G., Para, A., & Kay, S. A. (2009). A Functional Genomics Approach Reveals CHE as a Component of the Arabidopsis Circadian Clock. Science, 323(5920), 1481–1485. https://doi.org/10.1126/science.1167206

Puhakainen, T., Pihakaski-Maunsbach, K., Widell, S., & Sommarin, M. (1999). Cold acclimation enhances the activity of plasma membrane Ca2+ ATPase in winter rye leaves. Plant Physiology and Biochemistry, 37(3), 231–239. https://doi.org/10.1016/S0981-9428(99)80038-2

Quint, M., Delker, C., Franklin, K. A., Wigge, P. A., Halliday, K. J., & van Zanten, M. (2016). Molecular and genetic control of plant thermomorphogenesis. Nature Plants, 2, 15190. https://doi.org/10.1038/nplants.2015.190

Rantanen, M., Karpechko, A. Y., Lipponen, A., Nordling, K., Hyvärinen, O., Ruosteenoja, K., Vihma, T., & Laaksonen, A. (2022). The Arctic has warmed nearly four times faster than the globe since 1979. Communications Earth & Environment, 3(1), 1–10. https://doi.org/10.1038/s43247-022-00498-3

Reiser, L., Berardini, T. Z., Li, D., Muller, R., Strait, E. M., Li, Q., Mezheritsky, Y., Vetushko, A., & Huala, E. (2016). Sustainable funding for biocuration: The Arabidopsis Information Resource (TAIR) as a case study of a subscription-based funding model. Database, 2016, baw018. https://doi.org/10.1093/database/baw018

Rellstab, C., Dauphin, B., & Exposito-Alonso, M. (2021). Prospects and limitations of genomic offset in conservation management. Evolutionary Applications, 14(5), 1202–1212. https://doi.org/10.1111/eva.13205

Saidi, Y., Finka, A., & Goloubinoff, P. (2011). Heat perception and signalling in plants: A tortuous path to thermotolerance. New Phytologist, 190(3), 556–565. https://doi.org/10.1111/j.1469-8137.2010.03571.x

Scheepens, J. F., Deng, Y., & Bossdorf, O. (2018). Phenotypic plasticity in response to temperature fluctuations is genetically variable, and relates to climatic variability of origin, in Arabidopsis thaliana. AoB PLANTS, 10(4). https://doi.org/10.1093/aobpla/ply043

Sehgal, A., Sita, K., Siddique, K. H. M., Kumar, R., Bhogireddy, S., Varshney, R. K., HanumanthaRao, B., Nair, R. M., Prasad, P. V. V., & Nayyar, H. (2018). Drought or/and Heat-Stress Effects on Seed Filling in Food Crops: Impacts on Functional Biochemistry, Seed Yields, and Nutritional Quality. Frontiers in Plant Science, 9, 1705. https://doi.org/10.3389/fpls.2018.01705

Seki, M. (2003). RIKEN Arabidopsis full-length (RAFL) cDNA and its applications for expression profiling under abiotic stress conditions. Journal of Experimental Botany, 55(395), 213–223. https://doi.org/10.1093/jxb/erh007

Seo, P. J., Kim, M. J., Park, J.-Y., Kim, S.-Y., Jeon, J., Lee, Y.-H., Kim, J., & Park, C.-M. (2010). Cold activation of a plasma membrane-tethered NAC transcription factor induces a pathogen resistance response in Arabidopsis. The Plant Journal, 61(4), 661–671. https://doi.org/10.1111/j.1365-313X.2009.04091.x

Seo, P. J., & Park, C.-M. (2010). A membrane-bound NAC transcription factor as an integrator of biotic and abiotic stress signals. Plant Signaling & Behavior, 5(5), 481–483. https://doi.org/10.4161/psb.11083

Shen, Y., Lei, T., Cui, X., Liu, X., Zhou, S., Zheng, Y., Guérard, F., Issakidis-Bourguet, E., & Zhou, D. (2019). Arabidopsis histone deacetylase HDA 15 directly represses plant response to elevated ambient temperature. The Plant Journal, 100(5), 991–1006. https://doi.org/10.1111/tpj.14492

Silva, C. S., Nayak, A., Lai, X., Hutin, S., Hugouvieux, V., Jung, J.-H., López-Vidriero, I., Franco-Zorrilla, J. M., Panigrahi, K. C. S., Nanao, M. H., Wigge, P. A., & Zubieta, C. (2020). Molecular mechanisms of Evening Complex activity in Arabidopsis. Proceedings of the National Academy of Sciences, 117(12), 6901–6909. https://doi.org/10.1073/pnas.1920972117

Snowdon, R. J., Wittkop, B., Chen, T.-W., & Stahl, A. (2021). Crop adaptation to climate change as a consequence of long-term breeding. Theoretical and Applied Genetics, 134(6), 1613–1623. https://doi.org/10.1007/s00122-020-03729-3

Sweere, U., Eichenberg, K., Lohrmann, J., Mira-Rodado, V., Bäurle, I., Kudla, J., Nagy, F., Schafer, E., & Harter, K. (2001). Interaction of the response regulator ARR4 with phytochrome B in modulating red light signaling. Science (New York, N.Y.), 294(5544), 1108–1111. https://doi.org/10.1126/science.1065022

Tabas-Madrid, D., Méndez-Vigo, B., Arteaga, N., Marcer, A., Pascual-Montano, A., Weigel, D., Xavier Picó, F., & Alonso-Blanco, C. (2018). Genome-wide signatures of flowering adaptation to climate temperature: Regional analyses in a highly diverse native range of Arabidopsis thaliana. Plant, Cell & Environment, 41(8), 1806–1820. https://doi.org/10.1111/pce.13189

Tajima, T., Oda, A., Nakagawa, M., Kamada, H., & Mizoguchi, T. (2007). Natural variation of polyglutamine repeats of a circadian clock gene ELF3 in Arabidopsis. Plant Biotechnology, 24(2), 237–240. https://doi.org/10.5511/plantbiotechnology.24.237

The World Meteorological Organization (WMO). (2024). State of the Global Climate 2023 (WMO-No. 1347; WMO-No. 1347, p. 53). The World Meteorological Organization (WMO). https://library.wmo.int/idurl/4/68835

Thépaut, J-N., H., H. (2023). ERA5 hourly data on single levels from 1940 to present. Copernicus Climate Change Service (C3S) Climate Data Store (CDS). 10.24381/cds.adbb2d47

Uversky, V. N. (2015). The multifaceted roles of intrinsic disorder in protein complexes. FEBS Letters, 589(19PartA), 2498–2506. https://doi.org/10.1016/j.febslet.2015.06.004

Vacca, R. A., De Pinto, M. C., Valenti, D., Passarella, S., Marra, E., & De Gara, L. (2004). Production of Reactive Oxygen Species, Alteration of Cytosolic Ascorbate Peroxidase, and Impairment of Mitochondrial Metabolism Are Early Events in Heat Shock-Induced Programmed Cell Death in Tobacco Bright-Yellow 2 Cells. Plant Physiology, 134(3), 1100–1112. https://doi.org/10.1104/pp.103.035956

Valladares, F., Matesanz, S., Guilhaumon, F., Araújo, M. B., Balaguer, L., Benito-Garzón, M., Cornwell, W., Gianoli, E., Van Kleunen, M., Naya, D. E., Nicotra, A. B., Poorter, H., & Zavala, M. A. (2014). The effects of phenotypic plasticity and local adaptation on forecasts of species range shifts under climate change. Ecology Letters, 17(11), 1351–1364. https://doi.org/10.1111/ele.12348

Van Der Lee, R., Buljan, M., Lang, B., Weatheritt, R. J., Daughdrill, G. W., Dunker, A. K., Fuxreiter, M., Gough, J., Gsponer, J., Jones, D. T., Kim, P. M., Kriwacki, R. W., Oldfield, C. J., Pappu, R. V., Tompa, P., Uversky, V. N., Wright, P. E., & Babu, M. M. (2014). Classification of Intrinsically Disordered Regions and Proteins. Chemical Reviews, 114(13), 6589–6631. https://doi.org/10.1021/cr400525m

Vidigal, D. S., Marques, A. C. S. S., Willems, L. A. J., Buijs, G., Méndez-Vigo, B., Hilhorst, H. W. M., Bentsink, L., Picó, F. X., & Alonso-Blanco, C. (2016). Altitudinal and climatic associations of seed dormancy and flowering traits evidence adaptation of annual life cycle timing in Arabidopsis thaliana. Plant, Cell & Environment, 39(8), 1737–1748. https://doi.org/10.1111/pce.12734

Vierling, E. (1991). The Roles of Heat Shock Proteins in Plants. Annual Review of Plant Physiology and Plant Molecular Biology, 42(1), 579–620. https://doi.org/10.1146/annurev.pp.42.060191.003051

Vogt, G. (2022). Environmental Adaptation of Genetically Uniform Organisms with the Help of Epigenetic Mechanisms—An Insightful Perspective on Ecoepigenetics. Epigenomes, 7(1), 1. https://doi.org/10.3390/epigenomes7010001

Vu, L. D., Gevaert, K., & De Smet, I. (2019). Feeling the Heat: Searching for Plant Thermosensors. Trends in Plant Science, 24(3), 210–219. https://doi.org/10.1016/j.tplants.2018.11.004

Wang, Z., Wang, T., Zhang, X., Wang, J., Yang, Y., Sun, Y., Guo, X., Wu, Q., Nepovimova, E., Watson, A. E., & Kuca, K. (2024). Biodiversity conservation in the context of climate change: Facing challenges and management strategies. Science of The Total Environment, 937, 173377. https://doi.org/10.1016/j.scitotenv.2024.173377

Weinl, S., & Kudla, J. (2009). The CBL–CIPK Ca 2+ -decoding signaling network: Function and perspectives. New Phytologist, 184(3), 517–528. https://doi.org/10.1111/j.1469-8137.2009.02938.x

Weiskopf, S. R., Rubenstein, M. A., Crozier, L. G., Gaichas, S., Griffis, R., Halofsky, J. E., Hyde, K. J. W., Morelli, T. L., Morisette, J. T., Muñoz, R. C., Pershing, A. J., Peterson, D. L., Poudel, R., Staudinger, M. D., Sutton-Grier, A. E., Thompson, L., Vose, J., Weltzin, J. F., & Whyte, K. P. (2020). Climate change effects on biodiversity, ecosystems, ecosystem services, and natural resource management in the United States. Science of The Total Environment, 733, 137782. https://doi.org/10.1016/j.scitotenv.2020.137782

Wilczek, A. M., Cooper, M. D., Korves, T. M., & Schmitt, J. (2014). Lagging adaptation to warming climate in Arabidopsis thaliana. Proceedings of the National Academy of Sciences, 111(22), 7906–7913. https://doi.org/10.1073/pnas.1406314111

Wunderlich, M., Werr, W., & Schöffl, F. (2003). Generation of dominant-negative effects on the heat shock response in Arabidopsis thaliana by transgenic expression of a chimaeric HSF1 protein fusion construct. The Plant Journal: For Cell and Molecular Biology, 35(4), 442–451. https://doi.org/10.1046/j.1365-313x.2003.01815.x

Yoshida, T., Ohama, N., Nakajima, J., Kidokoro, S., Mizoi, J., Nakashima, K., Maruyama, K., Kim, J.-M., Seki, M., Todaka, D., Osakabe, Y., Sakuma, Y., Schöffl, F., Shinozaki, K., & Yamaguchi-Shinozaki, K. (2011). Arabidopsis HsfA1 transcription factors function as the main positive regulators in heat shock-responsive gene expression. Molecular Genetics and Genomics: MGG, 286(5–6), 321–332. https://doi.org/10.1007/s00438-011-0647-7

Yuan, P., Yang, T., & Poovaiah, B. W. (2018). Calcium Signaling-Mediated Plant Response to Cold Stress. International Journal of Molecular Sciences, 19(12), 3896. https://doi.org/10.3390/ijms19123896

Zarka, D. G., Vogel, J. T., Cook, D., & Thomashow, M. F. (2003). Cold Induction of Arabidopsis CBF Genes Involves Multiple ICE (Inducer of CBF Expression) Promoter Elements and a Cold-Regulatory Circuit That Is Desensitized by Low Temperature. Plant Physiology, 133(2), 910–918. https://doi.org/10.1104/pp.103.027169

Zhang, L., Eggers-Schumacher, G., Schöffl, F., & Prändl, R. (2001). Analysis of heat-shock transcription factor-DNA binding in Arabidopsis suspension cultures by UV laser crosslinking. The Plant Journal: For Cell and Molecular Biology, 28(2), 217–223. https://doi.org/10.1046/j.1365-313x.2001.01137.x

Zhang, L.-L., Li, W., Tian, Y.-Y., Davis, S. J., & Liu, J.-X. (2021). The E3 ligase XBAT35 mediates thermoresponsive hypocotyl growth by targeting ELF3 for degradation in Arabidopsis. Journal of Integrative Plant Biology, 63(6), 1097–1103. https://doi.org/10.1111/jipb.13107

Zhang, L.-L., Zhu, Q.-Y., Sun, J.-L., Yao, Z.-W., Qing, T., Ma, H., & Liu, J.-X. (2024). XBAT31 regulates reproductive thermotolerance through controlling the accumulation of HSFB2a/B2b under heat stress conditions. Cell Reports, 43(6). https://doi.org/10.1016/j.celrep.2024.114349

Zhang, M., Dunshea, F. R., Warner, R. D., DiGiacomo, K., Osei-Amponsah, R., & Chauhan, S. S. (2020). Impacts of heat stress on meat quality and strategies for amelioration: A review. International Journal of Biometeorology, 64(9), 1613–1628. https://doi.org/10.1007/s00484-020-01929-6

Zhang, X., Henriques, R., Lin, S.-S., Niu, Q.-W., & Chua, N.-H. (2006). Agrobacterium-mediated transformation of Arabidopsis thaliana using the floral dip method. Nature Protocols, 1(2), 641–646. https://doi.org/10.1038/nprot.2006.97

Zhang, Z., Luo, X., Yang, Y., & He, Y. (2023). Cold induction of nuclear FRIGIDA condensation in Arabidopsis. Nature, 619(7969), E27–E32. https://doi.org/10.1038/s41586-023-06189-z

CHAPTER 2 Biochemical characterisation of ELF3

2.1. Introduction

ELF3 from *A. thaliana* is a crucial component of the circadian clock and plays roles in photoperiodic flowering regulation and temperature sensing (Ezer et al., 2017; Jung et al., 2020; Yu et al., 2008). ELF3, with its partners ELF4 and LUX forms the Evening Complex (EC), a key part of the circadian clock (Hsu & Harmer, 2014; Nusinow et al., 2011; Pokhilko et al., 2012). ELF3 also acts as a scaffold protein, binding to many other protein partners including kinases, photoreceptors and transcription factors (Huang et al., 2016; Yang et al., 2024; Yu et al., 2008). Due to its promiscuous interactome, ELF3 plays a significant role in mediating circadian clock activity, light responses and temperature-dependent growth (Huang et al., 2016; Zhao et al., 2021).

ELF3's lack of defined secondary and tertiary structure across large segments of its sequence classifies it as an intrinsically disordered protein (IDP) (Arai et al., 2015; Z. Peng et al., 2014). IDPs generally contain low-complexity regions, enriched in hydrophilic and "disorder-promoting" amino acids such as serine, glutamine, glutamate, aspartate, asparagine, lysine, arginine, proline and glycine. As a result, regions rich in these amino acids tend to remain disordered and exposed to the aqueous environment. Glycine, with its small and flexible side chain, imposes minimal steric constraints on the polypeptide backbone, allowing glycine-rich regions to maintain high flexibility and disorder. Whereas proline disrupts regular secondary structures like alpha-helices and beta-sheets due to its constrained cyclic structure. Thus, IDPs tend to remain flexible and dynamic, existing as a heterogeneous ensemble of conformations (Das et al., 2020). This intrinsic disorder is believed to be essential for various cellular functions, particularly those requiring scaffolding or assembly of larger complexes with multiple partners. Remarkably, about 30% of eukaryotic proteins are classified as IDPs or contain intrinsically disordered regions (IDRs) (Monsellier et al., 2008; Peng et al., 2014; Ahrens et al., 2017).

IDRs and IDPs are crucial for proteins dynamics, reversible interactions and are hypothesized to be drivers of liquid-liquid phase separation (LLPS) (Turoverov et al., 2019; Uversky, 2017). Phase separation is a process by which proteins and other macromolecules form dense, droplet-like condensates that exclude solvent forming a more macromolecule-rich and solvent depleted phase (Alberti et al., 2019a). LLPS is driven by various types of weak, non-covalent interactions that allow molecules to transiently associate, including electrostatic, hydrophobic, π-π, cation-π and hydrogen bonding interactions (Turoverov et al., 2019; Uversky, 2017). Electrostatic interactions occur between charged amino acids, such as lysine or arginine (positively charged) and aspartate or glutamate (negatively charged) (Gupta & Uversky, 2024; Pak et al., 2016; J. Wang et al., 2018). Electrostatic attractions may be important for forming and maintaining phase-separated droplets, especially in proteins with prion-like domains or RNA-binding proteins possessing many charged residues (Hennig et al., 2015; King et al., 2012; Wang et al., 2018). Hydrophobic interactions occur between nonpolar amino acids, such as leucine, isoleucine, and valine that tend to cluster together to minimize their exposure to water (Cheung et al., 2002). This is thought to be one driver of phase separation by promoting the association of hydrophobic regions within proteins, leading to the formation of droplets (Lin et al., 2021; Simon et al., 2017). π-π interactions arise between aromatic amino acids like tyrosine, phenylalanine, and tryptophan and are energetically favorable stacking or edge-to-face orientations of the aromatic rings, allowing overlap of π orbitals. These interactions contribute to the cohesion of phase-separated

droplets, especially in proteins with aromatic-rich regions. Cation-π interactions occur between positively charged residues (e.g., lysine or arginine) and the electron-rich aromatic residues (e.g., tyrosine or phenylalanine) (Chong & Forman-Kay, 2016; Das et al., 2020; Qamar et al., 2018). Hydrogen bonding of polar amino acids with side chains containing hydroxyl, amine, or carbonyl groups (e.g., serine, threonine, glutamine) can form if a hydrogen bond donor and acceptor are in close proximity (approximately 3 Å) (Baker & Hubbard, 1984; Murthy et al., 2019). This multivalent nature amplifies weak individual interactions, making them collectively strong enough to drive phase separation (Bremer et al., 2022; Maharana et al., 2018; Martin et al., 2020; Pak et al., 2016). Multivalency also enables fine-tuning of LLPS, as small changes in the number of interacting sites or in the spacing between interacting sites can significantly impact the phase separation behavior (Bremer et al., 2022; Martin et al., 2020).

The interacting regions driving LLPS are often referred to as “stickers”, separated by spacers, or non-interacting linker sequences, in the so called “sticker and spacer” model. Stickers may be folded domains that are able to form intermolecular interactions, short interacting motifs or even single interacting amino acid “hotspots”. Spacers are regions that do not participate in intermolecular interactions and act to separate the sticker regions. For some phase separating IDPs, specific amino acids or short interacting motifs such as low-complexity aromatic rich kinked segments (LARKS) have been described that act as stickers (Hughes et al., 2020). LARKS are flexible regions within a single protein but are able to form extended beta sheet structures when protein concentration reaches a certain threshold, driving LLPS (Hughes et al., 2020). Of note, ELF3 contains a weak predicted LARK in the end of its PrD. LARK motifs are typically enriched in amino acids like glutamine, asparagine, and tyrosine (Hughes et al., 2020).

2.1.1. LLPS as an organizer of cellular processes in the plant

LLPS condensates may have the ability to form and dissipate spontaneously (Brangwynne et al., 2009; Riback et al., 2017) and to show high permeability (Schuster et al., 2018; Wei et al., 2017). Putative molecular functions of these condensates include sequestering interacting components, enhancing dwell time, and forming or dissolving in response to environmental change (Field et al., 2023). Protein-mediated LLPS is highly dependent on the protein concentration, redox state, ionic strength, pH, the presence of different “clients” or “cargos”, such as other protein partners and/or nucleic acids and most notable, temperature (Dignon et al., 2020; Elbaum-Garfinkle et al., 2015; Nott et al., 2015; Saha et al., 2016).

LLPS is thought to act as a general cellular organizing mechanism, forming membraneless organelles, such as nucleoli, stress granules, and P-bodies, which are involved in essential cellular processes including gene regulation, signal transduction, and response to changes in the environment and stress (Banani et al., 2017). The phase-separated state allows for the concentration of specific molecules, such as proteins and nucleic acids, thereby facilitating or impeding enzymatic reactions, controlling transcription, concentrating reactants or sequestering different factors. Although membraneless organelles are relatively well-characterized in animals and fungi, they are poorly studied in plants (Benkemoun & Saupe, 2006; Staples et al., 2023). However, recently studies in plants have shown that LLPS is involved in various cellular processes, including stress responses, growth regulation, and signal transduction (Hsiao, 2022). As plant cells must rapidly adapt to changing conditions such

as drought, temperature fluctuations, and pathogen attacks, LLPS provides an attractive mechanism to explain the fine regulation and quick induction of various response pathways.

One of the most well-studied examples of LLPS in plants are photobodies — liquid-like organelles that regulate the stability and activity of photoreceptors such as phytochromes like PhyB. Through LLPS, photobodies can concentrate phytochromes and their interacting partners, modulating light signaling pathways and ensuring proper photomorphogenic and thermomorphogenic responses (C. Kim et al., 2023a). ELF3 is a component of phytochrome B photobodies and plays an important role in photobody assembly, stability and cargo recruitment at temperatures below 22 °C (R. Yang et al., 2024). In addition to acting as an important component of photobodies, ELF3 also forms ELF3 bodies under warm temperature conditions. These membraneless organelles control the activity of the EC and result in de-repression of EC target genes through a sequestration mechanism (Jung et al., 2020).

Recently, it was demonstrated that the ELF3 PrD serves as a direct thermosensor by forming biomolecular condensates in a temperature-dependent manner as well as changes in the pH. Small pH changes of even 0.1 pH units can robustly trigger ELF3 LLPS (Hutin et al., 2023; Jung et al., 2020). It exhibits different dynamics of phase transition *in vitro* as a function of other environmental variables; changes in ionic strength alter LLPS which is in line with the finding that ELF3 enhances plants' resilience to salt stress (Sakuraba et al., 2017). This suggests that ELF3 may act as a multivalent environmental sensor.

The ELF3 LLPS is tuned by the length of the polyQ motifs but is not dependent on them for LLPS (Hutin et al., 2023). Surprisingly, the PrD region of ELF3 in solution assembles into a monodisperse higher-order oligomer consisting of about 30 copies of the polypeptide. These multimers undergo LLPS in a pH and temperature sensitive manner, with the polyQ region influencing the initial phases of this separation process, changing the dynamics and biomechanical properties of the condensates. The liquid phase can undergo rapid aging, culminating in the formation of a hydrogel, which assumes a semiordered structure (Hutin et al., 2023; Jung et al., 2020).

2.1.2. Biochemical studies of the ELF3 PrD

Understanding the role of specific amino acid sequences and motifs within the ELF3 PrD that drive multimerization and phase separation is critical to understanding its physiological function in membraneless organelle formation and, in the case of ELF3, temperature sensing. Identifying and experimentally validating the motifs that control not only phase separation but also the temperature-dependent behavior of the protein is a major challenge. In order to understand ELF3 LLPS, I used an *in vitro* biochemical approach to characterize the PrD region of ELF3. A benefit of *in vitro* studies is the ability to systematically sample different variables including amino acid sequence changes, protein concentration, ionic strength and temperature and to determine the phase separating behavior of the protein as a function of these variables. In addition, using different prediction tools and multiple sequence alignments, potential amino acids and motifs important to form LLPS could be targeted for mutagenesis and systematically compared to the wild type protein sequence. The biochemical characterization of the PrD of ELF3 relied on a number of different techniques including recombinant protein expression and purification, phase diagrams and site directed mutagenesis. Here I will provide a summary of the biochemical studies performed on the ELF3 PrD and discuss the implications of these results in terms of temperature-sensitive LLPS.

2.2. Results and discussion

2.2.1. Protein expression and purification

The AtELF3 PrD spans amino acids 429 to 609 and has been shown to undergo liquid-liquid phase separation (LLPS) *in vitro* in a temperature-dependent manner and this domain is sufficient for phase separation *in vivo* (Jung et al., 2020). The biochemical studies presented here were performed with a soluble construct previously identified that spans the PrD region (residues 388-625) and yields soluble protein when expressed recombinantly in *E. coli* (Hutin et al., 2023; Jung et al., 2020). Site-directed mutagenesis, deletion mutagenesis and phase diagrams studies were performed on this region (residues 388-625) of the ELF3 protein, called $ELF3^{PrD}$. All constructs were designed and cloned into the pESPRIT 002 vector, which contains an N-terminal 6x histidine tag followed by a TEV protease cleavage site. The deletion mutations were introduced by PCR amplification of flanking regions, amplifying the full vector minus the deletion regions and assembled using Gibbson assembly. Site-specific mutations were introduced using primers containing the mutation of interest followed by PCR amplification and Gibson assembly. All constructs were sequenced to confirm deletions and point mutations.

Protein expression was performed in *E. coli* Rosetta2 cell lines or RIL, *E. coli* strains that are engineered to express eukaryotic proteins from genes that have a different codon usage compared to bacterial genes. All protein expressions were carried out overnight at 18 °C. Protein purification was performed at room temperature using a Ni-affinity column

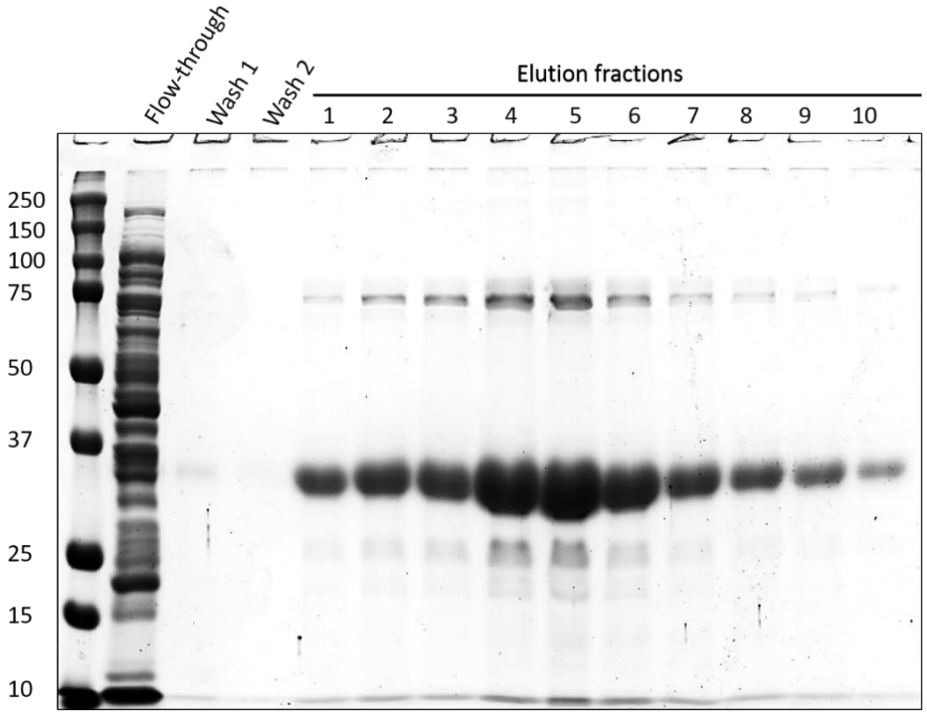

Figure 16. SDS PAGE Ni-column purification of WT ELF3 PrD protein. Molecular weight marker is shown in the first lane on far left followed by the supernatant, flow through, the first washing (Wash1), second washing (Wash2), elution fractions are noted with numbers.

purification protocols (Jung et al., 2020). As the ELF3^{PrD} proteins are predicted to be unfolded and prone to phase separation and/or aggregation, buffer conditions were systematically tested in order to obtain pure and monodisperse protein. Sodium chloride concentrations from 100 mM to 3 M and pH ranges from 6 to 10 were tested with an optimum buffer of 50 mM BTP, pH 9.6 and 500 mM NaCl identified (Hutin et al., 2023; Jung et al., 2020). This high salt and high pH buffer is likely necessary for solubility due to the high pI (8.8) and biased amino acid content, which was rich in glycine (10%), proline (16%) and glutamine (14%) residues of the protein. Typical yields from a 1 L expression were ~15 mg of purified protein (Figure 16). To pinpoint specific sites of interest for further mutagenesis, multiple sequence alignments of ELF3^{PrD} were performed.

2.2.2. Sequence alignments and LLPS predictions

ELF3 is represented in most plant taxa, and orthologs of this protein have been retrieved from the OrthoDB database. Using multiple sequence alignment containing 96 ELF3 sequences from 96 species selected for the presence of PrDs with PLAAC algorithm (Lancaster et al., 2014), from algae to dicots, I identified several regions with a high conservation rate score. One of the identified regions showed a predicted secondary structure, a β-hairpin, in the PrD domain (Figure 18). Using alignment data, a phylogenetic tree was constructed based on ELF3 sequences using the UPGMA method. The tree shows distinct clades corresponding to different plant families, with these groups represented by various colors in Figure 17. This phylogeny reflects the evolutionary relationships between plant species, demonstrating the diversification of ELF3 orthologs across taxa. A notable trend is the reduction in ELF3 protein length, observed as the species range from algae to Brassicaceae (Appendix, Multiple protein alignment). This pattern may be linked to the evolutionary adaptation of the ELF3 protein across plant species.

Multiple sequence alignment of ELF3 sequences from different species were used to identify conserved motifs and regions potentially critical for LLPS. Due to the high variability in sequence, the identification of ELF3 from distantly related plant species was challenging. I conducted a bioinformatic analysis of ELF3 orthologs containing the PrD region, identifying conserved motifs within the sequence. The conservation rate and protein alignment results showed in Figure 18.

Based on the sequence alignments, some regions of interest for mutagenesis studies were identified. To further refine the regions/motifs/sites of interest for mutagenesis studies, bioinformatics tools are used to predict which residues were likely to be involved in phase separation. These tools included PLAAC, which detects prion-like domains (Lancaster et al., 2014); Pscore, which identifies phase-separating regions based on low-complexity sequences (Vernon et al., 2018); PSPredictor, which estimates the propensity of a protein for phase separation using∗ sequence features (Chu et al., 2022); LARKSdb, which identifies low-complexity aromatic-rich kinked segments (LARKS) that drive phase separation (Hughes et al., 2020); and FuzDrop, which identifies sequences important for phase separation and aggregation (Hatos et al., 2022).

Two types of ELF3 mutants were designed and produced, deletions and amino acid substitutions with the aim to elucidate site specific areas in the PrD that facilitate LLPS formation and chosen for further analysis and experimental validation.

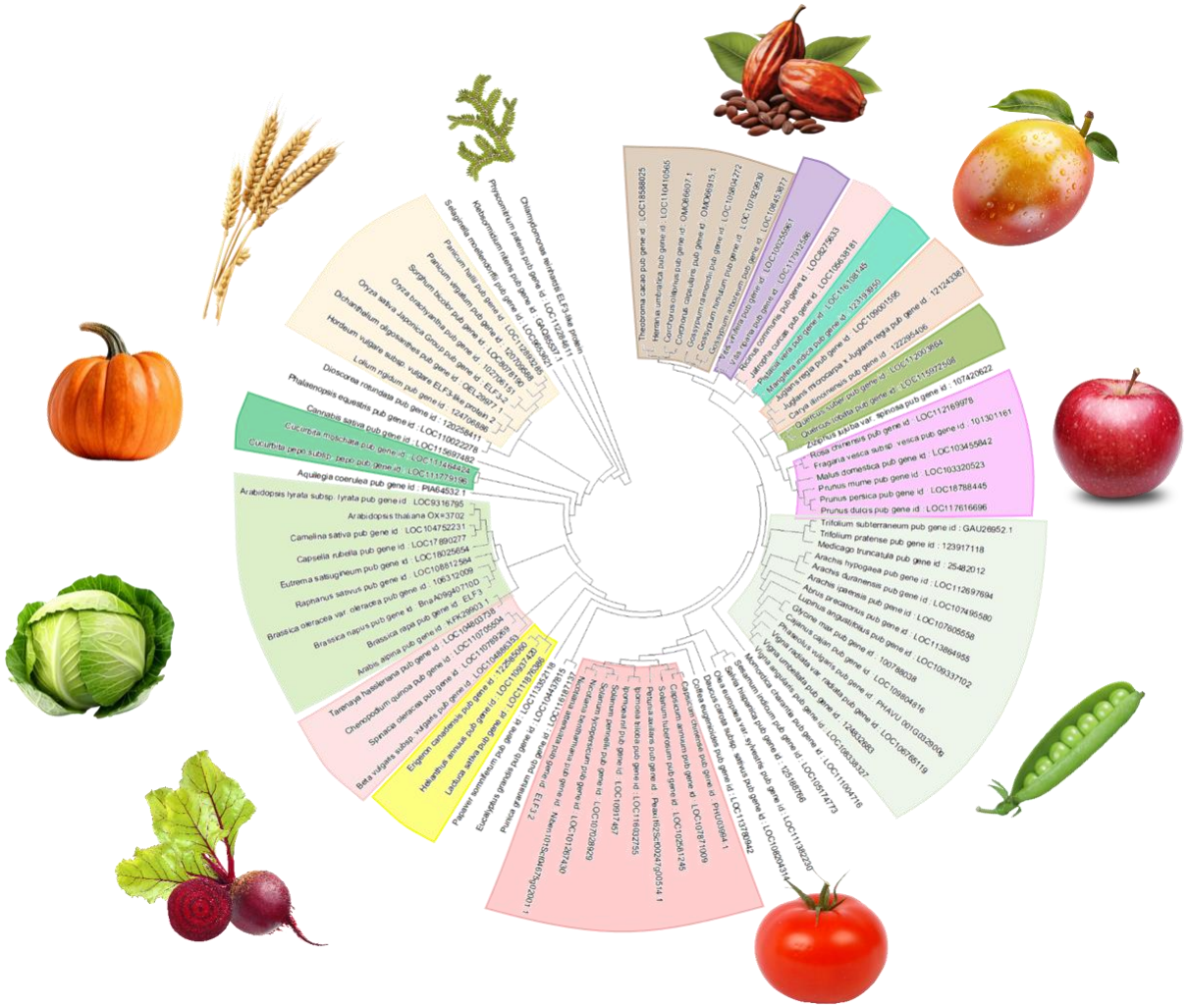

Figure 17. Phylogenetic tree of predicted ELF3 PrD-containing species. The tree includes 95 species across various plant taxa with predicted prion-like domains and one species without a PrD (*Brachypodium distachyon*), denoted with asterisk. For species with multiple ELF3 copies, only one PrD-containing protein was selected. The ELF3 orthologs represent several plant families, highlighted in different colors. Some families are illustrated with known representatives, emphasizing the evolutionary diversity of ELF3 PrD across plant lineages.

Figure 18. Multiple sequence alignments of ELF3 orthologs with predicted PrDs. Due to the large size of the alignment, only a small segment is displayed, corresponding to the *A. thaliana* ELF3 PrD from amino acid positions 430 to 604. Colors indicate conserved amino acids. A highly conserved region (positions 470-487), highlighted in a red box, is predicted to form a β-hairpin structure based on AlphaFold2 predictions.

2.2.3. Deletions

The deletion mutants collectively cover most of the ELF3^{PrD} sequence (Figure 19). Primer design, cloning and characterization of the mutants were carried out by Chloee Tymen with assistance from Stephanie Hutin. The first deletion mutant, the Δ411-428 mutant, lacks a short, evolutionarily conserved motif situated just before the predicted PrD region. The second mutant, is a deletion of amino acids Δ442-462, targeted proline rich motif (11 prolines). This mutation was chosen as prolines are disorder-promoting amino acids and over-represented many in proteins that undergo LLPS (Dao et al., 2024; X. Zhang et al., 2020). This deleted motif also contained three aromatic residues (two phenylalanine and one tyrosine), which could potentially engage in π-π or cation-π interactions. A third deletion mutant, Δ470-487, was based on secondary structure prediction that predicted this sequence may form a β-hairpin. The β-hairpin is a common structural motif that can stabilize protein-protein interactions, and its presence in the PrD region suggests a potential role in facilitating LLPS. Notably, this motif has a high conservation rate among ELF3 PrD regions across different plant taxa, further supporting its functional importance. A fourth deletion mutant targeted a proline- and glycine-rich motif (Δ490-525). This region is also enriched in aromatic residues and includes five tyrosines and one phenylalanine, as well as seven prolines and eight glycines, all of which could influence phase separation properties. A fifth mutant deleted amino acids 526 to 543 (Δ526-543 including a relatively conserved flanking region of polyglutamine (polyQ) tracks, as well as enrichment in tyrosine (three tyrosine residues), one phenylalanine, four prolines, and three methionines. The importance of polyQ regions in protein structure and function is well-documented (Pereira et al., 2023; Urbanek et al., 2020), with previous studies indicating that regions adjacent to polyQ stretches are able to promote the formation of alpha-helical structures or beta-sheets (Boatz et al., 2020; Nazarov et al., 2022; Urbanek et al., 2020). In ELF3, our lab has previously investigated the polyglutamine regions, measuring their impact to LLPS formation and temperature sensing function in plants. As results of the studies, polyglutamine stretches in ELF3 play a role in a fine-tuning mechanism of LLPS and affect plant physiology, but do not govern the formation of LLPS (Hutin et al., 2023b). This suggests that the deleted region may play a role in stabilizing the secondary structure of the PrD, thereby influencing its ability to undergo LLPS. A sixth deletion mutant targeted the region between amino acids 551 and 567 (Δ551-567). This segment is positioned between two polyglutamine regions, forming the left and right flanks for both PolyQ regions. The deleted region contains three glutamines, one methionine, and one phenylalanine, all of which could potentially contribute to the interactions necessary for phase separation.

Two additional deletion regions were designed based on the prediction of LARKS (Hughes et al., 2020). The LARKdb database specifically predicted a LARKS region within the motif spanning amino acids 597 to 606, hence this region was deleted (Δ597-606). Although this motif does not contain any aromatic residues, the prediction suggests this region may act as a kinked beta-sheet inducing motif. Lastly, a mutant with a deletion spanning amino acids 586 to 596 (Δ586-596) was designed. This region can be considered the right-side flanking region of the polyglutamine stretch and acts as a precursor to the LARKS region, with enrichment in proline and arginine residues. The particular location and residue composition of this motif suggest that it may play a role in the structural transitions that are critical for phase separation. A summary of the mutants is given in Figure 19 and Table 1.

A

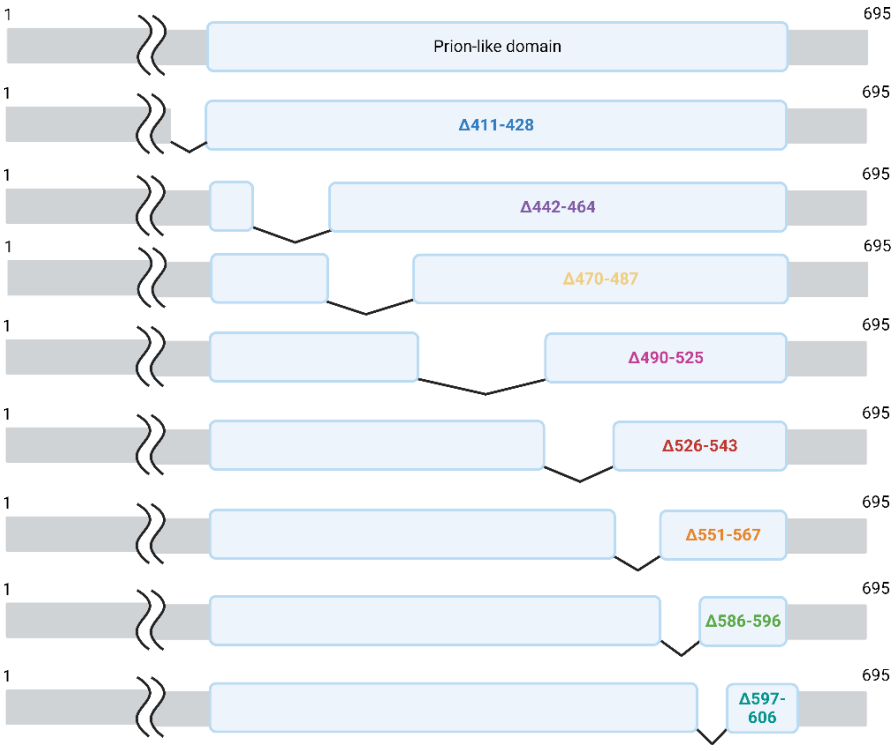

B

388	LLPSEFLVKPPLPHVVVKQRGDSEKTDQHKMESSA	422
423	ENVVGRLSNQGHHQQSNYMPFANNPPASPAPNGY	456
457	CFPPQPPPSGNHQQWLIPVMSPSE GLIYKPHPGM	517
518	AHTGHYGGYYGHYMPTPMVMPQYHPGMGFPPPG	523
524	NGYFPPYGMMPTIMNPYCSSQQQQQQQPNEQMN	556
557	QFGHPGNLQNTQQQQQRSDNEPAPQQQQQPTKSY	590
591	PRARKSRQGSTGSSPSGPQGISGSKSFRPFAAVDED	626
627	SNINNAPEQTMTTTTTTTRTTVTQTTRDGGGVTRV	661

Figure 19. Scheme of ELF3 deletion mutants. (**A)** Map of positions for deleted regions (**B)** Deleted amino acid sequences highlighted in colors in correspond to the map of mutations.

2.2.4. Single Amino-Acid Substitutions

Another mutagenesis strategy included a sequential substitution of amino acids putatively important for the temperature-dependent LLPS behavior of ELF3. Thermoresponsive proteins that are miscible at high temperatures and demix at low temperatures, exhibit what is called an upper critical solution temperature (UCST). ELF3, however, exhibits the opposite behavior and is miscible at lower temperatures and demixes at higher temperatures, thus displaying a lower critical solution temperature (LCST) behavior

(Dignon et al., 2019). Hydrophobic and aromatic residues are associated with LCST behavior. To better understand how specific amino acids contribute to ELF3's LCST behavior, two key mutants were studied. A mutant targeting all 9 histidine residues and replacing these with arginine was studied as well, kindly provided by the group of Phil Wigge from the Leibniz Institute (Figure 20). This mutant, called ELF3$^{PrD9xH/R}$ has a pI of 10 and also mimics the protonated state of the protein, as the pKa value of arginine (12.48) is significantly higher than that of histidine (6.04). A second mutant, called ELF3$^{PrD12xY/Q}$, has 12 tyrosines substituted to glutamine. This substitution removes the aromatic character of tyrosine and replaces it with a polar, non-aromatic side chain. This could affect the protein's hydrophobicity and overall structure, as aromatic rings often play crucial roles in stabilizing protein structures through hydrophobic interactions, π-cation and π-stacking. Glutamine has a longer, more flexible side chain compared to tyrosine, which would introduce more conformational flexibility.

Additional residues were targeted for mutagenesis based on proximity to conserved LARK motifs including the ELF3^{PrDR597A} mutant that replaces arginine at position 597 with an alanine, and ELF3$^{PrD2xR/A}$ that replaces two arginine residues with alanine in a short region positioned before the LARK and ELF3$^{PrD\ 3xR/A}$ replaces three arginine residues. Substituting Arg with Ala removes positive charges from the protein, reducing its overall charge and potentially disrupting beta structure of the LARK-like peptide (Figure 20, Table 1).

Figure 20. Scheme of mutation positions. In **purple** are mutations of tyrosine to glutamine; **orange –** Mutations of histidine to arginine; **green –** Mutations of arginine to alanine.

Table 1. List of mutants, described in the chapter and their measured effect on LLPS formation *in vitro*.

Mutants name	Mutation positions	Characteristics	Observed LLPS	Conditions for LLPS
Δ411-428	Deletion of 411-YFPPYGMMPTIMNNPY-429	Evolutionarily conserved motif situated just before the PrD region	Yes	Similar to WT
Δ442-464	Deletion of 441-YFPPYGMMPTIMNNPYCSS-464	A proline-rich motif	Yes	Similar to WT
Δ470-487	Deletion of 470-QWLIPVMSPSEGLIYKPH-487	Predicted β-hairpin motif	Yes	Undergoes LLPS at pH 9,6 – 9,0
Δ490-525	Deletion of 490-MAHTGHYGGYYGHYMPTPMVMPQYHPGMGFPPPGNG-525	An aromatic-rich motif	Yes	Undergoes LLPS at pH 9,6 – 9,0
Δ526-543	Deletion of 526-YFPPYGMMPTIMNNPYCSS-543	A conserved flanking region before polyglutamine stretch	Yes	Similar to WT
Δ551-567	Deletion of 551-PNEQMNQFGHPGNLQNT-567	Motif placed between two polyglutamine stretches	Yes	Similar to WT
Δ586-596	Deletion of 586-PTKSYPRARKS-596	A right-side flanking region of polyglutamine stretch	No	No observed LLPS
Δ597-604	Deletion of 597-RQGSTGSS-604	Second predicted LARKS region	Yes	Similar to WT
Δ586-596	Deletion of 430-SNQGHH-435	Predicted LARKS	Yes	Similar to WT
PrD R597A	R597A	Replacement of arginine to alanine in a second predicted LARKS region	Yes	No LLPS at pH 9.4–7.0; observed at 100–200 mM salt.
PrD 2xR/A	R592A, R594A	Replacement of arginine to alanine	No	No observed LLPS
PrD 3xR/A	R592A, R594A, R597A	Replacement of arginine to alanine	No	No observed LLPS
PrD 12x Y/Q	Y440Q, Y456Q, Y484Q, Y496Q, Y497Q, Y500Q, Y503Q, Y513Q, Y526Q, Y530Q, Y540Q, Y590Q	Mutant with tyrosine replaced to glutamine	No	No observed LLPS
PrD 9x H/R	H434R, H435R, H468R, H487R, H492R, H495R, H502R, H514R, H560R	Mutant with histidine replaced to arginine	Yes	Forms droplets at higher pH in range of 10,3-9,7

2.2.5. Phase diagrams

Phase diagrams map the conditions under which ELF3 undergoes LLPS as a function of different variables. The formation of liquid droplets is influenced by protein concentration, pH, temperature, and the ionic strength of the solution. Understanding how these variables affect LLPS is critical for characterizing the conditions under which ELF3 can transition into phase-separated states. To systematically investigate the effects of pH and protein concentration on LLPS, the pH of a dialysis solution was varied against different purified protein concentrations. Mutants were tested for their ability to undergo phase separation against different pH and salt concentrations as well. The protein samples were studied at four different concentrations — 4 mg/ml, 2 mg/ml, 1 mg/ml, and 0.5 mg/ml — to cover a range of conditions that might influence phase separation. For mutants displaying altered protein behavior regarding their pH range, salt gradient phase diagrams were used to further explore phase separation. The salt concentration was systematically adjusted from 500 mM to 100 mM NaCl in 100 mM decrements, while maintaining a constant pH, typically set to the lowest tested value. After 1 hour of dialysis, 5 µl of sample was examined under the bright field microscope to determine if the protein had undergone LLPS and/or formed a precipitate (Figure 21).

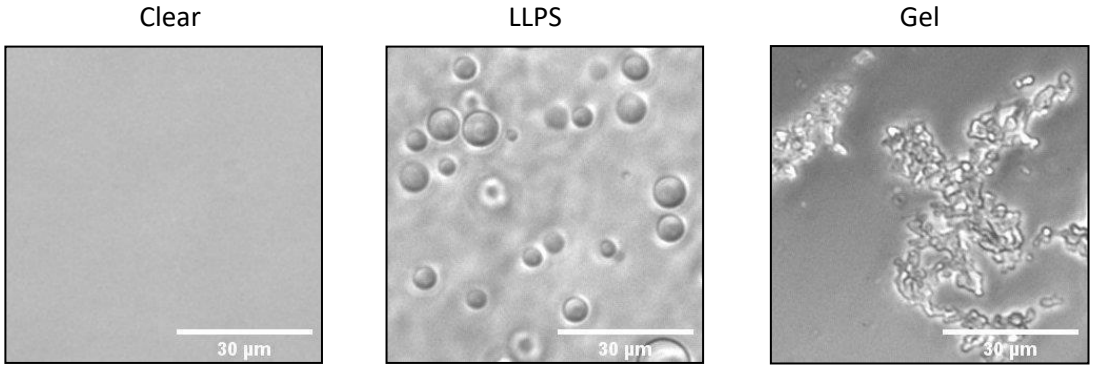

Figure 21. Purified WT ELF3 PrD at concentration 2 mg/ml forms liquid droplets *in vitro* under the conditions-pH 9.0-8.4, 500 mM NaCl, 5°C.

The results show that many of the ELF3 PrD constructs were able to undergo phase separation, resulting in the formation of liquid droplets, that have spherical shape and are able to fuse, indicating a liquid nature.

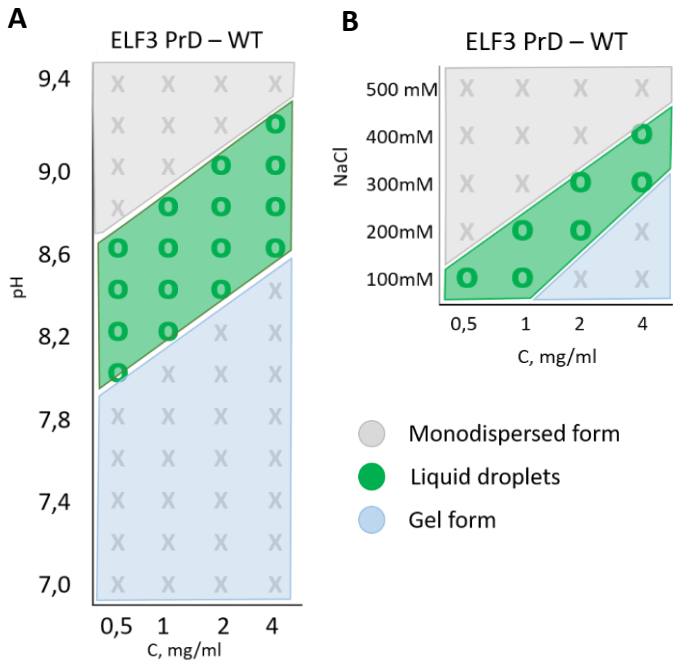

Figure 22. Phase diagrams illustrate under which conditions ELF3^{PrD} undergoes LLPS and gelation or precipitation. (**A**) Examples of ELF3 PrD phase diagrams examining pH versus protein concentration, in the dispersed/dilute (grey zone), liquid droplet (green) and gel-like phase (blue) **(B)** Phase diagram of ELF3 PrD showing the effect of salt concentration on protein concentration, mapping transitions between the same three phases at pH 9.4.

The WT protein forms liquid droplets within a pH range of 8.0 to 9.2, depending on its concentration (Figure 22). Below pH 8.0, the WT protein aggregates. LLPS was observed between 400 mM and 100 mM NaCl at pH 8.0. A few mutants showed different protein behavior as compared to the WT construct. Among the deletion mutants two of them showed mild alterations in the conditions for phase separation and only one did not undergo phase separation at any studied conditions (Figure 23).

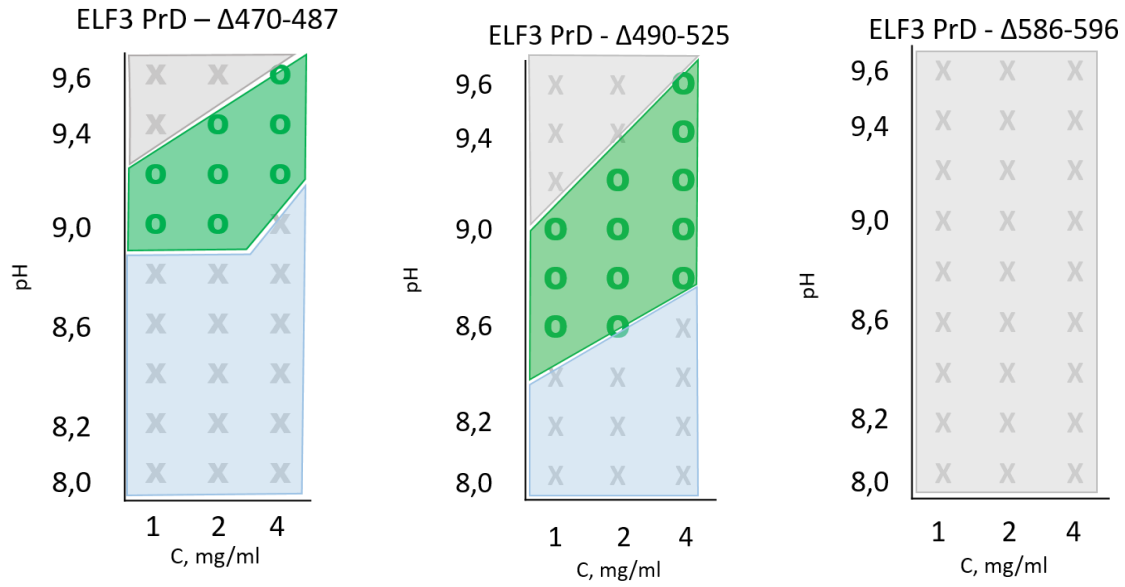

Figure 23. Phase diagrams of Δ470-487, Δ490-525 and Δ586-596 mutants. The mutants show slightly shifted phase separation conditions. Δ470-487 and Δ490-525 undergo LLPS ah higher pH conditions than WT. Δ586-596 mutant did not form liquid droplets at any pH conditions.

Phase diagrams of all tested mutants can be found in the Appendix figures 46, 47 and Table 5. The deletion mutant Δ470-487 underwent phase separation at higher pH conditions than WT and at higher salt concentration. This region was predicted to form a small β-sheet structure and its absent could potentially change protein stability. The mutant Δ490-525 showed a slight shift in formation of liquid droplets to higher pH than WT, but underwent LLPS and aggregation under the same salt conditions. Some of the most significant changes in protein behavior were observed in the deletion mutant Δ586-596, which deletes a region N-terminal to a predicted LARK motif (Figure 23). This short deletion disrupted the phase separation process, preventing the formation of liquid droplets under the assay conditions.

Point mutations targeting residues of interest were also performed. ELF3$^{PrD12xY/Q}$ and ELF3$^{PrD2xR/A}$ mutants did not phase separate in the pH and salt conditions tested, while ELF3^{PrDR597A} mutant forms liquid droplets at lower salt concentration and lower pH than WT (Figure 25 and 24).

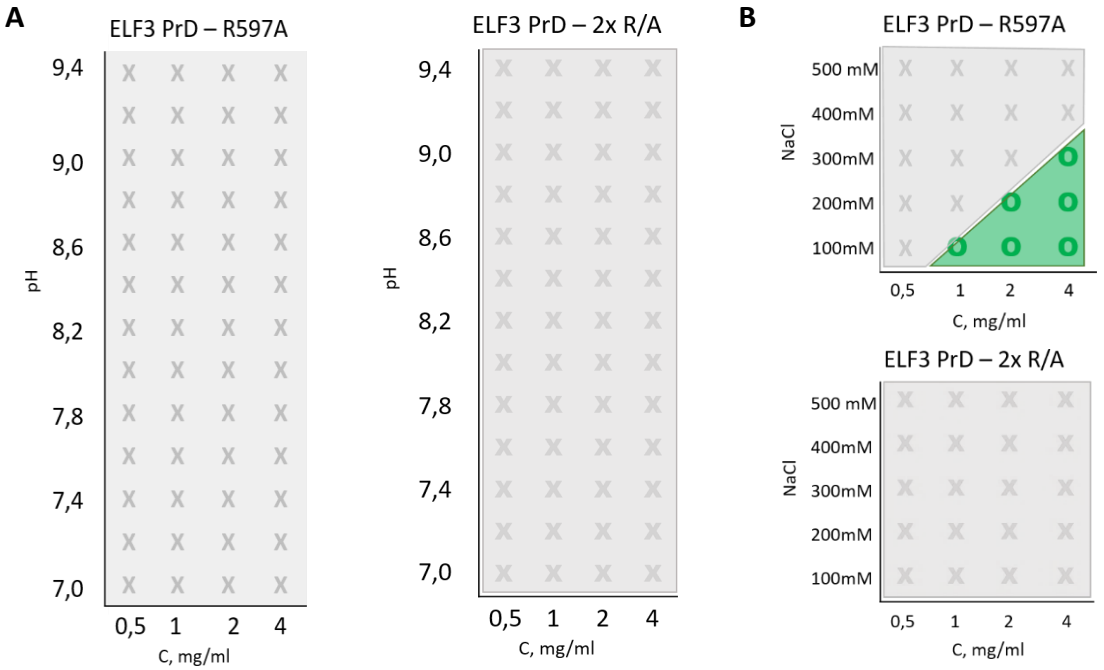

Figure 24. Phase diagrams of ELF3^{PrDR597A} and ELF3$^{PrD2xR/A}$ illustrate (**A)** no LLPS due to changes in pH condition and (**B)** LLPS behavior against salt reduction for **ELF3^{PrDR597A} (top).**

The ELF3$^{PrD9xH/R}$ mutant showed a high propensity for aggregation and was purified under denaturing conditions and refolded prior to phase diagram assays. This mutant underwent LLPS in a high pH and salt concentration range (Figure 25). These mutants show very different protein behavior than the WT protein and were more fully characterized structurally and functionally *in vitro* and *in planta* as discussed in later chapters.

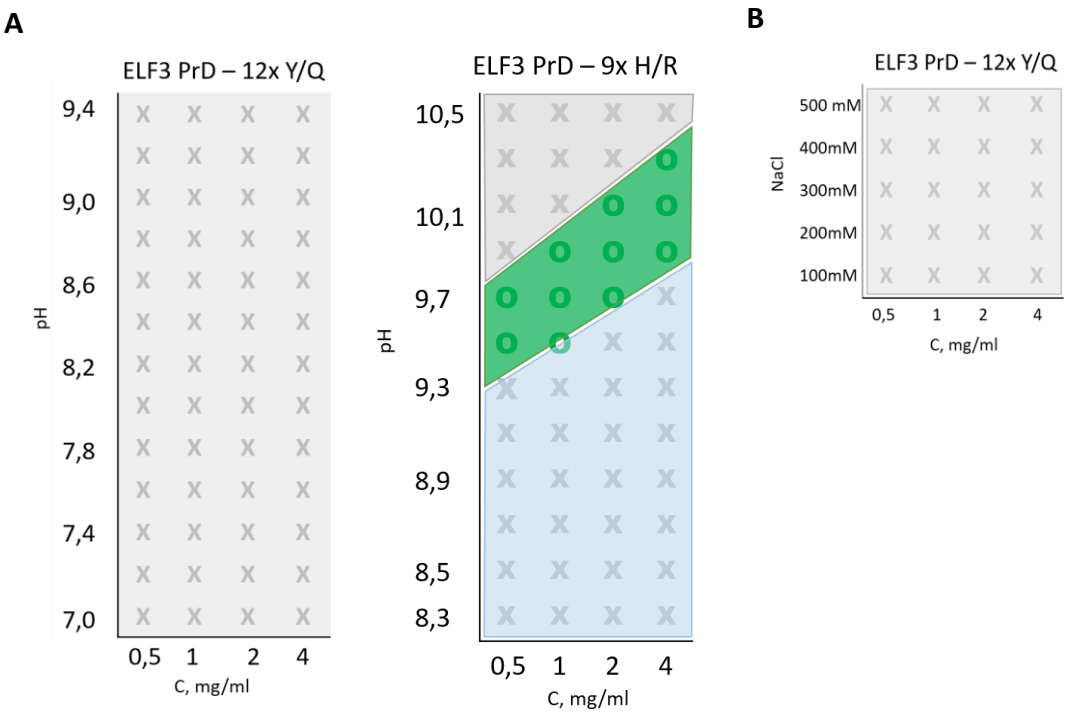

Figure 25. Phase diagrams of ELF3$^{PrD12xY/Q}$ and ELF3$^{Pr9x\ H/R}$.(A) ELF3$^{PrD12xY/Q}$ (left) does not undergo LLPS, while ELF3$^{PrD\ H/R}$ shows LLPS in increases pH condition samples.(**B)** LLPS behavior against salt reduction for **ELF3$^{PrD\ Y/Q}$.**

2.3. Conclusions

The ability of ELF3 to undergo phase separation is driven by its prion-like domain, and this process is thought to be regulated by specific amino acid motifs that promote multivalent interactions (Bremer et al., 2022; Martin et al., 2020; Murthy et al., 2019; Pak et al., 2016). By understanding the molecular drivers of phase separation in ELF3, we can better understand its role in plant circadian rhythms and environmental adaptation. The objective of these biochemical and mutagenesis studies was to determine the specific amino acids that are crucial for LLPS and aggregation. Based on a combination of sequence alignments and *in silico* predictions various motifs were identified as highly conserved, potential drivers of LLPS or exhibited an area enriched in amino acids such as proline, arginine or aromatic residues. Systematic deletion of different motifs revealed that arginine-rich stretches likely contribute to LLPS. Mutating all tyrosine residues to glutamine completely stopped phase separation. An important interaction often observed in folded proteins and believed to contribute to LLPS of IDPs are π -cation interactions. Arginine contains a positively charged guanidinium group that can interact with the aromatic π-electron cloud of tyrosine. This cation-π interaction is a non-covalent interaction that helps stabilize protein structures and plays an important role in protein-protein interactions and phase separation (Sherrill, 2013; Vernon et al., 2018). Thus, disrupting the number of π-cation interactions likely led to the observed decrease or impairment of LLPS. The addition of arginine residues via the substitution of histidines with

arginine resulted in a protein that underwent LLPS at higher salt concentrations and pH and that was much more prone to aggregation, further suggesting that arginine residues, likely in combination with tyrosine residues, are important for the LLPS and aggregation behavior of the ELF3 PrD. The extensive mutagenesis and biochemical assays allowed the identification of ELF3 PrD constructs with very different LLPS behavior and provide important tools for the testing of how LLPS may affect ELF3 function. The structural and functional implications of these changes, both *in vitro* and *in planta*, will be addressed in the following chapters.

2.4. Materials and methods

2.4.1. Phylogenetic analysis and protein alignment

ELF3 protein sequences were retrieved from OrthoDB (Kuznetsov et al., 2023). All the orthologs were revised and sorted manually for PrD prediction with PLAAC algorithm (Lancaster et al., 2014). Of 466 sequences across 160 species, only 95 species contained PrDs longer than 15 amino acids. For species with multiple ELF3 copies, only one was selected for analysis, prioritizing the predicted PrD. If multiple proteins contained a PrD, the longest sequence was chosen. For multiple alignment, MEGA11 program was used (Tamura et al., 2021). The Clustal algorithm was used for an alignment set with the following parameters: gap opening penalty 10.00, gap extension penalty 0.20 and delay divergent cutoff 30 % (Sievers et al., 2011). Color codes were used to visualize the conserved regions with a rate of conservation of more than 25 %. Protein alignment was visualized using Jalview program. A phylogenetic tree was constructed using the UPGMA method in MEGA11, with 500 bootstrap replications and the Jones-Taylor-Thornton substitution model for amino acids.

2.4.2. Cloning of ELF3 PrD mutants

For recombinant expression in *E. coli*, plasmids were constructed using the pESPRIT vector as previously described for the ELF3^{PrD} WT construct (Jung et al., 2020). The construct contains 6x His tag on N-terminus with a TEV cleavage site. The sequence of ELF3^{PrD} WT contains 714 bp encoding for 237 amino acids (residues 388 to 625). This construct was used as the template for mutagenesis. Mutations were introduced using the Gibson assembly (NEBBuilder, HiFi DNA Assembly Cloning Kit, NEB), following the manufacturer's protocol. Briefly, the pESPRIT ELF3^{PrD} plasmid was first PCR amplified using primers specifically designed to introduce the desired mutations/deletions (primer sequences listed in Appendix Table 4). The PCR reaction mix contained 1X Phusion HF buffer, 1 unit of Phusion DNA Polymerase, 0.5 µM each of forward and reverse primers, 200 µM dNTPs, 70-100 ng of template DNA, Nuclease-free water to a final volume of 50 µL.

The PCR program was set as follows:

- Initial denaturation at 94°C for 30 seconds;

  30 cycles of:
- Denaturation at 94°C for 30 seconds;
- Annealing at 55°-60°C for 30 seconds;
- Elongation at 72°C (30 seconds per kb);
- After 30 cycles, final elongation at 72°C for 5 minutes.

After PCR, the amplified fragments were gel-extracted for subsequent Gibson assembly. The purified fragments were mixed with a 1X Gibson assembly master mix and incubated at 50°C for 1 hour. The assembled constructs were then transformed into *E. coli* DH5α (NEB) cells for sequencing verification to confirm successful mutagenesis.

2.4.3. Protein expression and purification

E.coli BL21 (Rosetta2, Novagen) or RIL cells (Agilent Technologies) were transformed with the ELF3 constructs via heat shock and plated on LB agar plates supplemented with 50 µg/ml kanamycin. For the expression, a single colony was chosen and used to inoculate a 100 ml culture of LB medium supplemented with kanamycin (50 µg/mland grown at 37 °C over night. 3L of LB supplemented with kanamycin were inoculated with 20 ml of pre-culture. The cultures were grown at 37 °C, 150 rpm until an OD_{600} of 0.8 was reached. The protein expression was induced with 1 mM Isopropyl-β-D-Thiogalactopyranoside (IPTG) at 18 °C, 150 rpm and cells were grown overnight. Cells were collected by centrifugation at 4000 x g for 20 min at 4 °C.

Bacterial pellets were resuspended in resuspension buffer (50 mM Bis-Tris Propane (BTP) pH 9.4, 500 mM NaCl, 20 mM imidazole, 1 mM Tris(2-Carboxyethyl)Phosphine hydrochloride (TCEP)) and 1x complete EDTA-free protease-inhibitor cocktail at 4° C. Cells were lysed via sonication for 12 min. The lysates were centrifuged at 45,000 x g for 30 min at 4° C and the supernatant collected. A gravity column was prepared using 1.5-2 ml of Nickel-sepharose resin which was pre-equilibrated with resuspension buffer. The supernatant was loaded onto column at 4° C. Washing steps were performed with 50 ml of resuspension buffer and then with 50 ml of a high salt buffer (50 mM BTP, 1 M NaCl, 20 mM imidazole, 1 mM TCEP, pH 9.4) and eluted with 500 µl of elution buffer (50 mM BTP, 1 M NaCl, 300 mM imidazole, 1 mM TCEP, pH 9.4) in 10 fractions at 4 °C. The protein was stable in this buffer over night. Before use the eluted protein was dialyzed with a dialysis tubing (Fisher Scientific) for 1-2 hours at 4° C in 50 mM BTP pH 9.4, 1 M NaCl, 1 mM TCEP to remove the imidazole.

2.4.4. Protein quantification

Purified proteins were quantified for protein concentration with a NanoDrop machine (NanoDrop2000, Thermoscientific). 2 µl of buffer was used to blank the NanoDrop before 2 µl sample was measured. The final concentration was calculate using the calculated extinction coefficient, determined from the sequence using the software, ProtParam from Expasy (Gasteiger et al., 2005).

2.4.5. Phase Diagrams

After removing imidazole, the ELF3 PrD protein was diluted to concentrations 4, 2, 1 and 0.5 mg/ml, in first dialysis buffers (50 mM BTP pH 9.4, 500 mM NaCl and 1 mM TCEP). Further dialysis buffers were prepared with pHs between pH 9,4 – 7.0 with 0.2 units steps and cooled at 4 °C. The proteins with each concentration were dialyzed in dialysis tubing with a cutoff of 12-14 kDa against each buffer stepping down in pH for 1 hour. After dialysis, a 5 µl aliquot was removed and examined under the microscope OLYMPUS CKX41 coupled with camera CollSNAP cf2 on pre-cooled glass slides at 4 °C to identify the different phases (dispersed, LLPS and gel/aggregate). LLPS was scored based on the following criteria: at least 5 liquid droplets in an aliquot, no gel formation, fusion of droplets indicates liquid droplet phase.

A similar protocol was used to identify the protein state under salt gradient conditions. Protein samples at concentrations of 4, 2, 1, and 0.5 mg/ml were prepared. Dialysis buffers

containing 50 mM BTP (pH 8.0), 1 mM TCEP, and varying NaCl concentrations (from 500 mM to 100 mM, in 100 mM steps) were also prepared. The samples were then dialyzed sequentially against these buffers, starting with the highest salt concentration and progressing to the lowest, for 1 hour at 4 °C. After dialysis, a 5 µl aliquot of each sample was examined under a microscope to identify phase separation. The phase diagrams assessing pH and salt conditions were conducted in triplicate for accuracy. The figures were generated by manually plotting the observed protein states based on experimental results.

References

Ahrens, J. B., Nunez-Castilla, J., & Siltberg-Liberles, J. (2017). Evolution of intrinsic disorder in eukaryotic proteins. Cellular and Molecular Life Sciences: CMLS, 74(17), 3163–3174. https://doi.org/10.1007/s00018-017-2559-0

Alberti, S., Gladfelter, A., & Mittag, T. (2019). Considerations and Challenges in Studying Liquid-Liquid Phase Separation and Biomolecular Condensates. Cell, 176(3), 419–434. https://doi.org/10.1016/j.cell.2018.12.035

Arai, M., Sugase, K., Dyson, H. J., & Wright, P. E. (2015). Conformational propensities of intrinsically disordered proteins influence the mechanism of binding and folding. Proc Natl Acad Sci U S A. https://doi.org/10.1073/pnas.1512799112

Baker, E. N., & Hubbard, R. E. (1984). Hydrogen bonding in globular proteins. Progress in Biophysics and Molecular Biology, 44(2), 97–179. https://doi.org/10.1016/0079-6107(84)90007-5

Banani, S. F., Lee, H. O., Hyman, A. A., & Rosen, M. K. (2017). Biomolecular condensates: Organizers of cellular biochemistry. Nature Reviews Molecular Cell Biology, 18(5), 285–298. https://doi.org/10.1038/nrm.2017.7

Barbosa Pereira, P. J., Manso, J. A., & Macedo-Ribeiro, S. (2023). The structural plasticity of polyglutamine repeats. Current Opinion in Structural Biology, 80, 102607. https://doi.org/10.1016/j.sbi.2023.102607

Benkemoun, L., & Saupe, S. J. (2006). Prion proteins as genetic material in fungi. Fungal Genetics and Biology, 43(12), 789–803. https://doi.org/10.1016/j.fgb.2006.06.006

Boatz, J. C., Piretra, T., Lasorsa, A., Matlahov, I., Conway, J. F., & Van Der Wel, P. C. A. (2020). Protofilament Structure and Supramolecular Polymorphism of Aggregated Mutant Huntingtin Exon 1. Journal of Molecular Biology, 432(16), 4722–4744. https://doi.org/10.1016/j.jmb.2020.06.021

Brangwynne, C. P., Eckmann, C. R., Courson, D. S., Rybarska, A., Hoege, C., Gharakhani, J., Julicher, F., & Hyman, A. A. (2009). Germline P Granules Are Liquid Droplets That Localize by Controlled Dissolution/Condensation. Science, 324(5935), 1729–1732. https://doi.org/10.1126/science.1172046

Bremer, A., Farag, M., Borcherds, W. M., Peran, I., Martin, E. W., Pappu, R. V., & Mittag, T. (2022). Deciphering how naturally occurring sequence features impact the phase behaviours of disordered prion-like domains. Nature Chemistry, 14(2), 196–207. https://doi.org/10.1038/s41557-021-00840-w

Cheung, M. S., García, A. E., & Onuchic, J. N. (2002). Protein folding mediated by solvation: Water expulsion and formation of the hydrophobic core occur after the structural collapse. Proceedings of the National Academy of Sciences, 99(2), 685–690. https://doi.org/10.1073/pnas.022387699

Chong, P. A., & Forman-Kay, J. D. (2016). Liquid–liquid phase separation in cellular signaling systems. Current Opinion in Structural Biology, 41, 180–186. https://doi.org/10.1016/j.sbi.2016.08.001

Chu, X., Sun, T., Li, Q., Xu, Y., Zhang, Z., Lai, L., & Pei, J. (2022). Prediction of liquid–liquid phase separating proteins using machine learning. BMC Bioinformatics, 23(1), 72. https://doi.org/10.1186/s12859-022-04599-w

Dao, T. P., Rajendran, A., Galagedera, S. K. K., Haws, W., & Castañeda, C. A. (2024). Short disordered termini and proline-rich domain are major regulators of UBQLN1/2/4 phase separation. Biophysical Journal, 123(11), 1449–1457. https://doi.org/10.1016/j.bpj.2023.11.3401

Das, S., Lin, Y.-H., Vernon, R. M., Forman-Kay, J. D., & Chan, H. S. (2020). Comparative roles of charge, π , and hydrophobic interactions in sequence-dependent phase separation of intrinsically disordered proteins. Proceedings of the National Academy of Sciences, 117(46), 28795–28805. https://doi.org/10.1073/pnas.2008122117

Dignon, G. L., Best, R. B., & Mittal, J. (2020). Biomolecular Phase Separation: From Molecular Driving Forces to Macroscopic Properties. Annual Review of Physical Chemistry, 71(1), 53–75. https://doi.org/10.1146/annurev-physchem-071819-113553

Dignon, G. L., Zheng, W., Kim, Y. C., & Mittal, J. (2019). Temperature-Controlled Liquid–Liquid Phase Separation of Disordered Proteins. ACS Central Science, 5(5), 821–830. https://doi.org/10.1021/acscentsci.9b00102

Elbaum-Garfinkle, S., Kim, Y., Szczepaniak, K., Chen, C. C.-H., Eckmann, C. R., Myong, S., & Brangwynne, C. P. (2015). The disordered P granule protein LAF-1 drives phase separation into droplets with tunable viscosity and dynamics. Proceedings of the National Academy of Sciences, 112(23), 7189–7194. https://doi.org/10.1073/pnas.1504822112

Ezer, D., Jung, J.-H., Lan, H., Biswas, S., Gregoire, L., Box, M. S., Charoensawan, V., Cortijo, S., Lai, X., Stöckle, D., Zubieta, C., Jaeger, K. E., & Wigge, P. A. (2017). The evening complex coordinates environmental and endogenous signals in Arabidopsis. Nature Plants, 3, 17087. https://doi.org/10.1038/nplants.2017.87

Field, S., Jang, G.-J., Dean, C., Strader, L. C., & Rhee, S. Y. (2023). Plants use molecular mechanisms mediated by biomolecular condensates to integrate environmental cues with development. The Plant Cell, 35(9), 3173–3186. https://doi.org/10.1093/plcell/koad062

Gasteiger, E., Hoogland, C., Gattiker, A., Duvaud, S., Wilkins, M. R., Appel, R. D., & Bairoch, A. (2005). Protein Identification and Analysis Tools on the ExPASy Server. In J. M. Walker (Ed.), The Proteomics Protocols Handbook (pp. 571–607). Humana Press. https://doi.org/10.1385/1-59259-890-0:571

Gupta, M. N., & Uversky, V. N. (2024). Reexamining the diverse functions of arginine in biochemistry. Biochemical and Biophysical Research Communications, 705, 149731. https://doi.org/10.1016/j.bbrc.2024.149731

Hatos, A., Tosatto, S. C. E., Vendruscolo, M., & Fuxreiter, M. (2022). FuzDrop on AlphaFold: Visualizing the sequence-dependent propensity of liquid–liquid phase separation and aggregation of proteins. Nucleic Acids Research, 50(W1), W337–W344. https://doi.org/10.1093/nar/gkac386

Hennig, S., Kong, G., Mannen, T., Sadowska, A., Kobelke, S., Blythe, A., Knott, G. J., Iyer, K. S., Ho, D., Newcombe, E. A., Hosoki, K., Goshima, N., Kawaguchi, T., Hatters, D., Trinkle-Mulcahy, L., Hirose, T., Bond, C. S., & Fox, A. H. (2015). Prion-like domains in RNA binding proteins are

essential for building subnuclear paraspeckles. Journal of Cell Biology, 210(4), 529–539. https://doi.org/10.1083/jcb.201504117

Hsiao, A.-S. (2022). Plant Protein Disorder: Spatial Regulation, Broad Specificity, Switch of Signaling and Physiological Status. Frontiers in Plant Science, 13. https://www.frontiersin.org/articles/10.3389/fpls.2022.904446

Hsu, P. Y., & Harmer, S. L. (2014). Wheels within wheels: The plant circadian system. Trends in Plant Science, 19(4), 240–249. https://doi.org/10.1016/j.tplants.2013.11.007

Huang, H., Alvarez, S., Bindbeutel, R., Shen, Z., Naldrett, M. J., Evans, B. S., Briggs, S. P., Hicks, L. M., Kay, S. A., & Nusinow, D. A. (2016). Identification of Evening Complex Associated Proteins in Arabidopsis by Affinity Purification and Mass Spectrometry. Molecular & Cellular Proteomics: MCP, 15(1), 201–217. https://doi.org/10.1074/mcp.M115.054064

Hughes, M. P., Goldschmidt, L., & Eisenberg, D. S. (2020). The prevalence and distribution in genomes of low-complexity, amyloid-like, reversible, kinked segment (LARKS), a common structural motif in amyloid-like fibrils (p. 2020.12.08.415679). https://doi.org/10.1101/2020.12.08.415679

Hutin, S., Kumita, J. R., Strotmann, V. I., Dolata, A., Ling, W. L., Louafi, N., Popov, A., Milhiet, P.-E., Blackledge, M., Nanao, M. H., Wigge, P. A., Stahl, Y., Costa, L., Tully, M. D., & Zubieta, C. (2023a). Phase separation and molecular ordering of the prion-like domain of the Arabidopsis thermosensory protein EARLY FLOWERING 3. Proceedings of the National Academy of Sciences, 120(28), e2304714120. https://doi.org/10.1073/pnas.2304714120

Jung, J.-H., Barbosa, A. D., Hutin, S., Kumita, J. R., Gao, M., Derwort, D., Silva, C. S., Lai, X., Pierre, E., Geng, F., Kim, S.-B., Baek, S., Zubieta, C., Jaeger, K. E., & Wigge, P. A. (2020). A prion-like domain in ELF3 functions as a thermosensor in Arabidopsis. Nature, 585(7824), 256–260. https://doi.org/10.1038/s41586-020-2644-7

Kim, C., Kwon, Y., Jeong, J., Kang, M., Lee, G. S., Moon, J. H., Lee, H.-J., Park, Y.-I., & Choi, G. (2023). Phytochrome B photobodies are comprised of phytochrome B and its primary and secondary interacting proteins. Nature Communications, 14(1), 1708. https://doi.org/10.1038/s41467-023-37421-z

King, O. D., Gitler, A. D., & Shorter, J. (2012). The tip of the iceberg: RNA-binding proteins with prion-like domains in neurodegenerative disease. Brain Research, 1462, 61–80. https://doi.org/10.1016/j.brainres.2012.01.016

Lancaster, A. K., Nutter-Upham, A., Lindquist, S., & King, O. D. (2014). PLAAC: A web and command-line application to identify proteins with prion-like amino acid composition. Bioinformatics, 30(17), 2501–2502. https://doi.org/10.1093/bioinformatics/btu310

Lin, Y., Fichou, Y., Longhini, A. P., Llanes, L. C., Yin, P., Bazan, G. C., Kosik, K. S., & Han, S. (2021). Liquid-Liquid Phase Separation of Tau Driven by Hydrophobic Interaction Facilitates Fibrillization of Tau. Journal of Molecular Biology, 433(2), 166731. https://doi.org/10.1016/j.jmb.2020.166731

Maharana, S., Wang, J., Papadopoulos, D. K., Richter, D., Pozniakovsky, A., Poser, I., Bickle, M., Rizk, S., Guillén-Boixet, J., Franzmann, T. M., Jahnel, M., Marrone, L., Chang, Y.-T., Sterneckert, J.,

Tomancak, P., Hyman, A. A., & Alberti, S. (2018). RNA buffers the phase separation behavior of prion-like RNA binding proteins. Science, 360(6391), 918–921. https://doi.org/10.1126/science.aar7366

Martin, E. W., Holehouse, A. S., Peran, I., Farag, M., Incicco, J. J., Bremer, A., Grace, C. R., Soranno, A., Pappu, R. V., & Mittag, T. (2020). Valence and patterning of aromatic residues determine the phase behavior of prion-like domains. Science, 367(6478), 694–699. https://doi.org/10.1126/science.aaw8653

Monsellier, E., Ramazzotti, M., Taddei, N., & Chiti, F. (2008). Aggregation Propensity of the Human Proteome. PLoS Computational Biology, 4(10), e1000199. https://doi.org/10.1371/journal.pcbi.1000199

Murthy, A. C., Dignon, G. L., Kan, Y., Zerze, G. H., Parekh, S. H., Mittal, J., & Fawzi, N. L. (2019). Molecular interactions underlying liquid−liquid phase separation of the FUS low-complexity domain. Nature Structural & Molecular Biology, 26(7), 7. https://doi.org/10.1038/s41594-019-0250-x

Nazarov, S., Chiki, A., Boudeffa, D., & Lashuel, H. A. (2022). Structural Basis of Huntingtin Fibril Polymorphism Revealed by Cryogenic Electron Microscopy of Exon 1 HTT Fibrils. Journal of the American Chemical Society, 144(24), 10723–10735. https://doi.org/10.1021/jacs.2c00509

Nott, T. J., Petsalaki, E., Farber, P., Jervis, D., Fussner, E., Plochowietz, A., Craggs, T. D., Bazett-Jones, D. P., Pawson, T., Forman-Kay, J. D., & Baldwin, A. J. (2015). Phase Transition of a Disordered Nuage Protein Generates Environmentally Responsive Membraneless Organelles. Molecular Cell, 57(5), 936–947. https://doi.org/10.1016/j.molcel.2015.01.013

Nusinow, D. A., Helfer, A., Hamilton, E. E., King, J. J., Imaizumi, T., Schultz, T. F., Farré, E. M., & Kay, S. A. (2011). The ELF4-ELF3-LUX Complex Links the Circadian Clock to Diurnal Control of Hypocotyl Growth. Nature, 475(7356), 398–402. https://doi.org/10.1038/nature10182

Pak, C. W., Kosno, M., Holehouse, A. S., Padrick, S. B., Mittal, A., Ali, R., Yunus, A. A., Liu, D. R., Pappu, R. V., & Rosen, M. K. (2016). Sequence Determinants of Intracellular Phase Separation by Complex Coacervation of a Disordered Protein. Molecular Cell, 63(1), 72–85. https://doi.org/10.1016/j.molcel.2016.05.042

Peng, Z., Mizianty, M. J., & Kurgan, L. (2014). Genome-scale prediction of proteins with long intrinsically disordered regions. Proteins, 82(1), 145–158. https://doi.org/10.1002/prot.24348

Pokhilko, A., Fernández, A. P., Edwards, K. D., Southern, M. M., Halliday, K. J., & Millar, A. J. (2012). The clock gene circuit in Arabidopsis includes a repressilator with additional feedback loops. Molecular Systems Biology, 8, 574. https://doi.org/10.1038/msb.2012.6

Qamar, S., Wang, G., Randle, S. J., Ruggeri, F. S., Varela, J. A., Lin, J. Q., Phillips, E. C., Miyashita, A., Williams, D., Ströhl, F., Meadows, W., Ferry, R., Dardov, V. J., Tartaglia, G. G., Farrer, L. A., Kaminski Schierle, G. S., Kaminski, C. F., Holt, C. E., Fraser, P. E., … St George-Hyslop, P. (2018). FUS Phase Separation Is Modulated by a Molecular Chaperone and Methylation of Arginine Cation-π Interactions. Cell, 173(3), 720-734.e15. https://doi.org/10.1016/j.cell.2018.03.056

Riback, J. A., Katanski, C. D., Kear-Scott, J. L., Pilipenko, E. V., Rojek, A. E., Sosnick, T. R., & Drummond, D. A. (2017). Stress-Triggered Phase Separation Is an Adaptive, Evolutionarily Tuned Response. Cell, 168(6), 1028-1040.e19. https://doi.org/10.1016/j.cell.2017.02.027

Saha, S., Weber, C. A., Nousch, M., Adame-Arana, O., Hoege, C., Hein, M. Y., Osborne-Nishimura, E., Mahamid, J., Jahnel, M., Jawerth, L., Pozniakovski, A., Eckmann, C. R., Jülicher, F., & Hyman, A. A. (2016). Polar Positioning of Phase-Separated Liquid Compartments in Cells Regulated by an mRNA Competition Mechanism. Cell, 166(6), 1572-1584.e16. https://doi.org/10.1016/j.cell.2016.08.006

Sakuraba, Y., Bülbül, S., Piao, W., Choi, G., & Paek, N. (2017). Arabidopsis EARLY FLOWERING 3 increases salt tolerance by suppressing salt stress response pathways. The Plant Journal, 92(6), 1106–1120. https://doi.org/10.1111/tpj.13747

Schuster, B. S., Reed, E. H., Parthasarathy, R., Jahnke, C. N., Caldwell, R. M., Bermudez, J. G., Ramage, H., Good, M. C., & Hammer, D. A. (2018). Controllable protein phase separation and modular recruitment to form responsive membraneless organelles. Nature Communications, 9(1), 2985. https://doi.org/10.1038/s41467-018-05403-1

Sherrill, C. D. (2013). Energy component analysis of π interactions. Accounts of Chemical Research, 46(4), 1020–1028. https://doi.org/10.1021/ar3001124

Sievers, F., Wilm, A., Dineen, D., Gibson, T. J., Karplus, K., Li, W., Lopez, R., McWilliam, H., Remmert, M., Söding, J., Thompson, J. D., & Higgins, D. G. (2011). Fast, scalable generation of high-quality protein multiple sequence alignments using Clustal Omega. Molecular Systems Biology, 7(1), 539. https://doi.org/10.1038/msb.2011.75

Simon, J. R., Carroll, N. J., Rubinstein, M., Chilkoti, A., & López, G. P. (2017). Programming molecular self-assembly of intrinsically disordered proteins containing sequences of low complexity. Nature Chemistry, 9(6), 509–515. https://doi.org/10.1038/nchem.2715

Staples, M. I., Frazer, C., Fawzi, N. L., & Bennett, R. J. (2023). Phase separation in fungi. Nature Microbiology, 8(3), 375–386. https://doi.org/10.1038/s41564-022-01314-6

Turoverov, K. K., Kuznetsova, I. M., Fonin, A. V., Darling, A. L., Zaslavsky, B. Y., & Uversky, V. N. (2019). Stochasticity of Biological Soft Matter: Emerging Concepts in Intrinsically Disordered Proteins and Biological Phase Separation. Trends in Biochemical Sciences, 44(8), 716–728. https://doi.org/10.1016/j.tibs.2019.03.005

Urbanek, A., Popovic, M., Morató, A., Estaña, A., Elena-Real, C. A., Mier, P., Fournet, A., Allemand, F., Delbecq, S., Andrade-Navarro, M. A., Cortés, J., Sibille, N., & Bernadó, P. (2020). Flanking Regions Determine the Structure of the Poly-Glutamine in Huntingtin through Mechanisms Common among Glutamine-Rich Human Proteins. Structure, 28(7), 733-746.e5. https://doi.org/10.1016/j.str.2020.04.008

Uversky, V. N. (2017). Intrinsically disordered proteins in overcrowded milieu: Membrane-less organelles, phase separation, and intrinsic disorder. Current Opinion in Structural Biology, 44, 18–30. https://doi.org/10.1016/j.sbi.2016.10.015

Vernon, R. M., Chong, P. A., Tsang, B., Kim, T. H., Bah, A., Farber, P., Lin, H., & Forman-Kay, J. D. (2018). Pi-Pi contacts are an overlooked protein feature relevant to phase separation. ELife, 7. https://doi.org/10.7554/eLife.31486

Wang, J., Choi, J.-M., Holehouse, A. S., Lee, H. O., Zhang, X., Jahnel, M., Maharana, S., Lemaitre, R., Pozniakovsky, A., Drechsel, D., Poser, I., Pappu, R. V., Alberti, S., & Hyman, A. A. (2018). A

Molecular Grammar Governing the Driving Forces for Phase Separation of Prion-like RNA Binding Proteins. Cell, 174(3), 688-699.e16. https://doi.org/10.1016/j.cell.2018.06.006

Wei, M.-T., Elbaum-Garfinkle, S., Holehouse, A. S., Chen, C. C.-H., Feric, M., Arnold, C. B., Priestley, R. D., Pappu, R. V., & Brangwynne, C. P. (2017). Phase behaviour of disordered proteins underlying low density and high permeability of liquid organelles. Nature Chemistry, 9(11), 1118–1125. https://doi.org/10.1038/nchem.2803

Yang, R., Dong, H., Xie, X., Zhang, Y., & Sun, J. (2024). GSK3s promote the phyB-ELF3-HMR complex formation to regulate plant thermomorphogenesis. The New Phytologist. https://doi.org/10.1111/nph.20064

Yu, J.-W., Rubio, V., Lee, N.-Y., Bai, S., Lee, S.-Y., Kim, S.-S., Liu, L., Zhang, Y., Irigoyen, M. L., Sullivan, J. A., Zhang, Y., Lee, I., Xie, Q., Paek, N.-C., & Deng, X. W. (2008). COP1 and ELF3 control circadian function and photoperiodic flowering by regulating GI stability. Molecular Cell, 32(5), 617–630. https://doi.org/10.1016/j.molcel.2008.09.026

Zhang, X., Vigers, M., McCarty, J., Rauch, J. N., Fredrickson, G. H., Wilson, M. Z., Shea, J.-E., Han, S., & Kosik, K. S. (2020). The proline-rich domain promotes Tau liquid–liquid phase separation in cells. Journal of Cell Biology, 219(11), e202006054. https://doi.org/10.1083/jcb.202006054

Zhao, H., Xu, D., Tian, T., Kong, F., Lin, K., Gan, S., Zhang, H., & Li, G. (2021). Molecular and functional dissection of EARLY-FLOWERING 3 (ELF3) and ELF4 in Arabidopsis. Plant Science, 303, 110786. https://doi.org/10.1016/j.plantsci.2020.110786

CHAPTER 3 Structural characterisation of ELF3 mutants

3.1. Introduction

Structural studies of disordered proteins and disordered domains, such as the ELF3 prion-like domain, are particularly challenging due to their inherent flexibility and lack of a stable and defined secondary and tertiary structure (Hutin et al., 2023a). Common structural techniques like X-ray crystallography, which require a homogeneous conformational state of molecules, are unsuitable as these proteins sample many different conformations due to their flexibility and are thus not amenable to crystallization (Putnam et al., 2007). While electron microscopy does not require crystallization, this technique also relies on homogeneous conformations of molecules for particle picking and averaging, a challenge with disordered regions. NMR spectroscopy, while useful for capturing dynamic and flexible regions in solution, becomes difficult for large proteins like ELF3 PrD because of the complex and overlapping signals from many atoms. In addition, as protein size increases, rotational motion in solution slows down, leading to rapid signal decay, known as transverse relaxation, which reduces the resolution and intensity of NMR peaks. Tests on ELF3 PrD were performed and gave no useable signals, thus precluding further high-resolution studies by NMR (S. Hutin, unpublished).

While it is taught at university courses, that the structure of a protein dictates its function, IDPs are able to sample multiple conformations due to the low energy barriers between states. This dynamic nature enables IDPs to interact with various binding partners and, in the case of ELF3, undergo phase separation. One solution-state technique that is ideally suited to study the flexibility and conformations of IDPs is small-angle X-ray scattering (SAXS). SAXS is often used to complement high-resolution methods, such as NMR, and offers insight into the dynamic behavior of a given protein under different conditions (Eliezer, 2009; Mertens & Svergun, 2017). This is particularly important for the study of the ELF3 PrD and mutants. SAXS may be performed using different concentrations of protein, varying buffer conditions and under controlled temperatures. Combining SAXS data with Size Exclusion Chromatography (SEC-SAXS) and multi-angle laser light scattering (SEC-MALLS) allowed the determination of the approximate oligomerization state of different ELF3 PrD mutants in solution under different buffer conditions and allowed the investigation of structural changes to the protein upon phase separation (Brennich et al., 2017; Meisburger et al., 2016; Watanabe & Inoko, 2009). These studies offer insights into the steps involved in phase separation and the surprising appearance of internal organization of ELF3 PrD molecules in liquid droplets by demonstrating that droplet formation triggers a long-range ordering of ELF3 PrD oligomers (Hutin et al., 2023).

3.1.1. General principle of SAXS

SAXS stands as a versatile and powerful technique used in the structural analysis of polymers, nanoparticles, colloids and various biological macromolecules, including proteins, nucleic acids, and lipids (Barbosa et al., 2013; Blanchet & Svergun, 2013). The size range of molecules studied by SAXS spans from a few nanometers to hundreds of nanometers. It is most commonly used to analyze samples in the range of 10 to 100 nanometers in diameter and is thus well-suited for studying the overall shape and assembly of molecules and macromolecular assemblies in solution. Operating on the principle of X-ray scattering, SAXS provides data on the size, shape, and flexibility of the molecule under study. By exposing the

sample to an X-ray beam and measuring the scattered X-rays at low angles, SAXS captures information about the spatial arrangement of electron densities within the molecules in their native state. SAXS is particularly valuable for studying dynamic structures such as intrinsically disordered proteins (IDP) or intrinsically disordered regions of proteins (IDR) (Rambo & Tainer, 2011a; Tompa, 2011; Barbosa et al., 2013; Kikhney & Svergun, 2015).

SAXS relies on the difference in electron density between the molecules being studied and the surrounding solvent to generate its scattering signal. This is shown in a simplified schematic in figure 26.

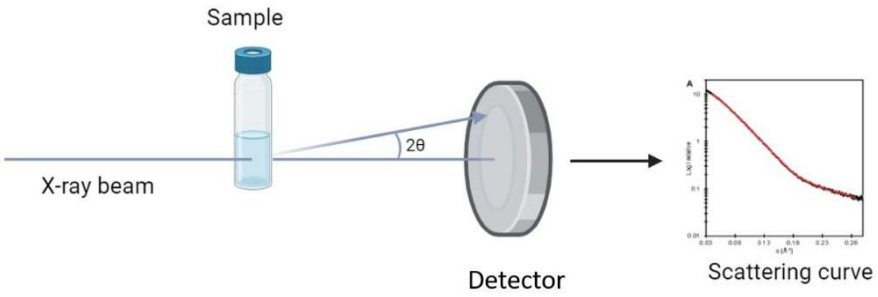

Figure 26. Schematic overview of a SAXS experiment. An X-ray beam hits the sample and scatters to the detector The resulting scattering curve represents the scattering intensity versus the scattering angle.

X-rays are scattered due to collisions with electron-rich particles present in a solution. The scattered electrons travel down a flight tube and then are measured on a direct electron detector. The detector image is then radially integrated. SAXS data is typically depicted as a scattering curve that shows the intensity of scattered X-rays (I) as a function of the scattering vector (q), which is related to the angle of scattering and the wavelength of the X-rays used.

$$q = \frac{4\pi}{\lambda} sin\theta$$

The scattering curve provides information about the overall shape and size of the molecule (Blanchet & Svergun, 2013; Pelikan et al., 2009). Key features include the slope at low q-values (related to overall size or radius of gyration, R_g) and features or oscillations at higher q-values, indicating more detailed structural features such as particle dimensions and shape. Here, λ is the wavelength of X-rays used in the experiment and θ is half of the total scattering angle, (the angle between the incident and scattered beams) (figure 26).

SAXS scattering intensity data not only contains information about how individual particles or molecules that scatter X-rays but also information about interactions between particles, such as the degree of order or aggregation in the sample. The form factor, P(q), describes the behavior of individual particles and is related to the internal structure and shape of an individual molecule and provides information on its size, shape, and electron density distribution. The form factor takes into account the spatial distribution of electron density within the macromolecule and contributes to the overall scattering profile, allowing extracting information about the size and shape of the scattering samples. The arrangement of particles in the solution and the interaction between them is called the structure factor and also contributes to the overall scattering intensity, I(q). The overall scattering intensity is given by the below equation:

$$I(q) = P(q)*S(q)$$

P(q) is the form factor, describing the shape of the scattering particle, S(q) is the structure factor, providing information about the intermolecular interactions of the particles and q is the momentum transfer related to the scattering angle and wavelength. In BioSAXS experiments the aim is to measure a non-interacting, homogenous sample. This will lead to the no S(q) scattering and then the I(q) is directly proportional to the P(q).

Scattering data provides information of several key structural parameters, including the radius of gyration (R_g), excluded particle volume, an estimation of the molecular weight, flexibility or disorder of the molecule, interparticle distances and the maximum dimension (D_{max}) of the macromolecules, these will be discussed in further detail below (Glatter & Kratky, 1982; Rambo & Tainer, 2013).

3.1.2. Radius of Gyration (Rg):

Guinier analysis is a method used in SAXS to determine the radius of gyration (R_g) of a scatterer by analyzing the low-angle region of the scattering curve (Guinier, 1939; Guinier & Fournet, 1955).

$$I(q) = I(0)e^{-q^2R_g^2/3}$$

R_g is a measure of the spread or distribution of mass within a macromolecule and characterizes the overall size and compactness of the protein. For well-behaved and non-aggregated proteins or proteins without strong inter-particle effects such as repulsion or attraction, the Guinier plot (ln I(q) vs. q^2) typically exhibits a linear relationship, enabling accurate R_g estimation for the overall size of the molecule, so long as $q*Rg < 1.3$ (Putnam et al., 2007). For example, two proteins of the same number of amino acids may adopt different structures in solution, resulting in differences in R_g even if the molecular weights are the same. A helical bundle protein with a spherical globular conformation would likely have a smaller R_g indicating a more compact conformation, versus a protein with an extended or multidomain structure (Gomes et al., 2021).

However, for intrinsically disordered proteins (IDPs), which have flexible and extended conformations, the Guinier region often exhibits non-linear behavior due to these heterogeneous structures (Kikhney & Svergun, 2015; Zheng & Best, 2018). Non-linear fit of the Guinier region of measured IDP leads to difficulty in accurate determination of the R_g. For this reason, it is possible to redefine the Rg range for an IDP as $q*Rg < 1.1$ (Zheng & Best, 2018). There are of course a number of alternative methods that rely on computing a pool of 1000s of individual structures, such as ensemble optimization methods (EOM), which can better capture the extended and dynamic conformations that IDPs offer (Ayuso-Tejedor et al., 2011; Bernado et al., 2010; Bonomi et al., 2017). The EOM process involves generating a large pool of random protein conformations and selecting a subset of conformations whose theoretical SAXS scattering curve best fits the experimental SAXS data. This subset represents an ensemble that should reflect the actual multiple conformations adopted by the IDP.

In the following sections an $q*Rg < 1.3$ was used to calculate the Guiner approximation, and the use of EOM was not required (Guinier & Fournet, 1955).

3.1.3. Kratky plot

The Kratky plot is a graphical method used to assess the «foldedness» or flexibility of the sample (Kratky & Porod, 1949; Glatter & Kratky, 1982)(Rambo & Tainer, 2011b). The standard Kratky plot shows $q^2I(q)$, scattering intensity multiplied by the square of the

scattering vector, plotted against q, where q is the magnitude of the scattering vector plotted over a low-q range s such the Kratky plot is dependent on the size and concentration of the sample. However, the dimensionless Kratky plot normalizes the data to I(0) and takes into account the Rg, and as such makes the plot independent of the concentration and size of the molecule, Rg and volume (Durand et al., 2010):

$$(qR_g)^2 I(q)/I(0)\ vs\ qR_g$$

In a dimensionless Kratky plot, for well-folded spherical proteins, the Kratky plot shows a bell-shaped curve (Gaussian), indicating a compact structure. In contrast, IDPs exhibit a plateau or continuous increase in the plot along the x-axis at higher q, reflecting their lack of a defined structure. The Kratky plot helps distinguish between folded, partially folded, and disordered states of proteins. By analyzing the shape of the Kratky plot, the degree of flexibility or disorder in the sample can be inferred (figure 27).

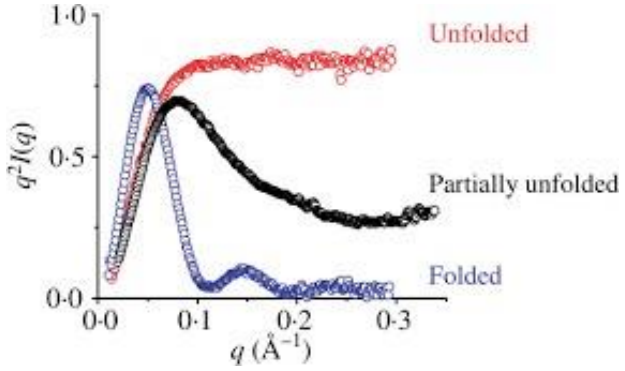

Figure 27. Kratky plot with overlaid curves for folded, partially unfolded and unfolded samples. Globular well-structured proteins due to the Porod's law have a bell-like shape on Kratky plot. Partially unfolded proteins have asymmetrical curve shoulders. Fully unfolded proteins lack of curve peak and have a plateau, increasing intensity at larger q range. Figure source Putnam et al., 2007.

3.1.4. Porod volume and Porod-Debye Law:

The excluded particle volume (V_p) or Porod volume is another parameter that can be derived from SAXS. Similarly, to the Kratky plot it can quickly distinguish between a structured and unstructured particle. V_p represents the volume that the protein occupies and the space it excludes to solvent molecules, thus offering insights into a molecules compactness and packing density or lack thereof.

$$V_p = 2\pi^2 \frac{I(0)}{Q}$$

Q is the Porod invariant and is a direct measurement of the electron density contrast, Δρ. Q can be calculated from the area under the peak in a Kratky plot, thus is defined for structured molecules which confer a defined area while the Kratky plot of a flexible molecule does not converge therefore preventing the determination of Q (Rambo & Tainer, 2013). The Porod-Debye law, a fourth power law approximation of q and the scattered intensities I(q):

$$I(q) \approx \Delta\rho^2 \cdot \frac{2\pi}{q^4} \cdot S$$

This suggests that a folded molecule will have a decay of q^{-4} and scales with the particles surface area, S (Rambo & Tainer, 2011a). For IDP's and flexible molecules the decay or slope of the scattering curve will then decrease to q^{-3} or q^{-2} in the Porod region denoting a

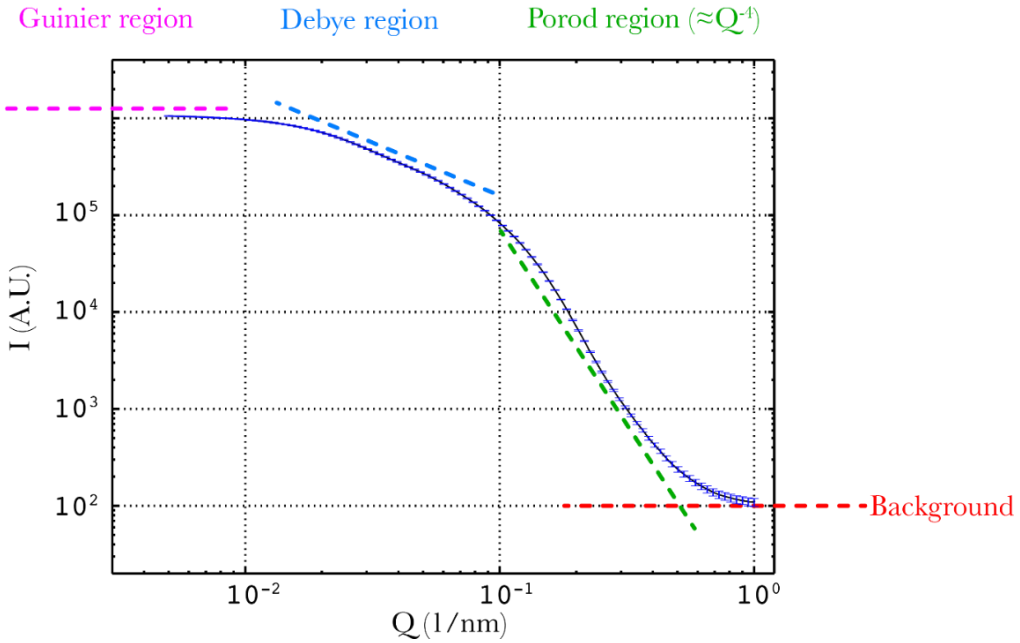

Figure 28. Scattering pattern with positioned Guinier region, Debye region, Porod region. Source of figure Pauw, 2013.

random coil or a mass fractal (Pauw, 2013). Together, these parameters help provide an idea of the average space a molecule occupies, whether folded or disordered (figure 28).

3.1.5. Molecular Weight:

Calculating MW in SAXS is important for validating the size and composition of the sample in solution, but is technically challenging, particularly for disordered proteins and samples of unknown concentration, as is the case for SAXS experiments performed using online size exclusion chromatography. To calculate MW, SAXS data is often compared with a known reference, such as BSA, or calibrated against absolute intensity standards (Mylonas & Svergun, 2007). Extrapolating the linear fit to the Guinier region to q=0 yields the parameter I(0). If no structure factor (S(q)) is present, and there are no interparticle effects or aggregation, the measured I(0) will depend on the molecular mass and the concentration of the protein in the solution (Orthaber et al., 2000).

The molecular weight (MW) of the scattering particle can also be determined using the volume of correlation, V_c:

$$V_c = \frac{I(0)}{\int_0^\infty qI(q) \cdot dq}$$

Where it was found that the relationship of Vc to Rg was proportional to the molecular weight, logarithmically:

$$MW = \left(\frac{V_c^2/R_g}{c}\right)^k$$

Where k and c are empirically defined constants. This estimation is also independent of the protein concentration, so can be used for SEC-SAXS measurements (Rambo & Tainer, 2011).

For samples of structured proteins with no aggregation or interparticle effects and of known concentration, MW estimation is straightforward, though generally accepted to be no better than 10 % accurate (Franke et al., 2018; Mylonas & Svergun, 2007). In contrast, IDPs are more challenging due to their flexible and heterogeneous conformations, leading to poorly estimated molecular weights that are often much larger compared to structured proteins of similar actual MW.

3.1.6. Pair Distance Distribution Function, P(r):

The P(r) describes the distribution of distances between scattering centers, it is essentially a histogram of all the distances within a molecule. It is crucial for constructing accurate structural models and validating the shape and size of the macromolecule in solution (Glatter & Kratky, 1982; Guinier & Fournet, 1955). It helps define the boundaries of the particle and complements other parameters like the radius of gyration (R_g) to provide a more comprehensive understanding of the protein's structure. The P(r) is obtained by an inverse Fourier transform of the SAXS data. To calculate D_{max}, the scattering intensity I(q) is calculated as a function of the scattering vector q, where the D_{max} is the maximum value of r for which P(r) is non-zero.

$$P(r) = \frac{1}{2\pi^2} \int_0^\infty I(q) \cdot qr \cdot \sin(qr) \cdot dq$$

D_{max} represents the maximum particle dimension and indicates the largest distance between any two points within the particle, it represents the overall size of the macromolecule (Glatter & Kratky, 1982; Guinier & Fournet, 1955).

3.1.7. Sample preparation and experimental modes

In Small-Angle X-ray Scattering (SAXS) experiments, good protein sample preparation is crucial for accurate measurements. As detailed above, interpretable SAXS scattering curves require samples to be homogeneous and exhibit little or no aggregation, they should be monodisperse. After protein purification using methods such as affinity chromatography and size-exclusion chromatography (SEC), samples are assessed for purity using SDS-PAGE and UV spectroscopy. Protein concentrations typically range from 2 to 10 mg/mL, but variables including pH, salt concentration, and temperature can affect the homogeneity of the sample and thus the quality of SAXS data (Kikhney & Svergun, 2015). The final purification buffer is also critical and ideally a dialysis step is performed, allowing accurate buffer matching for buffer subtraction in batch mode measurements (Lenton et al., 2022). In SEC-SAXS, proper column equilibration and a stable baseline is necessary for accurate buffer subtraction (Brennich et al., 2017). These modes — batch mode with a robotic temperature-controlled sample changer and an SEC-SAXS mode- are available at beamline BM29 and will be briefly described.

3.1.8. Batch mode

The development of automated sample changers has significantly advanced SAXS measurements, particularly in batch mode. This technology allows semi-high throughput

collection of experimental data from multiple protein samples with high efficiency and eliminates human pipetting errors during sample loading. The robotic sample changer can handle hundreds of individual samples under temperature-controlled conditions, and requires only a small sample volume (30-50 µL). By automating the loading process directly into the capillary, the system reduces the risk of sample loss and increases consistency and reliability in data collection. This setup allows the measurement of approximately 1 sample per 2 minute including buffer measurements and capillary washing between samples, with the time limiting factor the preparation of samples prior to the experiment. Batch mode is often used to determine protein concentrations and buffer requirements for good signal to noise ratios and to detect any potential problems with aggregation, particularly at higher protein concentrations.

3.1.9. SEC-SAXS

Size-exclusion chromatography coupled with small-angle X-ray scattering (SEC-SAXS) is often required for obtaining reliable SAXS data, especially for proteins prone to aggregation. In SEC, molecules are separated based on size as they pass through a column. Larger molecules elute first, followed by smaller ones, allowing for the isolation of monodisperse species, reduced of contaminants or aggregates (Brennich et al., 2017). As the data quality in a SAXS experiment depends on a homogeneous sample, SEC provides an ideal method of sample preparation. These fractions are then directly fed into the SAXS capillary for measurements in the X-ray beam (Inoue et al., 2019; Graewert et al., 2020).

SEC-SAXS is useful for studying challenging macromolecules, such as intrinsically disordered proteins, which often exhibit structural flexibility and have a high tendency to aggregate, particularly at high concentrations or over longer storage times. The method allows for the real-time characterization of the macromolecule as it is purified, avoiding the issues of aggregation or concentration dependent conformational changes seen in batch SAXS measurements (Brennich et al., 2017). Combining chromatography with SAXS measurements is easily performed at the ESRF BM29, which has SEC-SAXS workflows as standard protocols integrated into the data collection software (De Maria Antolinos et al., 2015; Tully et al., 2021). This technique is critical for studying ELF3^{PrD} and mutants under different conditions. While both batch and SEC-SAXS were performed for ELF3^{PrD} and variants, batch measurements were often too aggregated for reliable conclusions and SEC-SAXS provided the necessary purity and homogeneity to characterize ELF3^{PrD}.

3.2. Results and discussion

SAXS experiments were performed on a series of ELF3 constructs spanning the prion-like domain. All ELF3^{PrD} constructs had an N-terminal 6x histidine tag and were recombinantly overexpressed in *E. coli* and purified via affinity chromatography and online size exclusion chromatography to ensure sample homogeneity for all SAXS experiments (SEC-SAXS). ELF3^{PrD}, ELF3$^{PrDΔ470-487}$, ELF3$^{PrDΔ586-596}$, ELF3$^{PrDΔ586-596}$, ELF3^{PrDR597A}, ELF3$^{PrD2xR/A}$ ELF3$^{PrD12xY/Q}$, and ELF3$^{PrD9xH/R}$ samples were purified fractions were checked for purity by SDS PAGE prior to SEC-SAXS experiments and the highest concentration fractions selected for injection onto the online SEC column. Due to the propensity of the ELF3^{PrD} and variants to interact with concentrator membranes, further concentration of the samples was not performed. Based on sequence alignments, the series of deletion mutants and point mutants, presented in Chapter 2, were characterized by SEC-SAXS in order to determine whether the oligomeric state of the protein was affected. The results of these experiments are given in table 2 and the Scattering curves and Kratky plots given in figures 29-35 at the end of the chapter. All deletion mutants tested exhibited scattering curves consistent with large oligomeric species of ~ 30 copies, similar to the ELF3^{PrD} wild type protein. As most of these mutants also underwent LLPS, albeit under different salt and/or pH conditions, it is likely that oligomerization acts as a prerequisite for LLPS, as hypothesized previously (Hutin et al., 2023).

ELF3^{PrD} WT was used as a control for SEC-SAXS experiments as this construct has been well-studied (Hutin et al., 2023). ELF3^{PrD} at a concentration of ~ 5-10 mg/ml was injected onto an online size exclusion column and scattering curves were determined. The protein eluted as a symmetrical single peak after the void volume of the column, indicating the sample was monodisperse and non-aggregated. Analysis of the scattering data provided values for the radius of gyration (R_g, ~ 73 Å) and the maximum dimension (D_{max}, 273 Å). Unexpectedly, the molecular weight suggested that ELF3^{PrD} forms a multimeric assembly (~28-30-mer), confirmed by multi-angle light scattering (figure 29).

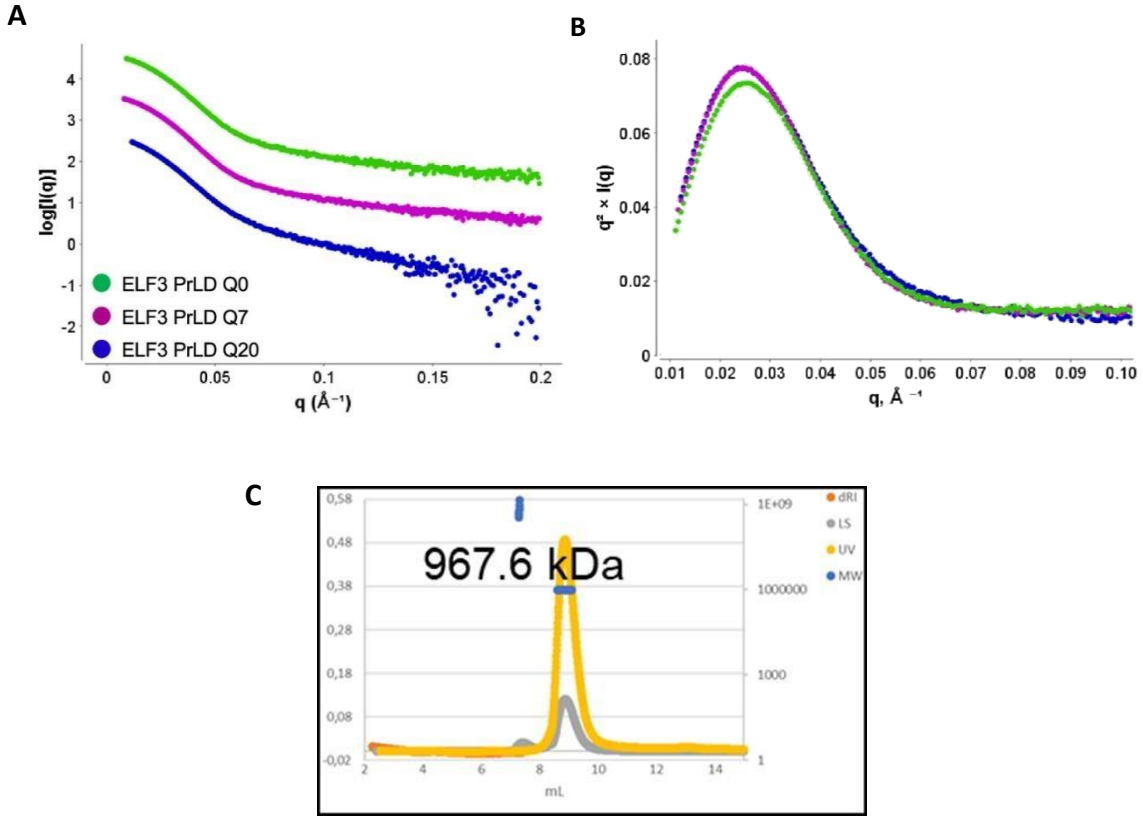

Figure 29. SAXS and SEC-MALLS analysis of ELF3^{PrD}. (A) Scattering curve, **(B)** Kratky plot, **(C)** SEC-MALLS, revealing a ~30-mer oligomer with a globular conformation. Data from Hutin et al., 2023.

SAXS results, indicated that ELF3^{PrD} adopts a relatively globular shape and a large oligomeric state (Figure 29) in contrast to typical extended conformations of intrinsically disordered proteins, suggesting weak multivalent interactions and hydrophobic sequences organize the molecules into an oligomer, even though little secondary structure is predicted for this region of the protein. This compact form might be a precursor to phase separation by ELF3, aligning with prior observations of proteins that undergo liquid-liquid phase separation (Hutin et al., 2023).

A series of ELF3^{PrD} mutants were expressed, purified and characterized using SEC-SAXS (Table 2). Oligomerization of proteins generally requires a folded domain or specific interacting secondary structures forming a geometrically complementary interface (Ali & Imperiali, 2005). Inspection of secondary structure predictions for ELF3^{PrD}, however, revealed the presence of a short β-hairpin and this structural motif was also highly conserved throughout evolution (see Chapter 2). In order to determine whether this region may play an important role in ELF3^{PrD} oligomerization, the ELF3$^{PrDΔ470-487}$ mutant was characterized by SEC-SAXS. In should be noted, as presented in Chapter 2, this mutant was still able to undergo LLPS. SAXS measurements showed a slight, but not significant difference is size of the macromolecule (Figure 30), likely due to the shorter construct that lacks 17 amino acids from the deletion. Interestingly, the β-hairpin does not appear important for 30-mer formation as the SAXS curves and Kratky plot were almost identical to those of ELF3^{PrD}. These data suggest that, while highly conserved, the evolutionary ancient β-hairpin in the prion-like domain of ELF3 does not affect oligomerization.

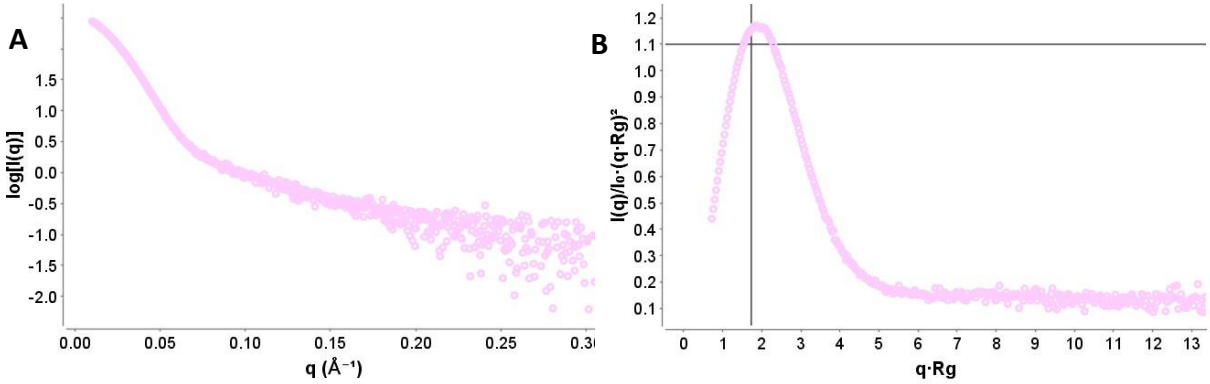

Figure 30. SAXS analysis of ELF3$^{PrDΔ470-487}$ mutant. (A) Scattering curve, **(B)** Kratky plot. The protein forms a large oligomer, similar to ELF3 PrD WT.

ELF3$^{PrD9xH/R}$ mutant, which undergoes LLPS at a higher pH compared to ELF3^{PrD} and was much more prone to precipitation, was also analyzed via SEC-SAXS (Figure 31). The results indicated that the mutant has a similar size and shape, forming a large oligomeric complex of approximately 30 subunits with a globular structure. Thus, the difference in LLPS behavior cannot be attributed to any large structural changes or changes in oligomeric state or shape in the protein.

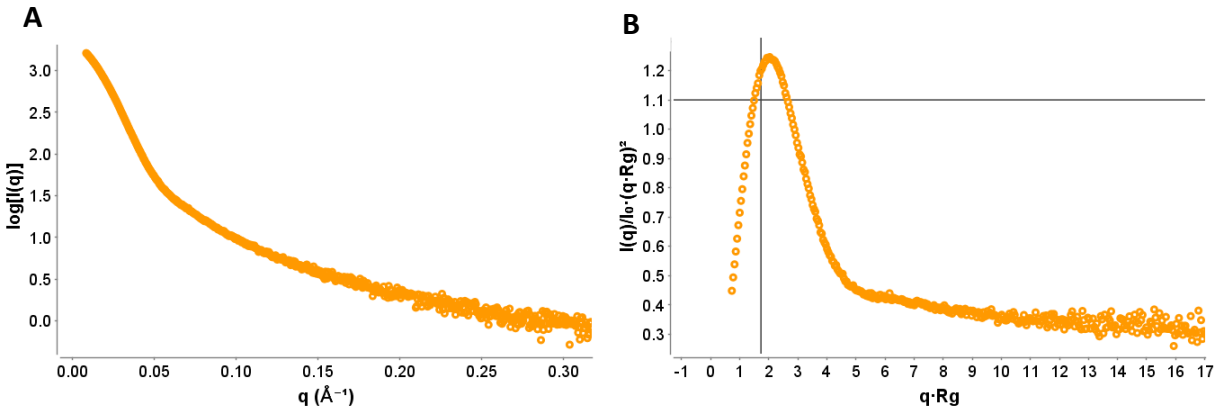

Figure 31. SAXS ELF3$^{PrD9xH/R}$. (A) Scattering SAXS curve and **(B)** Kratky plot. The data indicate that the mutant adopts an oligomeric globular shape, similar to that of the wild-type ELF3 PrD.

One deletion mutant with a significant change in biochemical behavior, with no LLPS observed but a high propensity for aggregation was ELF3$^{PrDΔ586-596}$. This mutant lacks the amino acids flanking the last polyglutamine stretch up to a predicted LARK sequence (figures 32). Despite the strongly altered LLPS behavior, SAXS analysis revealed that this mutant retained a size and shape similar to the WT, forming a large oligomer.

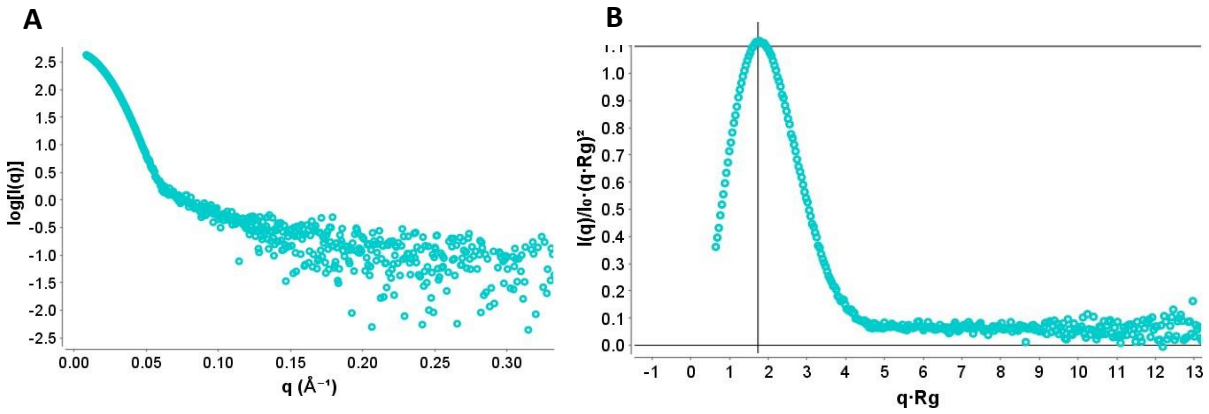

Figure 32. SAXS ELF3 ELF3$^{PrDΔ586-596}$, (A) Scattering SAXS curve (B) Kratky plot. The mutant displays an oligomeric globular conformation.

In order to investigate further the relationship between oligomerization and LLPS, mutants that had very impaired LLPS properties and did not easily precipitate were targeted for SEC-SAXS, as I hypothesized that these mutants were more likely to exhibit changes in oligomeric state. ELF3^{PrDR597A} showed no LLPS at different pHs under high salt (500 mM NaCl) and only underwent LLPS at relatively low salt concentrations as compared to wildtype. The scattering curve for the ELF3^{PrDR597A} mutant displayed no changes in shape compared to ELF3^{PrD}, suggesting the point mutation did not affect the formation of the protein oligomer (Figure 33). The Kratky plot was also nearly identical to the ELF3^{PrD}, further supporting the conclusion that the point mutation did not affect oligomerization or the overall globular form in solution of the 30-mer species.

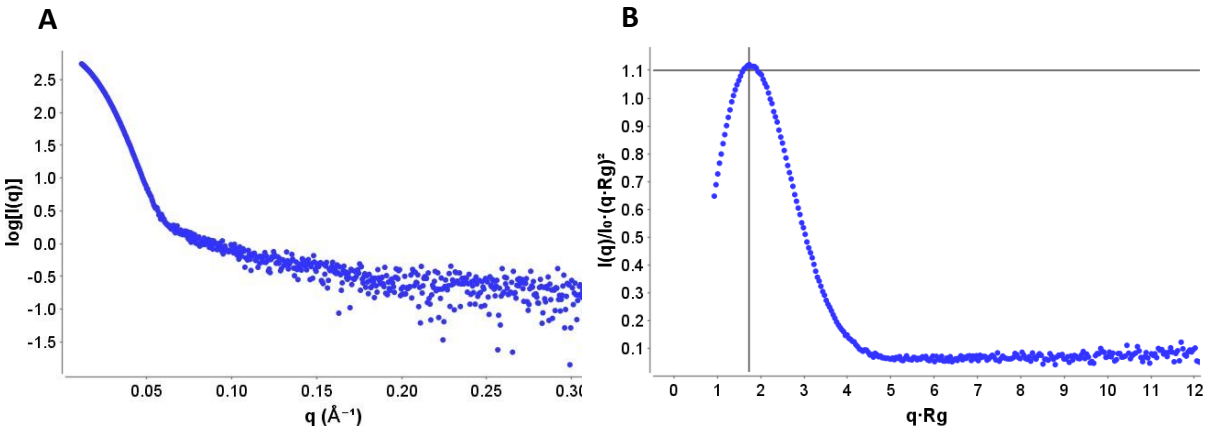

Figure 33. SAXS ELF3^{PrDR597A}. (A) Scattering SAXS curve (B) Kratky plot. The mutant is a large oligomer.

The ELF3$^{PrD2xR/A}$ double point mutant, with mutation positions R592A and R594A, did not undergo LLPS under any of the studied conditions. SEC-SAXS revealed, however, that the solution state ~ 30-mer form was predominant and that there were little or no structural changes in the protein, even though its LLPS behavior was markedly different from the wild type construct (figure 34). This suggests that oligomerization is a very robust property of the ELF3^{PrD} and likely driven by multiple residues and/or motifs, with small deletions and one or two point mutations being insufficient to disrupt oligomer formation.

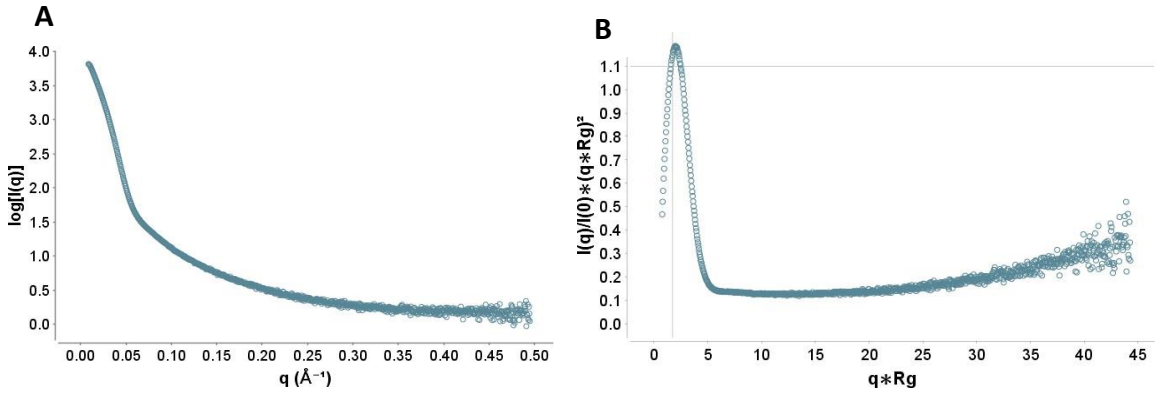

Figure 34. SAXS ELF3 $^{PrD2xR/A}$, (A) Scattering SAXS curve, (B) Kratky plot. The ELF3 $^{PrD2xR/A}$ is a globular ~30-mer.

In an attempt to disrupt the robust oligomerization and thus understand its formation a different mutagenesis strategy was taken. The aim was to disrupt the electrostatic interactions by mutating the tyrosine residues throughout the sequence. were targeted to. Tyrosines contain aromatic rings that enable the stabilizing of protein structures through aromatic π-π interactions, van der Waals forces, and hydrophobic interactions. Tyrosines can also form hydrogen bonds through their hydroxyl groups, π-cation interactions with arginine residues, for example, and often appear in the core of proteins, helping to maintain protein compaction and structure. In order to test the role of tyrosines, a construct replacing 12 tyrosines with glutamine, a disorder-inducing polar amino acid that is more flexible than tyrosine but has some hydrophobic character due to the aliphatic portion of its side chain and is likewise able to participate in hydrogen bonding interactions. Unlike all other constructs tested, ELF3$^{PrD12xY/Q}$ exhibits markedly different scattering curves in SEC-SAXS experiments (figure 35).

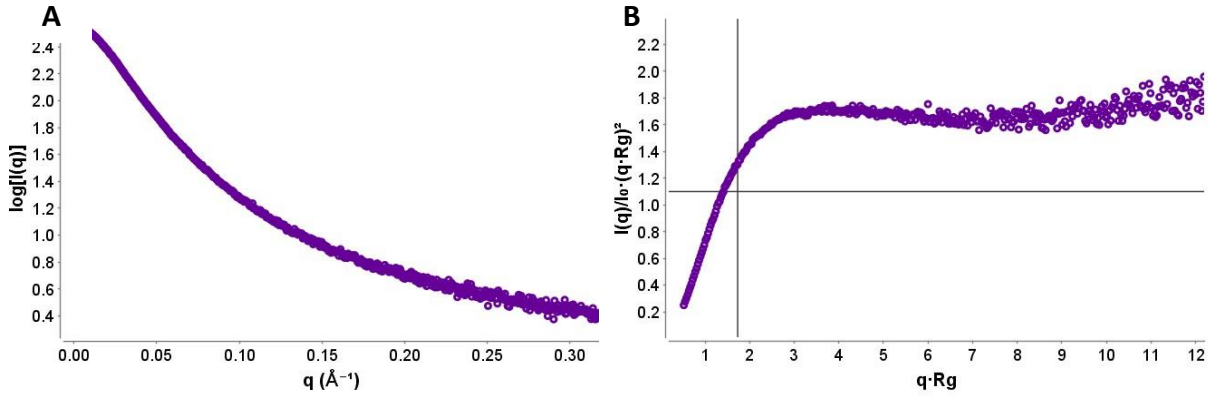

Figure 35. SAXS ELF3$^{PrD12xY/Q}$ (A) Scattering SAXS curve (B) Kratky plot. The mutant exhibits disordered behavior, remaining in a monomeric form.

As described in Chapter 2, ELF3$^{PrD12xY/Q}$ does not undergo LLPS in any condition tested and was not prone to precipitation as were other constructs. In SEC-SAXS, ELF3$^{PrD12xY/Q}$ exhibited scattering characteristic of a monomeric, intrinsically disordered protein. The Guinier region was linear and yielded an R_g of 51.25 Å, significantly smaller than the R_g values of 73.4 Å calculated for the other ELF3^{PrD} variants. The molecular weight estimation was consistent with a monomeric or dimeric species and the Kratky plot yielded a curve typical of an IDP, with a characteristic rise at low values of the scattering vector, q, followed by a plateau or gradual increase at higher q values, unlike the bell-shaped curve seen for globular proteins. This behavior reflects the extended and flexible conformation of IDPs, indicating a lack of stable secondary or tertiary structure. The gradual rise at higher q values suggests a random coil-like behavior, with the protein sampling many conformations in solution. Due to the low accuracy of molecular weight calculations from SAXS, additional studies using SEC-MALS were conducted to determine if ELF3$^{PrD12xY/Q}$ exists as a monomer or a dimer. The SEC-MALS experiment revealed a molecular mass of 29.9 kDa, confirming the presence of a monomer (Appendix, Figure 48).

Table 2. Measured Rg (radius of gyration), Dmax (maximum dimension) and Molecular Weight (MW) for ELF3 PrD mutants, with corresponding curve colors.

	ELF3 PrD mutants	R_g	D_{max}	Oligomeric state	Overall shape	MW approximation, kDa	SEC-MALLS, kDa
	ELF3 PrD	73.4	273	28-30 mer	Globular	1600	967,6
	ELF3 PrD Δ470-487	75.7	302	28-30 mer	Globular	1100	-
	ELF3 PrD 9x H/R	93.54	416	28-30 mer	Globular	1500	-
	ELF3 PrD Δ586-596	77.57	306	28-30 mer	Globular	1400	-
	ELF3 PrD R597A	79.09	277	27-30 mer	Globular	1600	777
	ELF3 PrD 2x R/A	83.7	391	28-30 mer	Globular	1500	-
	ELF3 PrD 12x Y/Q	51.25	187	Monomer	Elongated and disordered	2500	29,9

3.3. Conclusions

SEC-SAXS is particularly useful for proteins prone to aggregation, as it enables online purification by size exclusion chromatography, this ensuring data is collected from monodisperse fractions. The SEC-SAXS analysis of ELF3^{PrD} and variants reveals important insights into the oligomerization and phase separation behavior of the proteins. The SAXS data indicates that the wild-type ELF3^{PrD} forms a large, multimeric oligomer, with a relatively compact structure, suggesting the presence of weak multivalent interactions are sufficient to ensure oligomeric specificity and the formation of a single species in solution, even without predicted secondary structures (Hutin et al., 2023). Most mutations in the ELF3^{PrD}, including a series of deletions, were tolerated and still displayed similar oligomerization patterns, indicating that specific structural motifs, like the β-hairpin motif, are not determinant for the oligomerization state of the protein. This highlights the robustness of ELF3 oligomerization, driven by more extensive interactions rather than individual secondary structure elements. While some point mutants and deletion mutants did affect the LLPS behavior of the protein, as discussed in Chapter 2, they had a much more limited effect on oligomerization, with no significant differences for the ELF3^{PrD} variants except the ELF3$^{PrD12xY/Q}$ variant, which targeted alltyrosine residues in the ELF3 PrD sequence.

Interestingly, targeting the tyrosine residues with glutamine substitutions, demonstrated significant changes in oligomerization behavior and LLPS. The ELF3$^{PrD12xY/Q}$ mutant exhibited characteristics of IDP and was monomeric in solution based on molecular weight estimations by SEC-SAXS and confirmed by SEC-MALLS (Appendix, Figure 48). These results suggest that tyrosine residues are key players in both oligomerization and possibly LLPS, as the ELF3$^{PrD\ 12xY/Q}$ mutant did not undergo LLPS under any tested conditions (Chapter 2). Tyrosine residues have the potential to participate in many different interactions including π-cation interactions with arginine residues (Gupta & Uversky, 2024). It should be noted that different arginine mutations including R597A, and the double arginine mutation, R592A/R594A, exhibited impaired LLPS under the conditions assayed, including varying salt concentrations and lower pH (Chapter 2), suggesting these interactions may be pertinent to phase separation. However, SEC-SAXS demonstrated that arginine mutations do not affect oligomerization. Taken together these data suggest that tyrosine residues drive oligomerization and further participate in LLPS via interactions with arginine residues. These π-cation interactions will be sensitive to pH and ionic strength of the solution and act as determinants of LLPS, whereas they are indispensable for the oligomerization of the protein, as oligomerization still occurs in the arginine mutants. However, it is likely that oligomerization is a prerequisite for LLPS, as the monomeric ELF3$^{PrD12xY/Q}$ mutant was unable to undergo LLPS. The role of oligomerization in physiological activity of ELF3 is unfortunately not known. However, this series of mutants provides important tools for examining the role of oligomerization and LLPS in ELF3 *in vivo* function.

3.4. Materials and Methods

3.4.1. Protein expression and purification

All proteins were expressed and purified as described previously in Chapter 2. Briefly, *E.coli* BL21 (Rosetta2) cells were transformed with the ELF3 pEsprit PrD constructs, selected with 50 µg ml^{-1} kanamycin and grown in small volumes for a preculture. 1L of LB supplemented with 50 µg ml^{-1} kanamycin were inoculated with 10 ml of pre-culture. The cultures were grown at 37°C, 150 rpm until an OD_{600} of 0.8 was reached. The protein expression was induced with 1 mM Isopropyl-β-D-Thiogalactopyranoside (IPTG) at 18° C, 150 rpm overnight. Cells were collected by centrifugation at 4000 x g for 20 min. Bacterial pellets were resuspended in lysis buffer (50 mM Bis-Tris Propane (BTP) pH 9.4, 500 mM NaCl, 20 mM imidazole, 1 mM Tris(2-Carboxyethyl)Phosphine hydrochloride (TCEP)) and 1x complete EDTA-free protease-inhibitor, Roche) at 4 °C. Cells were lysed via sonication, centrifuged at 45,000 x g for 30 min at 4 °C and the supernatant collected. A gravity column was prepared using 1.5 ml of Nickel-sepharose resin which was pre-equilibrated with lysis buffer without protease inhibitors. The supernatant was loaded onto column and washing steps were performed with 50 ml of resuspension buffer and then with 50 ml of a high salt buffer (50 mM BTP, 1 M NaCl, 20 mM imidazole, 1 mM TCEP, pH 9.4) and eluted with 500 µl of elution buffer (50 mM BTP, 1 M NaCl, 300 mM imidazole, 1 mM TCEP, pH 9.4) in 10 fractions. The eluted protein was dialyzed for 2 hours at 4 °C in 50 mM BTP pH 9.4, 1 M NaCl, 1 mM TCEP to remove the imidazole. The protein purity was examined by SDS PAGE and the highest concentration fraction chosen. Proteins

were serially diluted to approximately 2 and 4 mg/ml for batch mode measurements. For SEC-SAXS measurements, the highest concentration of protein (generally ~ 10mg/ml) eluted directly from the Nickel-sepharose column was used directly for on-line size exclusion experiments.

3.4.2. SEC-SAXS

Buffers were degassed on-line and a flow rate of 0.05 ml/min at room temperature was used for all sample runs. Prior to each run the column was equilibrated with at least 5 column volumes of buffer and the baseline monitored. For SEC-SAXS experiments, an online HPLC system (Shimadzu) was attached directly to the sample inlet valve of the BM29 sample changer. Protein samples at 5-10 mg/ml were pipetted into vials and automatically injected onto the column (Superdex 200 3.2/300 Increase GE Healthcare) via an integrated syringe system. Due to column separation of the sample, some dilution effects will occur prior to measurement. 1600 frames (2 sec/frame) were collected.

3.4.3. SAXS data analysis

Initial data processing was performed automatically using the Dahu pipeline, generating integrated, calibrated and normalized 1-D profiles for each frame (Incardona et al., 2009; Kieffer et al., 2022). All frames were then further processed using Scatter IV (Tully et al., 2021), briefly, the frames were dropped into the software and in case of SEC-SAXS 50 – 100 frames selected for the background buffer. Using the heat plot a selection of similar frames were selected and merged. 30 frames corresponding to the highest protein concentration were merged and used for all further data processing and model fitting.

3.4.4. SEC-MALLS

For the ELF3$^{PrD12xY/Q}$ mutant, the calculated MW was confirmed using SEC-MALS (Appendix, Figure 48). The protein was purified via affinity column purification as described and the highest concentration fractions were selected for SEC-MALLS. 50 µl of ELF3$^{PrD12xY/Q}$ at a concentration of ~10 mg/ml was loaded onto an S200 Increase size-exclusion column (Superdex 200 Increase10/300 GL, GE Healthcare) at a flow rate of 0.5 mlmin^{-1}. The column was pre-equilibrated with 50 mM Bis Tris propane (BTP) at pH 9.4, 1 M NaCl, 1 mM TCEP and connected to a Hitachi Elite LaChrom UV detector and LAChrome Pump L-2130, a multi-angle laser light-scattering detector (DAWN HELEOS II, Wyatt Technology Corporation) and a refractive-index detector (Optilab T-rEX, Wyatt Technology Corporation). The data were processed with the OMNISEC software v11 (Malvern Panalytical). All SEC-MALLS experiments were performed as a service via the ISBG platform of the Grenoble within the Grenoble Partnership for Structural Biology (PSB).

References

Ali, M. H., & Imperiali, B. (2005). Protein oligomerization: How and why. Bioorganic & Medicinal Chemistry, 13(17), 5013–5020. https://doi.org/10.1016/j.bmc.2005.05.037

Ayuso-Tejedor, S., Garcia-Fandino, R., Orozco, M., Sancho, J., & Bernado, P. (2011). Structural analysis of an equilibrium folding intermediate in the apoflavodoxin native ensemble by small-angle X-ray scattering. J Mol Biol, 406(4), 604–619. https://doi.org/10.1016/j.jmb.2010.12.027

Barbosa, L. R. S., Spinozzi, F., Mariani, P., & Itri, R. (2013). Small-Angle X-Ray Scattering Applied to Proteins in Solution. In J. M. Ruso & Á. Piñeiro (Eds.), Proteins in Solution and at Interfaces (1st ed., pp. 49–72). Wiley. https://doi.org/10.1002/9781118523063.ch3

Bernado, P., Modig, K., Grela, P., Svergun, D. I., Tchorzewski, M., Pons, M., & Akke, M. (2010). Structure and Dynamics of Ribosomal Protein L12: An Ensemble Model Based on SAXS and NMR Relaxation. Biophys J, 98(10), 2374–2382. https://doi.org/10.1016/j.bpj.2010.02.012

Blanchet, C. E., & Svergun, D. I. (2013). Small-Angle X-Ray Scattering on Biological Macromolecules and Nanocomposites in Solution. Annual Review of Physical Chemistry, 64(1), 37–54. https://doi.org/10.1146/annurev-physchem-040412-110132

Bonomi, M., Heller, G. T., Camilloni, C., & Vendruscolo, M. (2017). Principles of protein structural ensemble determination. Current Opinion in Structural Biology, 42, 106–116. https://doi.org/10.1016/j.sbi.2016.12.004

Brennich, M. E., Round, A. R., & Hutin, S. (2017). Online Size-exclusion and Ion-exchange Chromatography on a SAXS Beamline. Journal of Visualized Experiments, 119, 54861. https://doi.org/10.3791/54861

De Maria Antolinos, A., Pernot, P., Brennich, M. E., Kieffer, J., Bowler, M. W., Delageniere, S., Ohlsson, S., Malbet Monaco, S., Ashton, A., Franke, D., Svergun, D., McSweeney, S., Gordon, E., & Round, A. (2015). ISPyB for BioSAXS, the gateway to user autonomy in solution scattering experiments. Acta Crystallographica Section D Biological Crystallography, 71(1), 76–85. https://doi.org/10.1107/S1399004714019609

Durand, D., Vivès, C., Cannella, D., Pérez, J., Pebay-Peyroula, E., Vachette, P., & Fieschi, F. (2010). NADPH oxidase activator p67phox behaves in solution as a multidomain protein with semi-flexible linkers. Journal of Structural Biology, 169(1), 45–53. https://doi.org/10.1016/j.jsb.2009.08.009

Eliezer, D. (2009). Biophysical characterization of intrinsically disordered proteins. Current Opinion in Structural Biology, 19(1), 23–30. https://doi.org/10.1016/j.sbi.2008.12.004

Franke, D., Jeffries, C. M., & Svergun, D. I. (2018). Machine Learning Methods for X-Ray Scattering Data Analysis from Biomacromolecular Solutions. Biophysical Journal, 114(11), 2485–2492. https://doi.org/10.1016/j.bpj.2018.04.018

Glatter, O., & Kratky, O. (1982). Small angle x-ray scattering.

Gomes, T., Martin-Malpartida, P., Ruiz, L., Aragón, E., Cordeiro, T. N., & Macias, M. J. (2021). Conformational landscape of multidomain SMAD proteins. Computational and Structural Biotechnology Journal, 19, 5210–5224. https://doi.org/10.1016/j.csbj.2021.09.009

Graewert, M. A., Da Vela, S., Gräwert, T. W., Molodenskiy, D. S., Blanchet, C. E., Svergun, D. I., & Jeffries, C. M. (2020). Adding Size Exclusion Chromatography (SEC) and Light Scattering (LS) Devices to Obtain High-Quality Small Angle X-Ray Scattering (SAXS) Data. Crystals, 10(11), 975. https://doi.org/10.3390/cryst10110975

Guinier, A. (1939). La diffraction des rayons X aux très petits angles: Application à l'étude de phénomènes ultramicroscopiques. Annales de Physique, 11(12), 161–237. https://doi.org/10.1051/anphys/193911120161

Guinier, A., & Fournet, G. (1955). SMALL-ANGLE SCATTERING OF X-RAYS.

Gupta, M. N., & Uversky, V. N. (2024). Reexamining the diverse functions of arginine in biochemistry. Biochemical and Biophysical Research Communications, 705, 149731. https://doi.org/10.1016/j.bbrc.2024.149731

Hutin, S., Kumita, J. R., Strotmann, V. I., Dolata, A., Ling, W. L., Louafi, N., Popov, A., Milhiet, P.-E., Blackledge, M., Nanao, M. H., Wigge, P. A., Stahl, Y., Costa, L., Tully, M. D., & Zubieta, C. (2023). Phase separation and molecular ordering of the prion-like domain of the Arabidopsis thermosensory protein EARLY FLOWERING 3. Proceedings of the National Academy of Sciences, 120(28), e2304714120. https://doi.org/10.1073/pnas.2304714120

Incardona, M. F., Bourenkov, G. P., Levik, K., Pieritz, R. A., Popov, A. N., & Svensson, O. (2009). EDNA: a framework for plugin-based applications applied to X-ray experiment online data analysis. J Synchrotron Radiat, 16(Pt 6), 872–879. https://doi.org/10.1107/S0909049509036681

Inoue, R., Nakagawa, T., Morishima, K., Sato, N., Okuda, A., Urade, R., Yogo, R., Yanaka, S., Yagi-Utsumi, M., Kato, K., Omoto, K., Ito, K., & Sugiyama, M. (2019). Newly developed Laboratory-based Size exclusion chromatography Small-angle x-ray scattering System (La-SSS). Scientific Reports, 9(1), 12610. https://doi.org/10.1038/s41598-019-48911-w

Kieffer, J., Brennich, M., Florial, J. B., Oscarsson, M., De Maria Antolinos, A., Tully, M., & Pernot, P. (2022). New data analysis for BioSAXS at the ESRF. Journal of Synchrotron Radiation, 29(Pt 5), 1318–1328. https://doi.org/10.1107/S1600577522007238

Kikhney, A. G., & Svergun, D. I. (2015). A practical guide to small angle X-ray scattering (SAXS) of flexible and intrinsically disordered proteins. FEBS Letters, 589(19 Pt A), 2570–2577. https://doi.org/10.1016/j.febslet.2015.08.027

Kratky, O., & Porod, G. (1949). Röntgenuntersuchung gelöster Fadenmoleküle. Recueil Des Travaux Chimiques Des Pays-Bas, 68(12), 1106–1122. https://doi.org/10.1002/recl.19490681203

Lenton, S., Tully, M. D., & Skepö, M. (2022). From dilute to concentrated solutions of intrinsically disordered proteins: Sample preparation and data collection. In Methods in Enzymology (Vol. 677, pp. 457–478). Elsevier. https://doi.org/10.1016/bs.mie.2022.08.036

Meisburger, S. P., Taylor, A. B., Khan, C. A., Zhang, S., Fitzpatrick, P. F., & Ando, N. (2016). Domain Movements upon Activation of Phenylalanine Hydroxylase Characterized by Crystallography and Chromatography-Coupled Small-Angle X-ray Scattering. Journal of the American Chemical Society, 138(20), 6506–6516. https://doi.org/10.1021/jacs.6b01563

Mertens, H. D. T., & Svergun, D. I. (2017). Combining NMR and small angle X-ray scattering for the study of biomolecular structure and dynamics. Archives of Biochemistry and Biophysics, 628, 33–41. https://doi.org/10.1016/j.abb.2017.05.005

Mylonas, E., & Svergun, D. I. (2007). Accuracy of molecular mass determination of proteins in solution by small-angle X-ray scattering. Journal of Applied Crystallography, 40(s1), s245–s249. https://doi.org/10.1107/S002188980700252X

Orthaber, D., Bergmann, A., & Glatter, O. (2000). SAXS experiments on absolute scale with Kratky systems using water as a secondary standard. Journal of Applied Crystallography, 33(2), 218–225. https://doi.org/10.1107/S0021889899015216

Pauw, B. R. (2013). SAXS regions. Looking at Nothing. https://lookingatnothing.com/index.php/archives/846

Pelikan, M., Hura, G., & Hammel, M. (2009). Structure and flexibility within proteins as identified through small angle X-ray scattering. General Physiology and Biophysics, 28(2), 174–189. https://doi.org/10.4149/gpb_2009_02_174

Putnam, C. D., Hammel, M., Hura, G. L., & Tainer, J. A. (2007). X-ray solution scattering (SAXS) combined with crystallography and computation: Defining accurate macromolecular structures, conformations and assemblies in solution. Quarterly Reviews of Biophysics, 40(3), 191–285. https://doi.org/10.1017/S0033583507004635

Rambo, R. P., & Tainer, J. A. (2011a). Characterizing flexible and intrinsically unstructured biological macromolecules by SAS using the Porod-Debye law. Biopolymers, 95(8), 559–571. https://doi.org/10.1002/bip.21638

Rambo, R. P., & Tainer, J. A. (2013). Accurate assessment of mass, models and resolution by small-angle scattering. Nature, 496(7446), 477–481. https://doi.org/10.1038/nature12070

Tompa, P. (2011). Unstructural biology coming of age. Current Opinion in Structural Biology, 21(3), 419–425. https://doi.org/10.1016/j.sbi.2011.03.012

Tully, M. D., Tarbouriech, N., Rambo, R. P., & Hutin, S. (2021a). Analysis of SEC-SAXS data via EFA deconvolution and Scatter. Journal of Visualized Experiments, 167, 61578. https://doi.org/10.3791/61578

Watanabe, Y., & Inoko, Y. (2009). Size-exclusion chromatography combined with small-angle X-ray scattering optics. Journal of Chromatography A, 1216(44), 7461–7465. https://doi.org/10.1016/j.chroma.2009.02.053

Zheng, W., & Best, R. B. (2018). An Extended Guinier Analysis for Intrinsically Disordered Proteins. Journal of Molecular Biology, 430(16), 2540–2553. https://doi.org/10.1016/j.jmb.2018.03.007

CHAPTER 4 Characterization of ELF3 plant mutants

4.1. Introduction

In *A. thaliana*, ELF3 is a key regulator of the circadian clock, photoperiodic flowering, and thermomorphogenesis. *ELF3* is highly expressed in various tissues, including rosette leaves, cauline leaves, inflorescence stems, apices, and siliques (Hicks, 2001). In the cotyledons, *ELF3* is highly expressed in the vasculature cells and lowly expressed in the mesophyll cells. Transcription of *ELF3* peaks at dusk and is controlled by the internal circadian clock and external light signals. Introduction of a premature stop codon in the *elf3-1* mutant results in a loss-of-function phenotype characterized by changes in impaired clock function, elongated hypocotyls and petioles, smaller leaf number and leaf blade and early flowering (Zagotta et al., 1996). Wild type *Arabidopsis* plants are capable of maintaining a stable ~ 24 hours oscillation rhythm of gene expression under constant light or dark conditions due to their circadian clock. However, in *elf3-1* mutants, this rhythmicity is disrupted under continuous light conditions, rendering the plants arrhythmic and unable to sustain the ~ 24 hour cycle. Interestingly, this arrhythmia does not occur under continuous darkness, highlighting the role of ELF3 in mediating light input to the circadian clock (Hicks et al., 1996). Hypocotyl elongation is significantly increased in the *elf3-1* mutant compared to wild-type plants (Zagotta et al., 1996). This resembles the phenotype of wild-type plants grown at elevated ambient temperatures, where ELF3 loss mimics warm-temperature signaling responses. ELF3 normally represses elongation in light-grown plants, but the *elf3-1* mutation removes this repressive function, causing elongation similar to high-temperature growth responses (Nieto et al., 2015). As the *elf3-1* mutant plant develops, petiole elongation is also evident, in contrast to the shorter petioles observed in wild-type plants grown under the same conditions (Figure 36). This elongation is accompanied by a reduction in leaf blade size, resulting in smaller and narrower leaves compared to wild-type plants (Figure 30). *elf3-1* plants initiate flowering after producing only 7-10 rosette leaves. As flowering progresses, the *elf3-1* mutant shows elongated and thinner inflorescence stems compared to Col-0 plants, caused by excessive cell elongation.

Figure 36. *Arabidopsis thaliana* Col-0 and *elf3-1* mutant plants. Loss of function of the ELF3 gene in *elf3-1* mutants results in phenotypic changes such as elongated shoots and early flowering, compared to the wild-type Col-0 plants. Plants were grown at 22° C under SD conditions.

Many of these phenotypic traits are due to the disruption of the activity of the Evening Complex (EC). As part of the EC, a three-protein repressive complex consisting of the DNA-binding protein, LUX ARRYTHMO (LUX) and the small alpha helical protein, ELF4, ELF3 helps maintain circadian rhythms and acts as an essential component of the clock (Helfer et al., 2011; Herrero et al., 2012; Hicks, 2001; Nusinow et al., 2011). LUX possesses a single ~ 60 amino acid MYB DBD, which folds into a characteristic three-helix bundle conformation. The protein binds DNA primarily through a helix that lies in the major groove and contains a plant-specific GARP family (named for GOLDEN2 from maize, ARR B-class from *Arabidopsis* and Psr1 from *Chlamydomonas*) signature motif, SH(A/L)QK(F/Y) (Silva et al., 2016). LUX is able to bind DNA with high affinity, ~ 100 nM, and target the EC to specific sites in the genome (Silva et al., 2020). The rest of the protein is predicted to be disordered. ELF4 is a small, ~ 100 amino acid alpha helical protein that is predicted to fold into a coiled-coil (Kolmos et al., 2009). As described in the previous chapters, ELF3 is largely disordered with some limited alpha-helical secondary structure in the middle of the protein, likely important for binding to LUX and ELF4. The EC represses some morning, day and evening phased genes, thus helping to ensure accurate timing of physiological processes and rhythmic oscillations in gene expression over a
~ 24 hour period (Helfer et al., 2011; Nusinow et al., 2011). The EC also directly regulates clock outputs, including PIF4, a major regulator of elongation growth, shade avoidance and thermomorphogenesis (Raschke et al., 2015).

ELF3 forms complexes with other proteins in addition to LUX and ELF4, including hormone biosynthesis regulators and transcription factors, thus enabling the transcriptional repression of diverse targets, in addition to EC targets (Table 4). For example, ELF3 localizes to photobodies to help regulate photoperiodic flowering in *Arabidopsis* by forming different protein-protein complexes (C. Kim et al., 2023). For example, ELF3 directly interacts with the red-light photoreceptor, PHYB, GI and the ubiquitin E3-ligase CONSTITUTIVE PHOTOMOPHOGENESIS 1 (COP1). A ELF3-COP1-GI complex leads to the degradation of ELF3 and GI, whereas the phyB - COP1 interaction inhibits COP1 activity, allowing the accumulation of ELF3 and GI (Yu et al., 2008). ELF3 also directly interacts with phyB, which stabilizes ELF3 in the evening under long-day conditions. In short-day conditions, reduced phyB activity leads to lower ELF3 stability, allowing GI-mediated *CO* expression, which induces flowering (Kubota et al., 2017). However, in short days, the light period is too short for CO to accumulate during the day, and it is degraded in the dark. This prevents CO from activating FT, leading to delayed flowering. As a result, *Arabidopsis* flowers later under short-day conditions because CO is not able to induce FT effectively in the shorter photoperiod (Song et al., 2018). ELF3 also competes with PIFs for binding to phyB. The PIF-phyB interaction leads to the phosphorylation of PIFs by kinases such as PHOTEREGULATORY PROTEIN KINASES (PPKs), and the phosphorylated PIFs subsequently undergo polyubiquitination by ubiquitin E3 ligases, such as BLADE-ON-PETIOLE (BOPs) for PIF4, and are then degraded by the 26S proteasome (Zhang et al., 2017). ELF3 directly interacts with PIF4, preventing it from binding to its target sequences, adding an additional layer of regulation to PIF4 activity (Nieto et al., 2015). The ELF3 interactions with different partners are crucial for photoperiodic regulation of flowering time in response to changing light conditions and acts as a signaling hub. These studies also suggest that ELF3 may function in large signaling complexes, participating in both protein degradation to indirectly alter downstream transcriptional outputs and direct transcriptional control through the formation of repressive complexes.

As part of the EC and as a direct interactor of PIF4, ELF3 plays an important role in thermosensing. The EC binds DNA in a temperature-dependent manner and regulates plant growth, with natural variation in EC components, particularly in ELF3, linked to altered thermal responses in *Arabidopsis* and crop plants (Andrade et al., 2022; Jung et al., 2020). For example, a tryptophan to glycine mutation at position 669 in ELF3 from *Hordeum vulgare* (barley) results in an early flowering phenotype (Zahn et al., 2023). This mutation is in the region of ELF3 that interacts with PIF4 and might disrupt this interaction (Nieto et al., 2015; Raschke et al., 2015).

Table 3. List of confirmed ELF3 interactors identified with physical methods, excluding genetic interaction evidence

ELF3 interactors	Interactors name	Experimental Technique	Molecular Function	References
ARF16	Auxin response factor 16	Y2H	Unknown	(Sun et al., 2020)
ARR6	Two-component response regulator ARR6	Y2H	Unknown	(Sun et al., 2020)
BBX18	B-box zinc finger protein 18	Y2H, pull down	Recruitment of ELF3 for COP1-mediated degradation	(Ding et al., 2018)
BBX19	B-box zinc finger protein 19	Y2H	Recruitment of ELF3 for COP1-mediated degradation	(C.-Q. Wang et al., 2015)
BBX23	B-box zinc finger protein 23	Y2H, pull down	Recruitment of ELF3 for COP1-mediated degradation	(Ding et al., 2018)
COP1	E3 ubiquitin-protein ligase COP1	Y2H, AP-MS	Degrade ELF3	(Huang et al., 2016a; Yu et al., 2008b)
CRF1	thylene-responsive transcription factor CRF1	Y2H	Unknown	(Sun et al., 2020)
CTR1	Serine/threonine-protein kinase CTR1	Y2H	Unknown	(Sun et al., 2020)
EIL1	ETHYLENE INSENSITIVE 3-like 1 protein	Y2H	Unknown	(Sun et al., 2020)
ELF4	EARLY FLOWERING 4	Y2H, Co-IP	Evening complex formation	(Choudhary et al., 2015; Herrero et al., 2012; Nusinow et al., 2011b)
ERF1	thylene-responsive transcription factor 1	Y2H	Unknown	(Sun et al., 2020)
GI	Gigantea	Y2H	COP1-mediated degradation of GI	(Yu et al., 2008a)
IAA16	Auxin-responsive protein IAA16	Y2H	Unknown	(Sun et al., 2020)
IAA3	Auxin-responsive protein IAA3	Y2H	Unknown	(Sun et al., 2020)

ELF3 interactors	Interactors name	Experimental Technique	Molecular Function	References
LUX	LUX ARRHYTHMO	Y2H, Co-IP	Evening complex formation DNA binding Transcription factor	(Huang et al., 2016a; Nusinow et al., 2011b)
PhyB	Phytocrome B	Y2H, AP-MS	Stabilize ELF3 during daytime	(Huang et al., 2016a; Liu et al., 2001)
PIF4	Phytochrome-interacting factor 4	Y2H, AP-MS, BiFC	Inhibit PIF4 binding to target genes	(Huang et al., 2016a; Nieto et al., 2015)
PIF7	Phytochrome-interacting factor 7	AP-MS, BiFC, Co-IP	Inhibit PIF7 binding to target genes	(Huang et al., 2016a; Y. Jiang et al., 2019)
TIC	Time for coffee	AP-MS	Unknown	(Huang et al., 2016a)
TOC1	Two-component response regulator-like APRR1	Y2H, AP-MS	Unknown	(Huang et al., 2016a)
XBAT31	Putative E3 ubiquitin-protein ligase XBAT31	Y2H, Co-IP	XBAT31-mediating ELF3 degradation	(L.-L. Zhang et al., 2024)
XBAT35	Putative E3 ubiquitin-protein ligase XBAT35	Co-IP, Pull down	XBAT35-mediating ELF3 degradation	(Zhang et al., 2021)

Furthermore, studies investigating the functional conservation of ELF3 across species have provided important insights and understanding of its role in thermal responsiveness (Jung et al., 2020; Zhu et al., 2023). *elf3* mutants transformed with a chimera construct expressing the N-terminal AtELF3 sequence with the C-terminal of ELF3 from *Brachypodium distachyon*, which lacks a predicted PrD, revealed that this substitution led to temperature insensitivity in *Arabidopsis.* This is probably due to a more active EC that no longer exhibits temperature dependent DNA binding (Jung et al., 2020). This finding suggests that the PrD region in ELF3 plays a crucial role in enabling plants to adapt their growth and flowering behavior to varying temperatures (Box et al., 2015; Raschke et al., 2015; Huang et al., 2016).

Increased ambient, growth permissive temperatures induce changes in development including accelerated growth, elongated hypocotyls, increased petiole length, fewer leaves, and early flowering (Box et al., 2015; Raschke et al., 2015). This adaptive response underscores the importance of temperature sensing in plant development. The molecular mechanisms of ELF3-mediated temperature sensing, as discussed in the previous thesis chapters, is likely due to LLPS of ELF3 that occurs as a function of increasing temperature (Jung et al., 2020). LLPS prevents the formation and/or DNA-binding of the EC, resulting in de-repression of EC target genes, such as *PIF4* (Hutin et al., 2024; Silva et al., 2020). Upon exposure to higher ambient temperatures, ELF3 undergoes reversible LLPS, a process driven by its PrD. When ELF3 forms condensates, it temporarily inhibits EC functions, leading to the de-repression of target genes involved in temperature-responsive growth (Jung et al., 2020) (Figure 13). This dynamic

regulation allows ELF3 to act as both a scaffold for transcription factor binding and a key mediator of temperature-driven developmental changes (Nieto et al., 2015; Zhao et al., 2021). In addition, ELF3 directly interacts with PIF4 and PIF7 proteins, key regulators of plant growth and development (Nieto et al., 2015; Y. Jiang et al., 2019). As PIFs integrate signals from light, temperature, and hormone pathways to control processes such as senescence, seed development, and fruit formation, changes in their stability and activity due to ELF3 binding has dramatic developmental effects (Khanna et al., 2004; Sharma et al., 2023). In darkness or shade, PIFs promote elongation of hypocotyls, petioles, and stems by activating growth pathways (Leivar & Quail, 2011). Conversely, under light conditions, due to binding and being phosphorylated by phytochromes, PIFs are rapidly degraded, leading to suppressed growth (Galvão et al., 2019; L. Li et al., 2012; Willige et al., 2021; C. Yang et al., 2021). ELF3 has been shown to add an additional layer of regulation by sequestering the PIF4 protein and preventing its ability to activate target genes (Nieto et al., 2015). PIF4 and PIF7 form heterodimers and interact with ELF3, suggesting ELF3 may also regulate PIF7 in a similar manner (Fiorucci et al., 2020).

Here, we tested whether different ELF3 mutants ($ELF3^{R597A}$ and $ELF3^{12xY/Q}$), which have altered *in vitro* phase separation and/or oligomerization, could still form a complex with LUX and ELF4, whether this complex could bind DNA, and if it exhibited temperature-sensitive DNA binding. We further examined the activity of these *ELF3* mutants *in planta* in the *elf3-1* mutant background to correlate *in vitro* phase separation and oligomerization with phenotype under different growth temperatures. While *in vitro* DNA-binding assays demonstrated binding to an EC target sequence for both mutants, $ELF3^{12xY/Q}$ exhibited binding at 4°C and room temperature whereas $ELF3^{R597A}$ exhibited a very similar binding profile as to WT, with robust binding at 4°C and strongly reduced binding at room temperature. The *in vitro* DNA-binding results suggest that $ELF3^{R597A}$ should complement the *elf3-1* phenotype, restoring WT-like activity with shorter hypocotyls and restored thermomorphogenesis. T1 *elf3-1* transgenic plants constitutively expressing $ELF3^{R597A}$ exhibited partial restoration of the hypocotyl and flowering time phenotypes. Surprisingly, no rescue was observed in *elf3-1* plants expressing $ELF3^{12xY/Q}$. Western blots showed no detectable protein for $ELF3^{12xY/Q}$, suggesting oligomerization and phase separation might be essential for stabilizing ELF3 *in planta*.

4.2. Results and discussion

4.2.1. *In vitro* EC reconstitution and DNA binding

The Evening Complex has been shown to bind DNA in a temperature-dependent manner, both *in vitro* and *in vivo* (Hutin et al., 2024; Jung et al., 2020; Silva et al., 2020). LUX possesses a DNA-binding domain (DBD), and this is essential for EC binding as neither ELF3 nor ELF4 possess a DBD (Helfer et al., 2011; Silva et al., 2016, 2020). LUX can also bind DNA independently of the EC, however LUX alone is not sufficient for gene regulation (Silva et al., 2020). Interestingly, while not involved in direct interactions with DNA, ELF3 is able to modulate EC binding in a temperature-dependent manner via LLPS, as discussed in the preceding chapters. In order to correlate LLPS with DNA binding *in vitro*, LUX, ELF4, ELF3^{WT}-mCherry, ELF3^{R597A}-mCherry and ELF3$^{12xY/Q}$-mCherry were recombinantly expressed, purified and used for EC reconstitution and DNA binding experiments.

ELF3^{WT}-mCherry, ELF3^{R597A}-mCherry and ELF3$^{12xY/Q}$-mCherry were produced using a codon optimized construct with an mCherry tag for easier monitoring of protein expression and purification. The mCherry fluorescent tag is highly stable, retaining its folded structure even in 8 M urea for over 24 hours, allowing mCherry-containing protein fractions to maintain their bright pink color, thus confirming successful purification. LUX and ELF4 were expressed and purified under native conditions, as previously reported (Silva et al., 2020). To form the EC with either ELF3^{WT}-mCherry, ELF3^{R597A}-mCherry or ELF3$^{12xY/Q}$-mCherry, denaturing conditions were used, (Hutin et al., 2024). The concentration of each protein sample was measured and ELF3, LUX and ELF4 were mixed together in a ratio 1:1:1.2 under denaturing conditions for EC reconstitution. Stepwise dialysis was used to decrease the urea concentration from 8 M to 1 M. In 1 M urea, the proteins should be refolded, but the low urea concentrations help avoid non-specific interactions and maintain the proteins in solution by reducing aggregation.

To investigate whether the ELF3^{R597A} and ELF3$^{12xY/Q}$ are able to interact with LUX and ELF4 and form a complex able to bind DNA, EMSA experiments were conducted. A 36 base pair Cy-5 labelled DNA from the *PRR9* promoter was used as a probe, as this sequence had been previously shown to bind to the wild type EC (Silva et al., 2020). ECs, consisting of LUX, ELF4 and either ELF3^{WT}-mCherry, ELF3^{R597A}-mCherry or ELF3$^{12xY/Q}$-mCherry were used at a concentration of approximately 1000 nM, with a DNA concentration of 10 nM. EC and Cy5-DNA were mixed and incubated on ice or at room temperature for 2 hours. The complexes were then run on a 2% agarose gel either at 4°C or room temperature and visualized based on the Cy-5 fluorescence (Figure 37). EC reconstituted with ELF3^{R597A} or ELF3^{WT} exhibited the same DNA band shift pattern, with binding at 4° C and no detectable binding at room temperature. These results suggest that ELF3^{R597A} may behave similarly to wild type ELF3 *in vivo* as well as *in vitro*. In contrast, ELF3$^{12xY/Q}$ was still able to bind DNA at room temperature, albeit with decreased intensity of the shifted bands. At 4°C, all three ELF3 constructs bound with similar intensity.

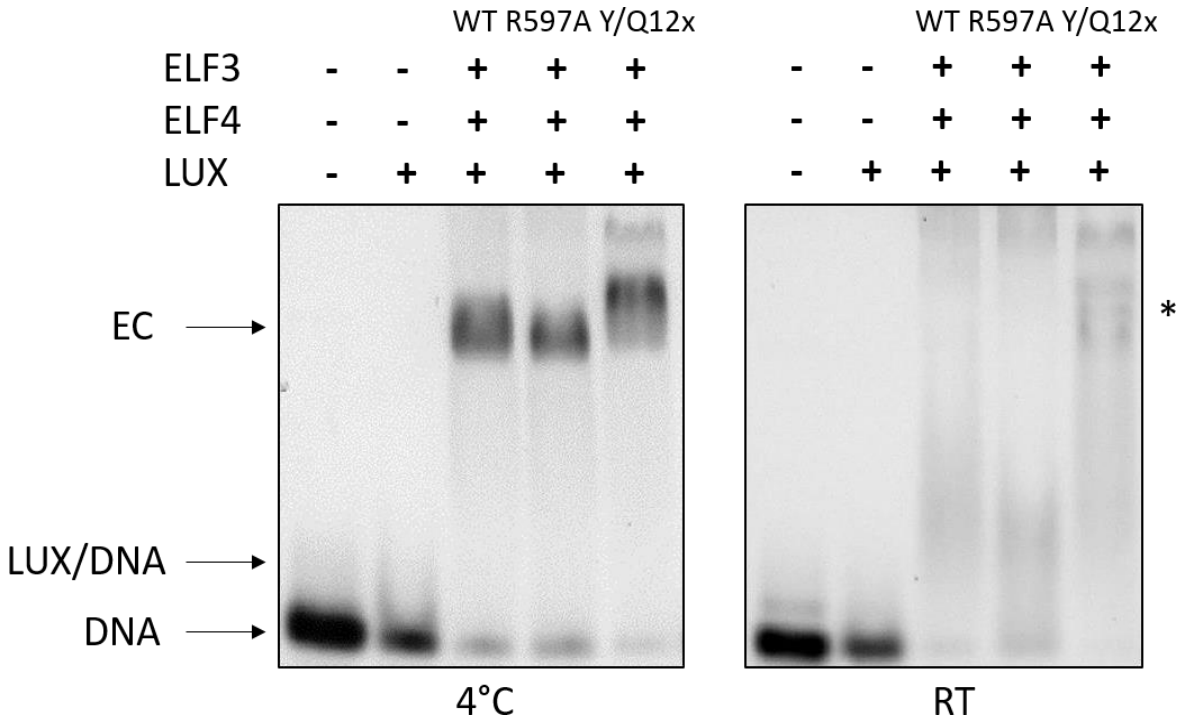

Figure 37. Interaction of Evening Complex and LUX with DNA. On the left, an EMSA was performed using a 2% agarose gel to examine DNA binding with LUX, the EC reconstituted with wild-type (WT) ELF3, and EC containing the ELF3 mutants **R597A** and **Y/Q 12x**. The experiment was conducted at 4°C, and a supershift was observed for each ELF3 variant. On the right, the experiment was repeated at room temperature (RT). At this temperature, the EC containing WT ELF3 and the **R597A** mutant did not bind DNA. However, the **12x Y/Q** mutant, marked with an asterisk, retained its DNA binding ability at RT, demonstrating less temperature sensitive binding of this mutant.

The ELF3^{PrDR597A} construct was oligomeric in the dilute phase and underwent some phase separation, albeit at lower salt and pH than the WT PrD (see Chapter 3, Figure 24). However, the EMSA conditions were under relatively low salt (150mM NaCl) and pH of 7.5, within the condensation/aggregation range of the PrD from both WT and ELF3^{PrDR597A} and the behavior of the full-length ELF3 constructs was consistent with these observations. ELF3$^{PrD12xY/Q}$ was monomeric in solution and was not able to undergo LLPS under any tested condition. Based on this, it was predicted that ELF3$^{12xY/Q}$-mCherry would likewise be monomeric in solution and not be sequestered away from the EC by LLPS higher temperatures. Indeed, the data are consistent with the observed DNA binding behavior in EMSAs when comparing ELF3$^{12xY/Q}$-mCherry to WT or ELF3^{R597A}-mCherry at room temperature. The EC with ELF3$^{12xY/Q}$-mCherry was still able to bind DNA, suggesting a more active complex that *in vivo* may still be able to inhibit its target genes even at higher temperatures. To determine whether this was indeed the case, *elf3-1* plants were transformed with ELF3^{WT}, ELF3$^{12xY/Q}$ and ELF3^{R597A,} and the phenotypes were determined.

4.2.2. Plant phenotypes

This investigation aimed to determine the minimal number of tyrosine mutations needed to alter ELF3 behavior. *In vitro*, ELF3$^{PrD12xY/Q}$ mutations disrupted LLPS, keeping ELF3

PrD in a monomeric or dimeric state. However, when labeled with GFP, it was revealed that ELF3$^{PrD7xY/Q\text{-}GFP}$ seemed to prevent LLPS while maintaining the oligomeric form (Appendix, Figure 46). *elf3-1* plants were transformed with ELF3*pro::ELF3*$^{7xY/Q}$ and ELF3*pro::ELF3*$^{7xY/Q}$*-GFP* constructs, which were cloned by Audrey Guillotin. Transformants in generation T2 were grown at 17°, 22° and 27° C on MS plates. After six days post-germination, hypocotyl lengths were measured to assess temperature-dependent phenotypes. *elf3-1* seedlings expressing the WT *ELF3, ELF3*$^{7xY/Q}$ and *ELF3*$^{7xY/Q\text{-}GFP}$ under the native promoter complemented the loss of function *elf3-1* phenotype*,* largely restoring hypocotyl temperature sensitivity (Figure 38). In contrast, the *ELF3*$^{7xY/Q\text{-}GFP}$ construct exhibited a different phenotype. At 17° C and 22° C, plants displayed hypocotyl length comparable to the WT, but at 27° C, the hypocotyls were significantly elongated. These results suggest that while the Y/Q 7x mutant retains its ability to undergo LLPS and maintain an oligomeric state without altering the plant phenotype the addition of the GFP tag affects its LLPS behavior, thus the phase separation dynamics and potential interactions with other proteins, which leads to hypocotyl elongation at high ambient temperature.

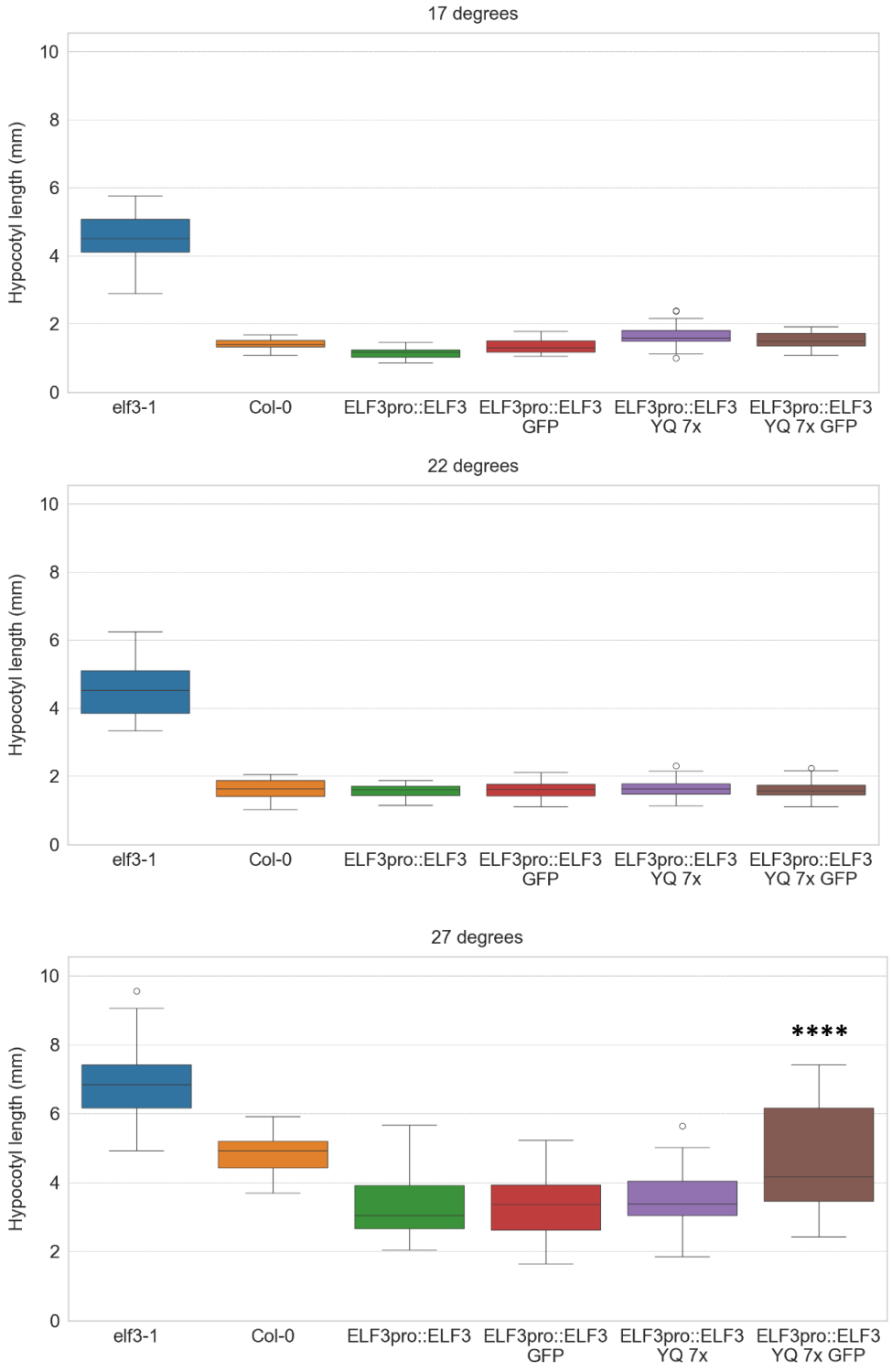

Figure 38. Hypocotyl length measurements. Seedlings of *elf3-1*, Col-0, *elf3*-expressing ELF3*pro::ELF3*, ELF3*pro::ELF3 GFP*, ELF3*pro::ELF3 Y/Q 7x* and ELF3*pro::ELF3 Y/Q 7x GFP* were grown after germination at **(A)** 17°C showing that the transformed seedlings resemble Col-0 as similar to (**B)** at 22°C; but at (**C)** 27°C the hypocotyls of ELF3*pro::ELF3 Y/Q* were significantly elongated. Statistics performed by Mann-Whitney U, comparing each genotype to controls, ****$p < .001$ n =42.

Due to difficulties in generating the large genomic constructs with native promoter and terminator, a simpler method was designed. Based on the ability of the *35S* promoter and cDNA construct for WT *ELF3* to complement much of the *elf3-1* mutant phenotype (Hicks, 2001; Zagotta et al., 1996), these technically simpler constructs were used to investigate the effects of ELF3$^{12xY/Q}$ and ELF3^{R597A} *in planta*. *elf3-1* plants were transformed with 35S*pro::ELF3*, 35S*pro::ELF3^{R597A}* and 35S*pro::ELF3$^{12xY/Q}$* in a GFP selection vector that expresses GFP in the seed coat, allowing for easy visual selection of transformants. Positive transformants were selected and T1 seedlings were grown on MS plates at 17° C, 22° C and 27° C for six days post- germination, and their hypocotyl lengths were measured.

The results revealed that *elf3-1* seedlings expressing *ELF3* had hypocotyl lengths comparable to Col-0, indicating that overexpression of wild-type *ELF3* effectively restores normal growth. *ELF3^{R597A}* expressing plants exhibited partial complementation of hypocotyl lengths, with seedlings displaying shorter hypocotyls than *elf3-1*, though still longer than both the wild-type and the *ELF3* complemented lines (Figure 39, 40).

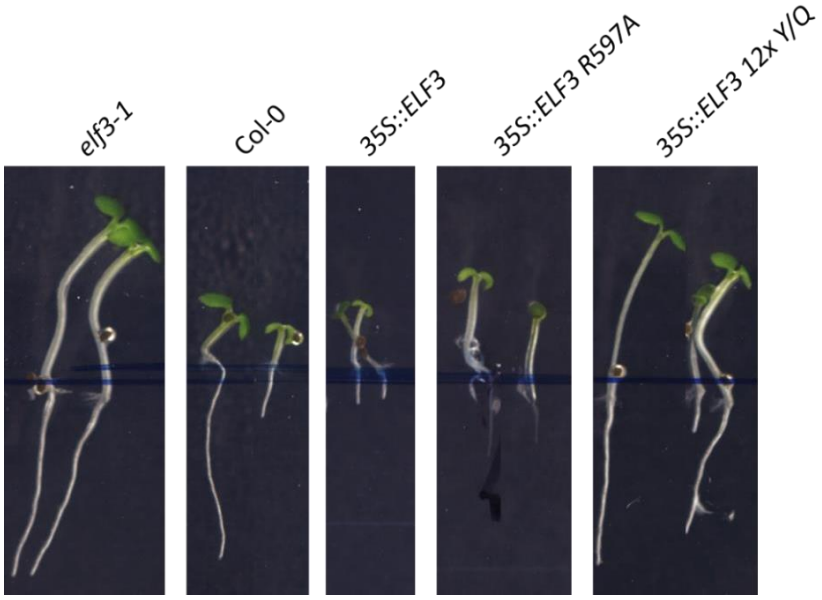

Figure 39. Hypocotyls from *elf3-1*, Col-0, *35S*::*ELF3*, *35S*::*ELF3^{R597A}* and *35S*::*ELF3$^{12xY/Q}$* seedlings grown at 22°C.

This may be due to the relatively low number of T1 plants, with only 22-43 T1 plants tested on MS plates at different temperature conditions for *ELF3^{R597A}*. While ELF3^{R597A} shows at least partial complementation whether there are some differences versus ELF3 WT will need to be confirmed in T2.

Despite these setbacks, the R597A mutant demonstrated partial complementation. Notably, the R597A mutant had elongated petioles, but had a larger overall rosette size compared to *elf3-1*. The leaf blades were broader, and the leaves were positioned more horizontally, unlike the *elf3-1* mutant, which typically shows more severe morphological changes (Hicks, 2001; Zagotta et al., 1996). These characteristics suggest partial restoration of ELF3 function in the R597A mutant, but with noticeable deviations from wild type.

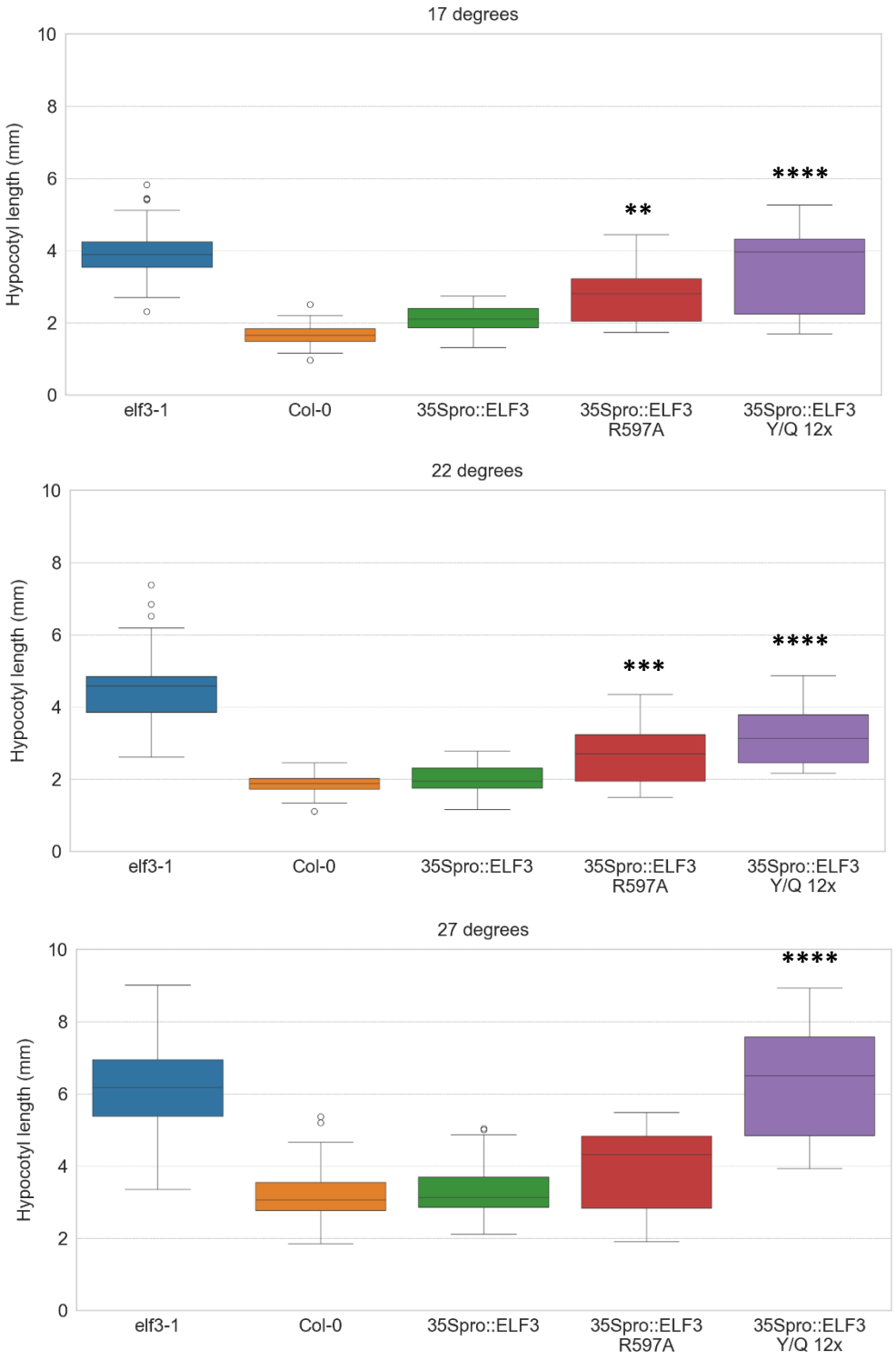

Figure 40. Hypocotyl length measurements. Plants of *elf3-1*, Col-0, 35S*::ELF3*, 35S*::ELF3 R597A*, 35S*::ELF3 12xY/Q* were grown after germination at **(A)** 17° C, showing a significant difference in hypocotyl length for ELF3^{R597A} and ELF3$^{12xY/Q}$, **(B)** at 22° C; **(C)** at 27° C. Statistics performed by Mann-Whitney U, comparing each genotype to control 35S::*ELF3, **p* < .01*; ***p* < .005*; ****p* < .001, n = 22.

The number of leaves, a classic trait used to estimate phenological stage of *Arabidopsis*, together with detecting of bolting moment indicates a quantitative evaluation of flowering time (Kinmonth-Schultz et al., 2021; Salomé et al., 2011). In this experiment, Col-0 plants produced 52 leaves, whereas *elf3-1* mutants had only 13 leaves. Interestingly, the R597A mutant produced 22 leaves on average, yet had not initiated bolting (Figure 41). The R597A mutant's intermediate phenotype provides further evidence that this mutation affects the temperature-sensitive regulation of growth, with partial retention of ELF3 function in regulating development and morphology.

Figure 41. The effect of ELF3 point mutation in position R597A in *A. thaliana* plants. On the left, Col-0 plant with short petioles, big number of the rosette leaves, no flowering. In the middle is 35Spro::ELF3 R597A plant that has elongated petioles, intermediate number of leaves, wide rosette size. On the right, *elf3-1* plant, with smaller rosette size, leaves are smaller and turned upwards, petioles are elongated. Plants were grown at 17°C under SD conditions.

The *elf3-1* plants expressing *ELF3*$^{12xY/Q}$ showed no complementation of the hypocotyl phenotype at any temperature (17° C, 22° C and 27° C) (Figure 40). This was a surprising result as *in vitro* experiments demonstrated robust binding of the EC when reconstituted with ELF3$^{12xY/Q}$ and binding at low and high temperatures. Based on the current model, the monomeric form of ELF3 is the active form, able to form the EC with LUX and ELF4, whereas under higher temperatures, ELF3 would undergo LLPS, abrogating the ability of the EC to bind via sequestration or destabilization of the complex. As ELF3$^{PrD12xY/Q}$ is only monomeric and unable to undergo LLPS, I predicted the protein would be more active. In order to further investigate this counterintuitive result, Western blots were performed using an anti-ELF3 antibody to examine the protein levels in the different lines.

4.2.3. ELF3 WT and mutants expression *in planta*

In order to determine the protein expression in Col-0, *elf3-1*, 35S*::ELF3*^{R597A}, and 35S::*ELF3*$^{12xY/Q}$ mutant plants, samples from each genotype were collected 4 hours after the onset of darkness, immediately frozen in liquid nitrogen, and processed to extract total proteins. The extracted proteins were resolved by 12% SDS-PAGE and transferred onto a nitrocellulose membrane. The membrane was then probed with an ELF3-specific antibody, followed by incubation with a secondary anti-rabbit HRP antibody. Protein detection was achieved using enhanced chemiluminescence reagents.

The results revealed a detectable level of ELF3 in both Col-0 and *35S::ELF3*^{R597A} transformants, confirming ELF3 protein expression in these plants (Figure 42). However, the ELF3$^{12xY/Q}$ mutant did not show any ELF3 band, suggesting that the mutant protein is either not produced or rapidly degraded *in planta*. The absence of a detectable band for the ELF3$^{12xY/Q}$ mutant may imply that the mutations lead to degradation of the ELF3 protein, whereas the R597A mutation does not significantly affect protein stability and accumulation. To further explore the rapid protein degradation hypothesis, additional experiments including measuring the levels of target mRNA by qPCRs will be necessary.

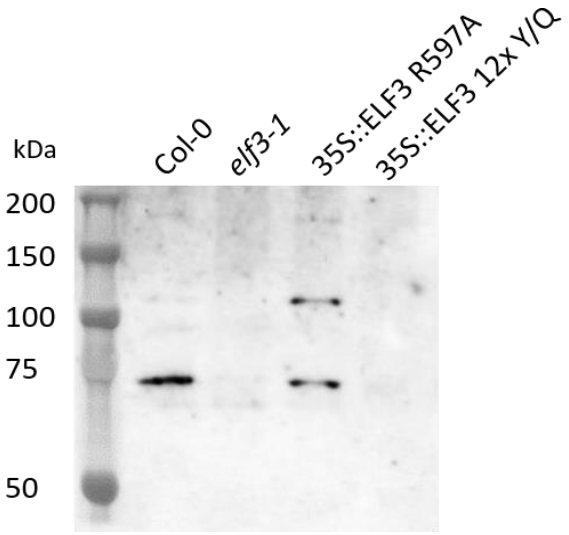

Figure 42. Detection of ELF3 protein in leaf extracts from *A.thaliana* plants Col-0, *elf3-1*, ELF3^{R597A} and ELF3$^{12xY/Q}$. Plants were grown at 22°C under short-day conditions prior to total protein extraction. Western blot analysis was performed using an anti-ELF3 antibody.

4.3. Conclusions

Based on these results, the likely active form of ELF3 is a monomeric species that forms the EC with its partners, LUX and ELF4. The band shift assays from the EC with ELF3-mCherry, ELF3^{R597A}-mCherry and ELF3$^{12xY/Q}$-mCherry were very similar even though ELF3PrD-mCherry and ELF3PrD^{R597A}-mCherry formed high molecular weight oligomers in solution based on

results presented in Chapter 3, whereas ELF3$^{12xY/Q}$-mCherry would be monomeric based on detailed structural studies of the ELF3$^{PrD12xY/Q}$ construct by SAXS. In addition, if the oligomeric form of ELF3 is able to interact with LUX and ELF4 to form an active complex able to bind DNA, multiple bands would be present on the agarose gel, as the binding of multiple LUX proteins would occur due to ~ 30 copies of ELF3. However, this was not observed, further supporting the idea of monomeric ELF3 as the species present in the EC. This leads to the question what is the role of oligomerization? Oligomerization seems to be conserved as it was observed for *Arabidopsis* ELF3 and *Brachypodium* ELF3, suggesting oligomer formation has a functional role even when the ELF3 protein does not undergo LLPS, as in the case of *Bd*ELF3. Oligomerization may play a key role in determining active monomer levels *in planta* and potentially protecting the ELF3 protein from degradation. Based on initial western blots presented here, no protein could be detected for the ELF3$^{12xY/Q}$ transformants, explaining their inability to complement the *elf3-1* loss of function phenotype and leading to the intriguing hypothesis that ELF3 oligomerization is required for protein accumulation *in vivo*.

LLPS is required for temperature sensitivity (Jung et al., 2020; Z. Zhang et al., 2023; Zhu et al., 2023). Plants expressing *ELF3^{R597A}* show partially complementation of the elongated hypocotyl phenotype of the *elf3-1* loss of function mutant. Based on studies of the PrD domain presented in Chapter 2 and 3, this mutant was predicted to have impaired LLPS and should be more active *in planta*, resulting in a shorter hypocotyl phenotype versus the WT. However, this was not observed in the T1 transformants. Due to the low number of T1 plants, however, this result needs to be confirmed and mRNA and protein levels determined for the *ELF3^{R597A}* expressing plants and rigorously compared to *ELF3* complemented lines using the same promoter. As the PrD was assayed under high pH and salt concentrations, higher than conditions *in planta*, differences in LLPS observed under these conditions *in vitro* may not be physiological relevant.

Future experiments will be required fully decouple oligomerization from LLPS and to investigate how LLPS may influence ELF3 stability and activity *in vivo*. To better understand the observed phenotypes, mRNA quantification and Western blots should be performed to assess protein levels under various temperature conditions and at multiple timepoints. In addition, ELF3 from different species with and without predicted PrDs may be used to test complementation of the *elf3-1* loss of function mutants to better understand if LLPS is a temperature sensing mechanism or plays a more general role in controlling ELF3 speciation and availability of active monomer in solution.

4.4. Materials and methods

4.4.1. Recombinant protein expression and purification

LUX (The *Arabidopsis* Information Resource [TAIR] At3g46640.1) and *ELF4* (TAIR At2g40080.1) were cloned into the expression vector pESPRIT002 (Guilligay et al., 2008; Hart & Tarendeau, 2006) using standard protocols, with all constructs containing a TEV protease-cleavable N-terminal 6xHis tag. Full-length *ELF3* (TAIR At2g25930.1) was codon opimised for expression in bacteria (Shinegene) and placed upstream of a C-terminal mCherry tag in the pESPRIT002 vector. Recombinant proteins were expressed in *E. coli* RIL cells (Agilent). Bacteria were grown in LB supplemented with kanamycin (50 μg/ml) and chloramphenicol (37 μg/ml) at 37 °C to an OD600 of 0.6–0.8. The temperature was reduced to 18 °C and protein expression was induced by addition of 1 mM of isopropyl-β-D-1-thiogalactoside (IPTG) overnight. Cells were harvested by centrifugation. LUX and ELF4 bacterial pellets were resuspended in resuspension buffer (50 mM Bis-Tris Propane (BTP) pH 9.4, 500 mM NaCl, 20 mM imidazole, 1 mM e TCEP) and 1x complete EDTA-free protease-inhibitor cocktail at 4°C (ThermoFisher). Cells were lysed via sonication. The lysates were centrifuged at 45,000 x g for 30 min at 4°C and the supernatant collected. A gravity column was prepared using 1.5 ml of Nickel-sepharose resin which were pre-equilibrated with resuspension buffer. The supernatant was loaded onto the column at 4°C. Washing steps were performed with 50 ml of resuspension buffer and with 50 ml of a high salt buffer (50 mM BTP, 1 M NaCl, 20 mM imidazole, 1 mM TCEP, pH 9.4). The proteins were eluted with 500 µl aliquots in elution buffer (50 mM BTP, 1 M NaCl, 300 mM imidazole, 1 mM TCEP, pH 9.4) in 10 fractions at 4°C. The eluted protein was dialyzed for 2 hours at 4° C in 50 mM BTP pH 9.4, 1 M NaCl, 1 mM TCEP to remove the imidazole. The purity was controlled on a SDS PAGE.

ELF3 full-length proteins from codon-optimized constructs were purified under denaturing conditions. Bacterial pellets of WT proteins and R597A, Y/Q 12x mutants were resuspended in denaturing resuspension buffer (8 M urea 20 mM Imidazole, 1 mM TCEP) and sonicated. The lysate was centrifuged at 45,000 x g for 30 min and the supernatant was applied to a 1,5 ml Ni-Sepharose column pre-equilibrated with 8 M urea resuspension buffer. The unbound proteins were washed away with 50 ml of the denaturing resuspension buffer and eluted with elution buffer (8 M urea, 250 mM imidazole, 1 mM TCEP) in 0.5 ml fractions. Fractions of interest were identified by SDS PAGE and protein concentration quantified by measuring the absorbance at 280 nm on a NanoDrop machine.

4.4.2. Evening Complex reconstitution and EMSA experiments

The evening complex was reconstituted by dialyzing all three EC components together under denaturing conditions. Briefly, LUX, ELF4 and ELF3 proteins in a 1:1,2:1 ratio were combined in 8M urea, 1 mM TCEP. The proteins were dialyzed for 1 hour at 4° C against 6 M urea, 1 mM TCEP; 1h against 4 M urea, 1 mM TCEP; 1 h against 2 M urea, 50 mM sodium phosphate pH 7.3, 150 mM NaCl, 1 mM TCEP and finally against 1 M urea, 50 mM sodium phosphate pH 7.3, 150 mM NaCl, 1 mM TCEP. The EC complex was used immediately for the EMSA experiments (M. Peng et al., 2024a).

For electrophoretic mobility shift assays, Cy5 labelled DNA was annealed (sequence below with LUX binding site highlighted in bold) (Silva et al., 2020a). EC complex (or LUX alone) and DNA were incubated at 4°C and RT in binding buffer (10 mM Tris, pH 7.0, 50 mM NaCl, 1 mM $MgCl_2$, 1 mM TCEP, 3% glycerol, 28 ng/µL herring sperm DNA, 20 µg/mL bovine serum albumin (BSA), 2.5% 3-cholamidopropyl dimethylammonio 1-propanesulfonate (CHAPS), 1.25 mM spermidine, 10 nM DNA probe) for 2 hours. After incubation, the samples were loaded on a 2% agarose gel and run in 1x tris-borate-EDTA (TBE) buffer for 20 min at room temperature and 65 min at 4° C and voltage of 75 V.

DNA oligo	DNA sequence
Oligo fwd	5′-ATGATGTCTTCTCA**AGATTCGA**TAAAAATGGTGTTG-3′
Oligo rev	5′-CAACACCATTTTTA**TCGAATCT**TGAGAAGACATCAT-3′

4.4.3. Western blot

Single leaves from *elf3-1*, Col-0, 35S::*ELF3 R597A* and 35S::*ELF3 12xY/Q* were collected 4 hours after dark and immediately frozen in liquid nitrogen. Total proteins were extracted from the leaves using lysis buffer (5% SDS, 50 mM Tris-HCl pH 6.8, 90 mM Na3PO4) while avoiding light exposure. The proteins were separated by 12% SDS-PAGE, transferred to a nitrocellulose membrane (Amersham), and incubated overnight at 4°C with ELF3 antibody (Agrisera). The membrane was then incubated with a secondary anti-rabbit antibody for 1 hour at 4°C (Agrisera). Protein detection was performed using enhanced chemiluminescence reagents (Thermo Scientific).

4.4.4. Plant materials

Arabidopsis thaliana Columbia (Col-0) ecotype was used. A previously characterized null mutant, *elf3-1,* which has a premature stop codon in exon 3 was used as background for agrobacterium-mediated transformation and complementation experiments (M. Zagotta et al., 1992). Plants were grown in temperature-controlled growth chambers in long day conditions (16h light**/**8h dark) at 22°C.

4.4.5. Cloning of plant constructs

A ELF3 full-genomic construct under control of the native ELF3 promoter provided by Philip Wigge, Potsdam University, Germany was used to subclone ELF3 (WT), ELF3-GFP and ELF3$^{7xY/Q}$ in the pFP101 vector (Bensmihen et al., 2004) using the previously reported ELF3 genomic construct and native promoter and terminator (Jung et al., 2020). The vector backbone, pFP100, allows GFP expression in the seed coat for selection of transformants (Bensmihen et al., 2004). Constructs were generated by Gibson assembly according to the manufacturer's instructions and primers used are listed in Table 3. For all constitutive expression constructs of ELF3 cDNA and mutants, the 35S promoter was used. Briefly, 35S cDNA constructs were made with T4 ligation of the ELF3 cDNA insertion into pCA26 35S constructs, kindly provided by Gabrielle Tichtinsky. The plasmid was linearized with BamHI and ApaI enzymes. Amplified ELF3 cDNA was inserted into the vector with T4 ligation. For mutation insertion, pCA26 *35S::ELF3* was amplified via PCR in 3 fragments. The PrD region was amplified from the pESPRIT002 vector, containing Y/Q12x, R597A mutations. pCA26 35S::*ELF3* vector fragments and mutant PrDs were combined via Gibbson assembly. A map of plasmid in given in figure 43. Correct construction of vectors and inserts were confirmed by sequencing.

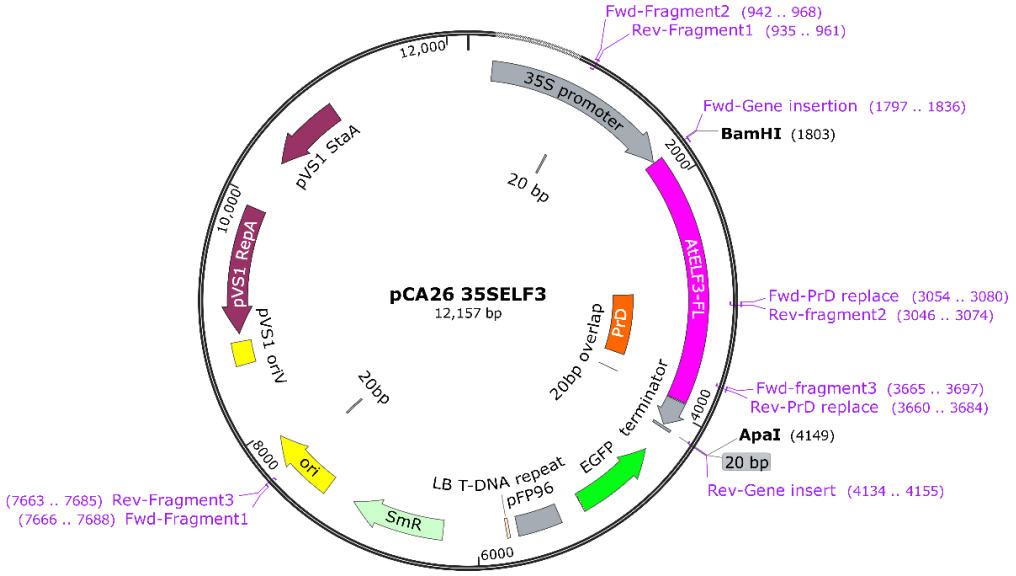

Figure 43. pCA26 35S::ELF3 construct map. Initial vector contained LHY gene that was cut from the plasmid with BamHI and ApaI enzymes. Amplified ELF3 coding DNA was inserted using T4 ligation. Insertion of mutations were obtained by switching PrD region with amplified fragment from pESPRIT002 constructs.

4.4.6. Generation of transgenic plants

Pfp101 ELF3pro::ELF3 and *pCA26 35Spro::ELF3* constructs were transformed into the *elf3-1* mutant by the floral-dip method (Clough & Bent, 1998). After dipping, plants were grown for 24 hours in the dark at 22° C and covered to maintain humidity. After 24 h plants were moved to LD conditions at 22° C with blue/red light and grown until the first siliques became yellow. Siliques were placed in paper bags to prevent spreading of seeds and grown until plant death. Transformants were selected based on the fluorescence of GFP-positive

seeds. Positive transformants were sown in pots and grown under LD conditions at 22° C. The flowering time of plant mutants was examined in the T2 generation for Pfp101 ELF3*pro::ELF3*.

4.4.7. Plants growth conditions

Seeds were placed at -80°C for 2 hours to limit potential insect contamination and then sown in pots which contained 6:1 substrate and vermiculite. Sowed seeds were stratified at 5°C for 48 hours and then moved to temperature controlled growing chambers or phytotrons. Plants were exposed to long-day conditions (16 h light, 8 hours dark) with red and blue light (OsramL 58 W/77 FLUORA T8|) and spectra (430 and 540 nm). Temperature experiments were carried in short day conditions with 8 hours light and 16 hours dark with similar light conditions. Watering of plants was regular, according to needs.

For hypocotyl length measurements, plants were grown on plates with MS agar medium without sugar at pH 5.7 (Murashige & Skoog, 1962). Seeds were disinfected with 2% hypochlorite solution, washed with ethanol and dried on sterile Whatman paper. Seeds were then transferred to MS plates and stratified at 5° C for 48 hours. The MS plates were then placed in phytotrons with short day conditions at 22° C until seeds germinated. After 48 hours, plates were moved to three temperatures: 17°, 22° and 27° C with the same day length and light conditions and examined 6 days after germination. Hypocotyl length measurements were quantified using ImageJ (Schneider et al., 2012), and data visualization was performed with the Matplotlib library in Python. Statistical analysis was conducted using the Mann-Whitney U test in Python, N = 30.

4.4.8. Plant genotyping

To control gene insertion, a set of primers designed against the GFP tag and a fragment spanning part of the 35S promoter were used (Table 4, Appendix). Briefly, total DNA was extracted from young leaves of T1 plants, using Edwards extraction buffer (200m mM Tris-HCL pH 7.5, 250 mM NaCl, 25 mM EDTA, 0,5% SDS). The PCR reaction (2 µL total DNA, 0,5 µL 10 µM primers, 1x HF Phusion buffer, 0,5µL 10 µM dNTPs and 0,25 µL Phusion polymerase (NEB)) was performed using 40 cycles of amplification and a 58-60°C annealing temperature. Results were visualized by electrophoresis on a 2% agarose gel stained with SYBRSafe (Invitrogen).

To detect if the mutant construct were correctly transformed into *elf3-1*, the PrD spanning sequence of ELF3 was amplified via PCR and the resulting fragment sequenced. A table of primers is given in Appendix, Table 4.

References

Andrade, L., Lu, Y., Cordeiro, A., Costa, J. M. F., Wigge, P. A., Saibo, N. J. M., & Jaeger, K. E. (2022). The evening complex integrates photoperiod signals to control flowering in rice. Proceedings of the National Academy of Sciences, 119(26), e2122582119. https://doi.org/10.1073/pnas.2122582119

Bensmihen, S., To, A., Lambert, G., Kroj, T., Giraudat, J., & Parcy, F. (2004a). Analysis of an activated ABI5 allele using a new selection method for transgenic Arabidopsis seeds. FEBS Letters, 561(1–3), 127–131. https://doi.org/10.1016/S0014-5793(04)00148-6

Box, M. S., Huang, B. E., Domijan, M., Jaeger, K. E., Khattak, A. K., Yoo, S. J., Sedivy, E. L., Jones, D. M., Hearn, T. J., Webb, A. A. R., Grant, A., Locke, J. C. W., & Wigge, P. A. (2015). ELF3 controls thermoresponsive growth in Arabidopsis. Current Biology: CB, 25(2), 194–199. https://doi.org/10.1016/j.cub.2014.10.076

Choudhary, M. K., Nomura, Y., Wang, L., Nakagami, H., & Somers, D. E. (2015). Quantitative Circadian Phosphoproteomic Analysis of Arabidopsis Reveals Extensive Clock Control of Key Components in Physiological, Metabolic, and Signaling Pathways. Molecular & Cellular Proteomics, 14(8), 2243–2260. https://doi.org/10.1074/mcp.M114.047183

Clough, S. J., & Bent, A. F. (1998). Floral dip: A simplified method for Agrobacterium -mediated transformation of Arabidopsis thaliana . The Plant Journal, 16(6), 735–743. https://doi.org/10.1046/j.1365-313x.1998.00343.x

Ding, L., Wang, S., Song, Z.-T., Jiang, Y., Han, J.-J., Lu, S.-J., Li, L., & Liu, J.-X. (2018). Two B-Box Domain Proteins, BBX18 and BBX23, Interact with ELF3 and Regulate Thermomorphogenesis in Arabidopsis. Cell Reports, 25(7), 1718-1728.e4. https://doi.org/10.1016/j.celrep.2018.10.060

Fiorucci, A.-S., Galvão, V. C., Ince, Y. Ç., Boccaccini, A., Goyal, A., Allenbach Petrolati, L., Trevisan, M., & Fankhauser, C. (2020). PHYTOCHROME INTERACTING FACTOR 7 is important for early responses to elevated temperature in Arabidopsis seedlings. New Phytologist, 226(1), 50–58. https://doi.org/10.1111/nph.16316

Galvão, V. C., Fiorucci, A.-S., Trevisan, M., Franco-Zorilla, J. M., Goyal, A., Schmid-Siegert, E., Solano, R., & Fankhauser, C. (2019). PIF transcription factors link a neighbor threat cue to accelerated reproduction in Arabidopsis. Nature Communications, 10(1), 4005. https://doi.org/10.1038/s41467-019-11882-7

Guilligay, D., Tarendeau, F., Resa-Infante, P., Coloma, R., Crepin, T., Sehr, P., Lewis, J., Ruigrok, R. W., Ortin, J., Hart, D. J., & Cusack, S. (2008). The structural basis for cap binding by influenza virus polymerase subunit PB2. Nat Struct Mol Biol, 15(5), 500–506. https://doi.org/10.1038/nsmb.1421

Hart, D. J., & Tarendeau, F. (2006). Combinatorial library approaches for improving soluble protein expression in Escherichia coli. Acta Crystallogr D Biol Crystallogr, 62(Pt 1), 19–26. https://doi.org/10.1107/S0907444905036097

Helfer, A., Nusinow, D. A., Chow, B. Y., Gehrke, A. R., Bulyk, M. L., & Kay, S. A. (2011). LUX ARRHYTHMO Encodes a Nighttime Repressor of Circadian Gene Expression in the Arabidopsis Core Clock. Current Biology, 21(2), 126–133. https://doi.org/10.1016/j.cub.2010.12.021

Herrero, E., Kolmos, E., Bujdoso, N., Yuan, Y., Wang, M., Berns, M. C., Uhlworm, H., Coupland, G., Saini, R., Jaskolski, M., Webb, A., Gonçalves, J., & Davis, S. J. (2012). EARLY FLOWERING4 Recruitment of EARLY FLOWERING3 in the Nucleus Sustains the Arabidopsis Circadian Clock. The Plant Cell, 24(2), 428–443. https://doi.org/10.1105/tpc.111.093807

Hicks, K. A. (2001). EARLY FLOWERING3 Encodes a Novel Protein That Regulates Circadian Clock Function and Flowering in Arabidopsis. THE PLANT CELL ONLINE, 13(6), 1281–1292. https://doi.org/10.1105/tpc.13.6.1281

Huang, H., Alvarez, S., Bindbeutel, R., Shen, Z., Naldrett, M. J., Evans, B. S., Briggs, S. P., Hicks, L. M., Kay, S. A., & Nusinow, D. A. (2016). Identification of Evening Complex Associated Proteins in Arabidopsis by Affinity Purification and Mass Spectrometry. Molecular & Cellular Proteomics : MCP, 15(1), 201–217. https://doi.org/10.1074/mcp.M115.054064

Hutin, S., Wigge, P. A., & Zubieta, C. (2024a). In Vitro Determination of Temperature-Dependent DNA Binding of the Evening Complex Using Electrophoretic Mobility Shift Assays. In M. Chen (Ed.), Thermomorphogenesis: Methods and Protocols (pp. 135–147). Springer US. https://doi.org/10.1007/978-1-0716-3814-9_14

Jiang, Y., Yang, C., Huang, S., Xie, F., Xu, Y., Liu, C., & Li, L. (2019). The ELF3-PIF7 Interaction Mediates the Circadian Gating of the Shade Response in Arabidopsis. IScience, 22, 288–298. https://doi.org/10.1016/j.isci.2019.11.029

Jung, J.-H., Barbosa, A. D., Hutin, S., Kumita, J. R., Gao, M., Derwort, D., Silva, C. S., Lai, X., Pierre, E., Geng, F., Kim, S.-B., Baek, S., Zubieta, C., Jaeger, K. E., & Wigge, P. A. (2020). A prion-like domain in ELF3 functions as a thermosensor in Arabidopsis. Nature, 585(7824), 256–260. https://doi.org/10.1038/s41586-020-2644-7

Khanna, R., Huq, E., Kikis, E. A., Al-Sady, B., Lanzatella, C., & Quail, P. H. (2004). A Novel Molecular Recognition Motif Necessary for Targeting Photoactivated Phytochrome Signaling to Specific Basic Helix-Loop-Helix Transcription Factors[W]. The Plant Cell, 16(11), 3033–3044. https://doi.org/10.1105/tpc.104.025643

Kim, C., Kwon, Y., Jeong, J., Kang, M., Lee, G. S., Moon, J. H., Lee, H.-J., Park, Y.-I., & Choi, G. (2023). Phytochrome B photobodies are comprised of phytochrome B and its primary and secondary interacting proteins. Nature Communications, 14(1), 1708. https://doi.org/10.1038/s41467-023-37421-z

Kinmonth-Schultz, H., Lewandowska-Sabat, A., Imaizumi, T., Ward, J. K., Rognli, O. A., & Fjellheim, S. (2021). Flowering Times of Wild Arabidopsis Accessions From Across Norway Correlate With Expression Levels of FT, CO, and FLC Genes. Frontiers in Plant Science, 12, 747740. https://doi.org/10.3389/fpls.2021.747740

Kolmos, E., Nowak, M., Werner, M., Fischer, K., Schwarz, G., Mathews, S., Schoof, H., Nagy, F., Bujnicki, J. M., & Davis, S. J. (2009). Integrating ELF4 into the circadian system through combined structural and functional studies. HFSP Journal, 3(5), 350–366. https://doi.org/10.2976/1.3218766

Kubota, A., Ito, S., Shim, J. S., Johnson, R. S., Song, Y. H., Breton, G., Goralogia, G. S., Kwon, M. S., Laboy Cintrón, D., Koyama, T., Ohme-Takagi, M., Pruneda-Paz, J. L., Kay, S. A., MacCoss, M. J., & Imaizumi, T. (2017). TCP4-dependent induction of CONSTANS transcription requires GIGANTEA in photoperiodic flowering in Arabidopsis. PLOS Genetics, 13(6), e1006856. https://doi.org/10.1371/journal.pgen.1006856

Leivar, P., & Quail, P. H. (2011). PIFs: Pivotal components in a cellular signaling hub. Trends in Plant Science, 16(1), 19–28. https://doi.org/10.1016/j.tplants.2010.08.003

Li, L., Ljung, K., Breton, G., Schmitz, R. J., Pruneda-Paz, J., Cowing-Zitron, C., Cole, B. J., Ivans, L. J., Pedmale, U. V., Jung, H.-S., Ecker, J. R., Kay, S. A., & Chory, J. (2012). Linking photoreceptor excitation to changes in plant architecture. Genes & Development, 26(8), 785–790. https://doi.org/10.1101/gad.187849.112

Liu, X. L., Covington, M. F., Fankhauser, C., Chory, J., & Wagner, D. R. (2001). ELF3 Encodes a Circadian Clock–Regulated Nuclear Protein That Functions in an Arabidopsis PHYB Signal Transduction Pathway. The Plant Cell, 13(6), 1293–1304. https://doi.org/10.1105/TPC.000475

Murashige, T., & Skoog, F. (1962). A Revised Medium for Rapid Growth and Bio Assays with Tobacco Tissue Cultures. Physiologia Plantarum, 15(3), 473–497. https://doi.org/10.1111/j.1399-3054.1962.tb08052.x

Nieto, C., López-Salmerón, V., Davière, J.-M., & Prat, S. (2015). ELF3-PIF4 Interaction Regulates Plant Growth Independently of the Evening Complex. Current Biology, 25(2), 187–193. https://doi.org/10.1016/j.cub.2014.10.070

Nusinow, D. A., Helfer, A., Hamilton, E. E., King, J. J., Imaizumi, T., Schultz, T. F., Farré, E. M., & Kay, S. A. (2011). The ELF4–ELF3–LUX complex links the circadian clock to diurnal control of hypocotyl growth. Nature, 475(7356), 398–402. https://doi.org/10.1038/nature10182

Peng, M., Hutin, S., Mironova, A., Zubieta, C., & Wigge, P. A. (2024). Analysis of Phase Separation of EARLY FLOWERING 3. In M. Chen (Ed.), Thermomorphogenesis (Vol. 2795, pp. 123–134). Springer US. https://doi.org/10.1007/978-1-0716-3814-9_13

Raschke, A., Ibañez, C., Ullrich, K. K., Anwer, M. U., Becker, S., Glöckner, A., Trenner, J., Denk, K., Saal, B., Sun, X., Ni, M., Davis, S. J., Delker, C., & Quint, M. (2015). Natural variants of ELF3 affect thermomorphogenesis by transcriptionally modulating PIF4-dependent auxin response genes. BMC Plant Biology, 15, 197. https://doi.org/10.1186/s12870-015-0566-6

Salomé, P. A., Bomblies, K., Laitinen, R. A. E., Yant, L., Mott, R., & Weigel, D. (2011). Genetic Architecture of Flowering-Time Variation in Arabidopsis thaliana. Genetics, 188(2), 421–433. https://doi.org/10.1534/genetics.111.126607

Schneider, C. A., Rasband, W. S., & Eliceiri, K. W. (2012). NIH Image to ImageJ: 25 years of image analysis. Nature Methods, 9(7), 671–675. https://doi.org/10.1038/nmeth.2089

Sharma, A., Samtani, H., Sahu, K., Sharma, A. K., Khurana, J. P., & Khurana, P. (2023). Functions of Phytochrome-Interacting Factors (PIFs) in the regulation of plant growth and development: A comprehensive review. International Journal of Biological Macromolecules, 244, 125234. https://doi.org/10.1016/j.ijbiomac.2023.125234

Silva, C. S., Lai, X., Nanao, M., & Zubieta, C. (2016). The Myb domain of LUX ARRHYTHMO in complex with DNA: expression, purification and crystallization. Acta Crystallogr F Struct Biol Commun, 72(Pt 5), 356–361. https://doi.org/10.1107/S2053230X16004684

Silva, C. S., Nayak, A., Lai, X., Hutin, S., Hugouvieux, V., Jung, J.-H., López-Vidriero, I., Franco-Zorrilla, J. M., Panigrahi, K. C. S., Nanao, M. H., Wigge, P. A., & Zubieta, C. (2020a). Molecular mechanisms of Evening Complex activity in Arabidopsis. Proceedings of the National Academy of Sciences of the United States of America, 117(12), 6901–6909. https://doi.org/10.1073/pnas.1920972117

Song, Y. H., Kubota, A., Kwon, M. S., Covington, M. F., Lee, N., Taagen, E. R., Laboy Cintrón, D., Hwang, D. Y., Akiyama, R., Hodge, S. K., Huang, H., Nguyen, N. H., Nusinow, D. A., Millar, A. J., Shimizu, K. K., & Imaizumi, T. (2018). Molecular basis of flowering under natural long-day conditions in Arabidopsis. Nature Plants, 4(10), 824–835. https://doi.org/10.1038/s41477-018-0253-3

Sun, K., Xue, X., Liu, N., Zhu, Z., & Li, H. (2020). A point-to-point protein–protein interaction assay reveals the signaling interplays among plant hormones and environmental cues. Plant Direct, 4(5), e00228. https://doi.org/10.1002/pld3.228

Wang, C.-Q., Sarmast, M. K., Jiang, J., & Dehesh, K. (2015). The Transcriptional Regulator BBX19 Promotes Hypocotyl Growth by Facilitating COP1-Mediated EARLY FLOWERING3 Degradation in Arabidopsis. The Plant Cell, 27(4), 1128–1139. https://doi.org/10.1105/tpc.15.00044

Willige, B. C., Zander, M., Yoo, C. Y., Phan, A., Garza, R. M., Wanamaker, S. A., He, Y., Nery, J. R., Chen, H., Chen, M., Ecker, J. R., & Chory, J. (2021). PHYTOCHROME-INTERACTING FACTORs trigger environmentally responsive chromatin dynamics in plants. Nature Genetics, 53(7), 955–961. https://doi.org/10.1038/s41588-021-00882-3

Yang, C., Huang, S., Zeng, Y., Liu, C., Ma, Q., Pruneda-Paz, J., Kay, S. A., & Li, L. (2021). Two bHLH transcription factors, bHLH48 and bHLH60, associate with phytochrome interacting factor 7 to regulate hypocotyl elongation in Arabidopsis. Cell Reports, 35(5), 109054. https://doi.org/10.1016/j.celrep.2021.109054

Yu, J.-W., Rubio, V., Lee, N.-Y., Bai, S., Lee, S.-Y., Kim, S.-S., Liu, L., Zhang, Y., Irigoyen, M. L., Sullivan, J. A., Zhang, Y., Lee, I., Xie, Q., Paek, N.-C., & Deng, X. W. (2008a). COP1 and ELF3 control circadian function and photoperiodic flowering by regulating GI stability. Molecular Cell, 32(5), 617–630. https://doi.org/10.1016/j.molcel.2008.09.026

Zagotta, M., Shannon, S., Jacobs, C., & Meeks-Wagner, D. (1992). Early-Flowering Mutants of Arabidopsis thaliana. Functional Plant Biology, 19(4), 411. https://doi.org/10.1071/PP9920411

Zagotta, M. T., Hicks, K. A., Jacobs, C. I., Young, J. C., Hangarter, R. P., & Meeks-Wagner, D. R. (1996). The Arabidopsis ELF3 gene regulates vegetative photomorphogenesis and the photoperiodic induction of flowering. The Plant Journal, 10(4), 691–702. https://doi.org/10.1046/j.1365-313X.1996.10040691.x

Zahn, T., Zhu, Z., Ritoff, N., Krapf, J., Junker, A., Altmann, T., Schmutzer, T., Tüting, C., Kastritis, P. L., Babben, S., Quint, M., Pillen, K., & Maurer, A. (2023). Novel exotic alleles of EARLY FLOWERING 3 determine plant development in barley. Journal of Experimental Botany, 74(12), 3630–3650. https://doi.org/10.1093/jxb/erad127

Zhang, B., Holmlund, M., Lorrain, S., Norberg, M., Bakó, L., Fankhauser, C., & Nilsson, O. (2017). BLADE-ON-PETIOLE proteins act in an E3 ubiquitin ligase complex to regulate PHYTOCHROME INTERACTING FACTOR 4 abundance. ELife, 6, e26759. https://doi.org/10.7554/eLife.26759

Zhang, L.-L., Li, W., Tian, Y.-Y., Davis, S. J., & Liu, J.-X. (2021). The E3 ligase XBAT35 mediates thermoresponsive hypocotyl growth by targeting ELF3 for degradation in Arabidopsis. Journal of Integrative Plant Biology, 63(6), 1097–1103. https://doi.org/10.1111/jipb.13107

Zhang, L.-L., Zhu, Q.-Y., Sun, J.-L., Yao, Z.-W., Qing, T., Ma, H., & Liu, J.-X. (2024). XBAT31 regulates reproductive thermotolerance through controlling the accumulation of HSFB2a/B2b under heat stress conditions. Cell Reports, 43(6). https://doi.org/10.1016/j.celrep.2024.114349

Zhang, Z., Luo, X., Yang, Y., & He, Y. (2023). Cold induction of nuclear FRIGIDA condensation in Arabidopsis. Nature, 619(7969), E27–E32. https://doi.org/10.1038/s41586-023-06189-z

Zhao, H., Xu, D., Tian, T., Kong, F., Lin, K., Gan, S., Zhang, H., & Li, G. (2021). Molecular and functional dissection of EARLY-FLOWERING 3 (ELF3) and ELF4 in Arabidopsis. Plant Science, 303, 110786. https://doi.org/10.1016/j.plantsci.2020.110786

Zhu, Z., Esche, F., Babben, S., Trenner, J., Serfling, A., Pillen, K., Maurer, A., & Quint, M. (2023). An exotic allele of barley EARLY FLOWERING 3 contributes to developmental plasticity at elevated temperatures. Journal of Experimental Botany, 74(9), 2912–2931. https://doi.org/10.1093/jxb/erac470

CHAPTER 5 Conclusions and perspectives

Plants rely on precise mechanisms to detect and adapt to changes in temperature, which affect critical developmental processes throughput the life cycle of the plant, from initial hypocotyl elongation to the timing of flowering (Chen et al., 2022; Haider et al., 2021; Hayes et al., 2021; Jung et al., 2023; Li et al., 2019; Mizuno et al., 2014). The scaffold protein ELF3, a core component of the circadian clock, plays a crucial role in regulating these temperature responses through its interactions with other protein partners (Huang et al., 2016; Jiang et al., 2019; Nieto et al., 2015; Nusinow et al., 2011). For example, by interacting with LUX and ELF4, ELF3 forms the Evening Complex (EC), which regulates the expression of downstream genes involved in growth and flowering in a temperature-dependent manner, thus acting as a direct read-out mechanism of non-stress ambient temperature (Ezer et al., 2017; Jung et al., 2020; Silva et al., 2020). The molecular mechanisms underlying this activity likely involve the complex speciation of ELF3, which is able to sample a dilute phase with monomeric and oligomeric species and to undergo liquid-liquid phase separation, forming a condensed phase that further ages into a stable and lamellar stacked hydrogel (Hutin et al., 2023a). LLPS can occur in response to changes in environmental conditions such as pH, salt concentration, and, most importantly for this work, temperature (Hutin et al., 2023; Jung et al., 2020). How LLPS is triggered, what are the amino acid sequences that control this phenomenon, and whether LLPS can be a target to alter thermomorphogenesis *in planta* are the major questions the thesis work tried to address. Studying ELF3 through biochemistry, biophysical assays, structural studies, and *in vivo* experiments is critical for a comprehensive understanding of liquid-liquid phase separation and thermosensing. Biochemistry and biophysical techniques allow us to investigate the molecular mechanisms, interactions, and temperature-dependent behaviors of ELF3. Structural studies provide insights into how ELF3 organizes itself at the molecular level, revealing its oligomerization state and molecular interactions under different conditions. *In vivo* studies are essential to link this knowledge at the molecular level to physiological outcomes and temperature-sensitive phenotypes in plants.

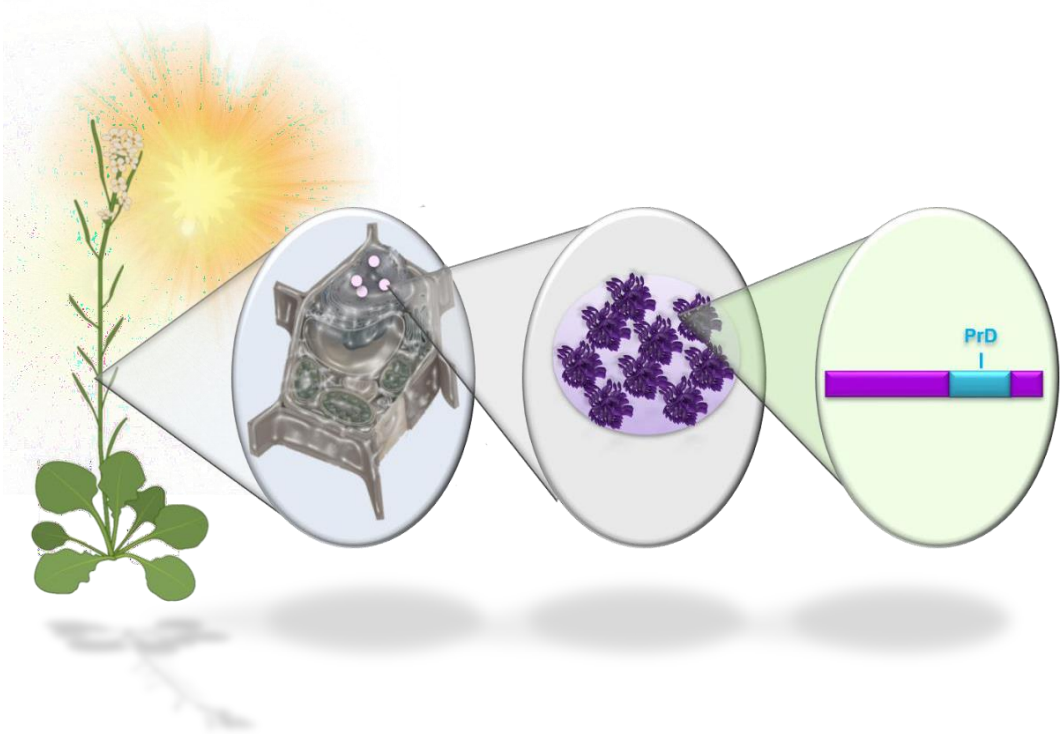

Figure 44. Schematic representation of ELF3 action in plants. At elevated ambient temperatures, ELF3 localizes to the cell nucleus, where it undergoes LLPS. This process is facilitated by the presence of a PrD in ELF3, which drives the phase separation, potentially affecting downstream processes related to temperature response and circadian regulation.

5.1. Biochemical characterization-limitations and alternatives

Previous studies have identified the PrD of ELF3 responsible for driving liquid-liquid phase separation (Hutin et al., 2023). The PrD construct used in the biochemical studies presented in Chapter 2 formed the basis of many conclusions as to the putative behavior of the full-length protein. This is an important limitation for the detailed biochemical studies, including phase diagrams, which demonstrate the relationship between protein concentration, ionic strength and/or pH, and LLPS and SEC-MALLS, which determined the molecular weight of the WT and mutants in solution. Ideally, working with full length protein would have been optimal, however, I was unable to obtain a sufficient amount of ELF3 full-length protein or point mutants for phase diagrams that required milligram quantities of soluble protein. While it is clear that the PrD is required for phase separation, the behavior of the full-length protein should not be assumed to be the same. Domains or sequences adjacent to the PrD will have an effect on LLPS. While I was able to express mCherry tagged full-length ELF3 in sufficient quantities for EMSAs, it required purification under denaturing conditions. It may be possible to scale up protein production and optimize the purification, cleave the mCherry tag and/or use microfluidic chips to minimize the amount of protein required for phase diagrams (and structural studies using SAXS, Chapter 3). This will require extensive

optimization of expression and purification protocols. The PrD spanning construct was thus chosen as the largest soluble construct, therefore the most promising way, to study LLPS of ELF3. It showed a better solubility and stability, making it easier to work with *in vitro* experiments or for structural studies. Often, proteins have distinct functional domains, and isolating and working with these specific domains can still provide insights into their biological function. Even if only a portion of the protein can be studied, structural information from this fragment can offer clues about the overall architecture and/or behavior of the full-length protein. In general, studying a fragment allows one to test hypotheses about the protein's function, interactions, or activity in a more controlled environment. This can be a stepping stone towards solving solubility issues or engineering the full-length protein to be more stable. I could show that mutations in the PrD clearly altered the behavior of this construct, however, the effect of these mutations may be different in the context of the full-length protein.

A second major drawback of any study attempting to relate *in vitro* protein behavior to *in vivo* function is the highly simplified few-component system used. The assay conditions for the biochemical characterization of the ELF3 PrD were very different from physiological conditions in terms of protein concentration, pH and salt concentration. These *in vitro* conditions do not recapitulate cellular conditions so it cannot be excluded that the behavior observed *in vitro* is an artefact of the assay conditions used and is quite different in a cellular environment. On the other hand, *in vitro* experiments have different requirements in terms of protein concentration, quantity and stability. The amounts and concentrations needed for phase diagrams and structural studies are probably much higher than cellular ELF3 concentrations, but were needed in order to obtain enough signal. In addition, ELF3 protein is a scaffold and no protein binding partners were used in biochemical studies in Chapter 2. These are important limitations of the study, although most *in vitro* experiments suffer from this and extrapolation to *in vivo* physiological behavior and function should be done cautiously. Alternatives such as using cell extract in LLPS assays as opposed to purified proteins in controlled buffer conditions or mimicking the crowded cellular environment through the use of polymers such as polyethylene glycols (PEGs) have been proposed in the literature as alternatives to more traditional protein methods of examining LLPS behavior of a protein (Alberti et al., 2019). However, it is not clear if these methods act as better proxies or not for intracellular conditions.

5.2. Structural studies – SAXS and future experiments

Small angle X-ray scattering provides one of the few methods to obtain structural data from macromolecules in solution, albeit at low resolution. The SAXS studies performed here allowed structural characterization of the ELF3 PrD and different mutants. SAXS showed that most ELF3 PrD constructs formed large homogeneous globular oligomers in solution, even for constructs that exhibited large differences in their LLPS. Interestingly, only the ELF3 PrD mutant with twelve tyrosine residues replaced with glutamine residues exhibited a dramatic change in structure. This mutant was no longer oligomeric and adopted a flexible elongated structure consistent with an intrinsically disordered protein. These experiments provide important descriptive results for the ELF3 PrD mutants under study. As for the biochemical assays, a limitation of the structural work is the use of only the PrD as opposed to the full-

length protein. Unpublished results by Dr. Stephanie Hutin (CNRS, LPCV, Grenoble) on full length ELF3 wild-type protein tagged with mCherry also revealed the formation of a large oligomeric species in the dilute phase, suggesting that what I observed for the PrD also occurs for the full-length context.

The resolution limitation of SAXS does not allow us to determine how interactions at the amino acid level contribute to oligomerization or what is the potential protein-protein interface. As the ELF3 PrD does not have much predicted secondary structure, structural methods such as protein crystallography are not applicable to the system as the likelihood of crystallization is extremely low due to the high flexibility of the molecule. Nuclear magnetic resonance is one method that does allow the atomic level determination of protein structure in the solution state, however, due to the size of the oligomer, solution state NMR studies were not successful. This is because large proteins tumble more slowly in solution, resulting in broadened and weak NMR signals with reduced resolution and sensitivity of the NMR data. Additionally, the increased complexity of larger proteins results in more overlapping signals, coupled with line broadening, which makes the assignment and interpret resonance peaks difficult. ELF3 PrD, with its megadalton molecular weight, for example, gives virtually no NMR peaks (S. Hutin, unpublished). One alternative would be solid state NMR (ssNMR), which circumvents some of the limitations of solution state NMR, such as molecule size and slow tumbling dynamics. In ssNMR, the sample is often immobilized in a solid or semi-solid state such as a hydrogel. This technique has been applied to aggregate and gel-forming polyQ proteins and offers a potential future direction for high-resolution studies of the ELF3 PrD (van der Wel, 2024).

5.3. *In vitro* DNA binding studies

In Chapter 4, electrophoretic mobility shift assays (EMSA) were presented showing a shift of a Cy5-probe shift due to the binding of the Evening Complex with mCherry tagged ELF3 wild type protein and different ELF3 mutants. As previously described, the EC consists of ELF3, ELF4 and the DNA-binding protein, LUX ARRYTHMO (LUX). Additional EMSA experiments for the ELF3$^{9xH/R}$ mutant, for example, would be very illuminating with respect to the observed phenotype of short hypocotyls and late flowering under all tested temperature conditions (P. Wigge, unpublished, see Appendix Figure 49). Phase diagrams and structural studies revealed that this mutant undergoes LLPS under high pH and salt conditions, aggregated easily and was oligomeric in the dilute phase. However, its possible effect on DNA binding in the context of the EC was not determined. As the replacement of histidine residues, which are not charged at physiological pH, with positively charged arginine residues may alter DNA binding affinity due to charge complementarity, these EMSA experiments are important to see if *in vitro* behavior can be correlated with observed phenotype. The delayed flowering of the mutant could be related to increased DNA-binding activity due to arginine-rich protein content and not related to LLPS behavior per se.

Interactions with other transcription factors such as PIF4 and PIF7 were not tested by EMSA, but would be interesting as to determine whether ELF3 temperature-induced LLPS also affects PIF4 and/or PIF7 DNA binding. Testing different binding partners, determining their

effect on LLPS, ELF3 oligomeric state and DNA-binding are all potential future directions for the project. If LLPS and sequestration of binding partners is a general mechanism used by ELF3 (Hutin et al., 2024b; Silva et al., 2020b), similar results for temperature-dependent EMSAs should be observed for the different TF partners.

5.4. *In planta* experiments- caveats and future directions

Understanding how ELF3 regulates temperature adaptation may have broad implications for improving crop temperature tolerance in varying climate conditions. As shown in the initial plant studies in *Arabidopsis thaliana* presented here (Chapter 4), ELF3 mutants that disrupt or alter phase separation can alter plant temperature sensitivity, suggesting a link between the molecular events of oligomerization and LLPS and thermomorphogenesis. Studies of *elf3-1* plants expressing $ELF3^{9xH/R}$ and $ELF3^{12xY/Q}$ demonstrate that changes in the PrD dramatically effect plant phenotype. *elf3-1* loss of function plants expressing $ELF3^{9xH/R}$ were no longer temperature responsive and exhibited short hypocotyls and late flowering over a 17-27° C temperature range, whereas the $ELF3^{12xY/Q}$ expressing plants also exhibited less temperature sensitivity than WT over this range but with long hypocotyls and early flowering phenotypes similar to the loss of function *elf3* mutant. The *elf3-1* plants expressing $ELF3^{R597A}$ phenocopied WT plants, even though this mutant, *in vitro*, exhibited attenuated LLPS, suggesting it would be more active than WT ELF3. Based purely on LLPS behavior these phenotypes are unexpected as $ELF3^{9xH/R}$ and $ELF3^{R597A}$ would be predicted to result in faster entry into LLPS (and a more sensitive temperature response) and attenuated entry into LLPS (and a weaker temperature response with shorter hypocotyls and late flowering), respectively. Likewise, $ELF3^{R597A}$ expressing plants would be predicted to have weaker temperature response with shorter hypocotyls and late flowering. However, the opposite was observed. *In vitro* DNA binding assays demonstrated that the EC containing $ELF3^{R597A}$ behaved very similarly to the complex with ELF3 WT, correlating well with *in vivo* observations. $ELF3^{9xH/R}$ has not been assayed *in vitro* as part of the EC. However, the addition of arginine residue may increase DNA binding affinity with positively charged arginines interacting with the negatively charged phosphates of DNA (DeRouchey et al., 2013; Leng & Felsenfeld, 1966). Perhaps most interestingly, *in vitro*, the EC containing $ELF3^{12xY/Q}$ exhibits robust binding at low temperatures and retains DNA binding at higher temperatures, as opposed to the EC with WT ELF3 which does not exhibit binding at higher temperatures. $ELF3^{12xY/Q}$ also does not undergo phase separation and is monomeric, unlike all other ELF3 constructs tested. These *in vitro* results would suggest a highly active protein and stronger DNA binding over a wider temperature range than WT ELF3 and thus shorter hypocotyls and later flowering. This was not observed in T1 plants, leading me to wonder if the protein was present or not. Based on initial western blots, while protein could be detected for ELF3 WT and $ELF3^{R597A}$, no $ELF3^{12xY/Q}$ was detected. These results let me to speculate that the monomeric form of ELF3 might be prone to degradation due to its accessible conformation, while its multimers are more stable (Figure 45). Additional experiments must be performed to confirm this result, including qPCR to confirm proper gene expression. While preliminary, these experiments suggest an important role for oligomerization as being required to maintain ELF3 protein levels *in planta*.

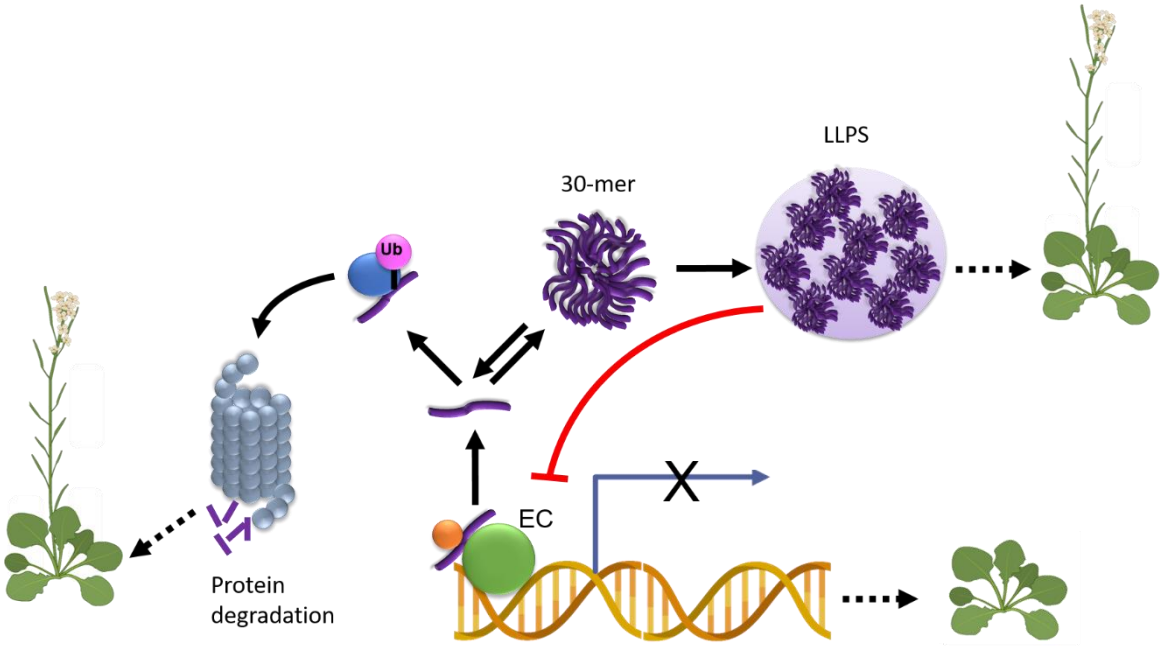

Figure 45. Suggested model of ELF3 regulation *in planta*. At low ambient temperature, ELF3 forms EC with LUX and ELF4, binding tightly to DNA and repressing flowering. At warmer temperatures, ELF3 undergoes LLPS, forming liquid droplets. However, in mutants unable to undergo LLPS, ELF3 is targeted for proteasomal degradation, leading to the de-repression of flowering and earlier flowering onset.

5.5. Implications and future work

Studies of ELF3-mediated temperature sensing provides critical insights into the evolution of plant response to changing environmental conditions. Understanding how proteins like ELF3 function in crops could provide agricultural strategies aiming to improve resilience to climate change. The identification and characterization of ELF3 orthologs in diverse species, including crops like wheat and barley, suggests a potential for manipulating this pathway to enhance or attenuate thermosensitivity and influence productivity in agriculturally important plants. In wheat and barley, ELF3 orthologs have been shown to modulate developmental timing under varying temperature conditions, often influencing traits like flowering onset (Zhu et al., 2023b; Zikhali et al., 2016). Cross-species analysis and expanding the study to diverse plants and non-model systems will allow us to evaluate how phase separation-mediated temperature sensing evolved across plant taxa. The recent discovery of an ELF3 ortholog in *Chlamydomonas reinhardtii*, a species representing an early plant divergence (Gururaj et al., 2022), suggests the evolutionary importance of ELF3 and opens up opportunities to study changes in protein function, copy number variation, and the emergence of new traits during evolution.

The combined results of these future experiments might have significant implications for agricultural innovation. By improving our understanding of ELF3-mediated temperature regulation, it may be possible to engineer plants with altered thermoresponse, thereby

increasing productivity in warmer climates or regions facing rapid temperature changes. Understanding the evolutionary aspect of ELF3's function can also assist in applying these findings to a wide range of species, making this research highly relevant to global food security and crop resilience strategies.

Appendix

Multiple protein alignment of 96 species ELF3 PrD-containing protein can be found on the repository: https://github.com/plant-research/ELF3_Phase_Separation.git

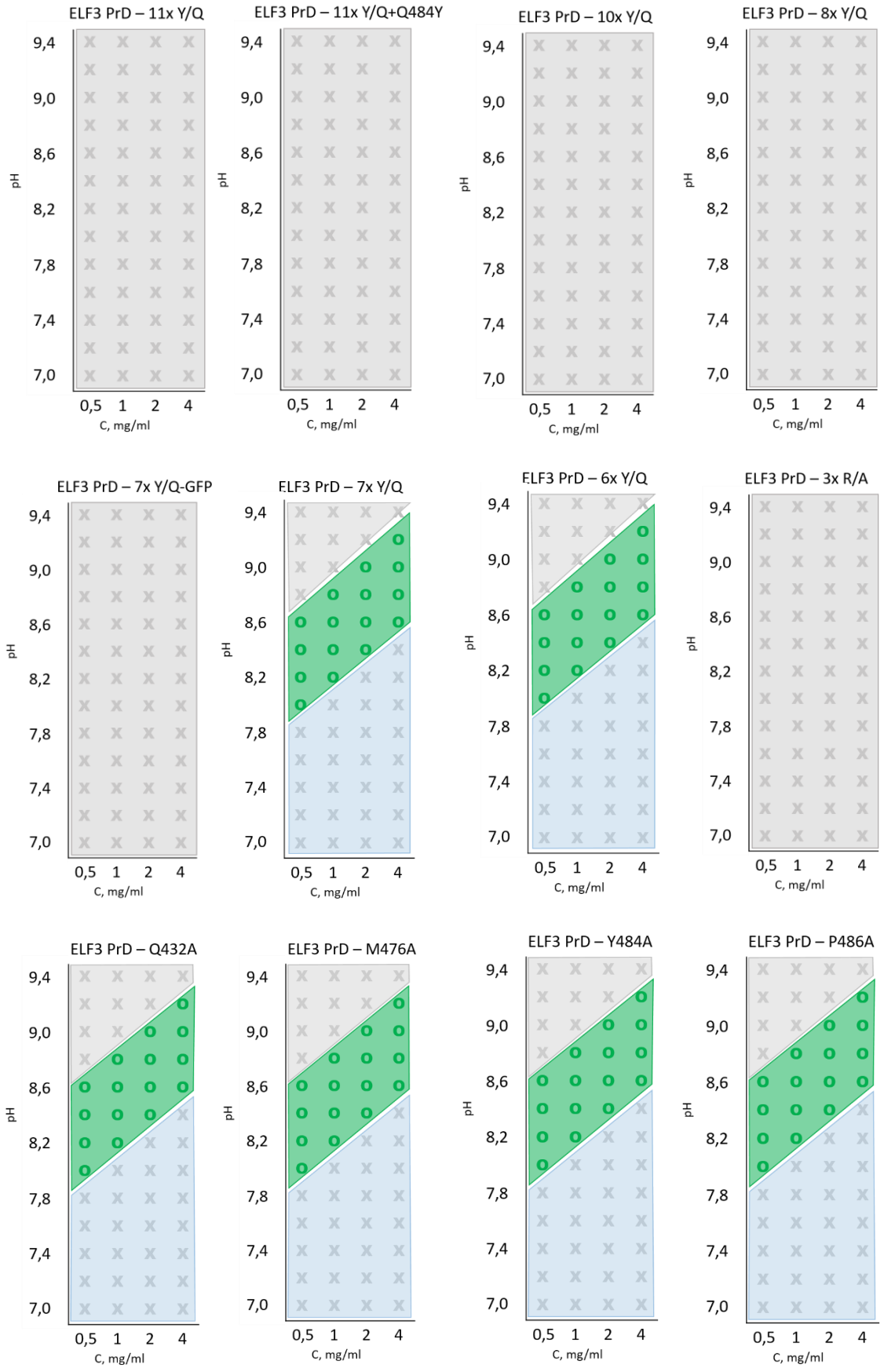

Figure 46. Phase diagrams of ELF3 mutants illustrate under which conditions a protein undergoes LLPS and gelation or precipitation. Examples of phase diagrams examining pH versus protein concentration.

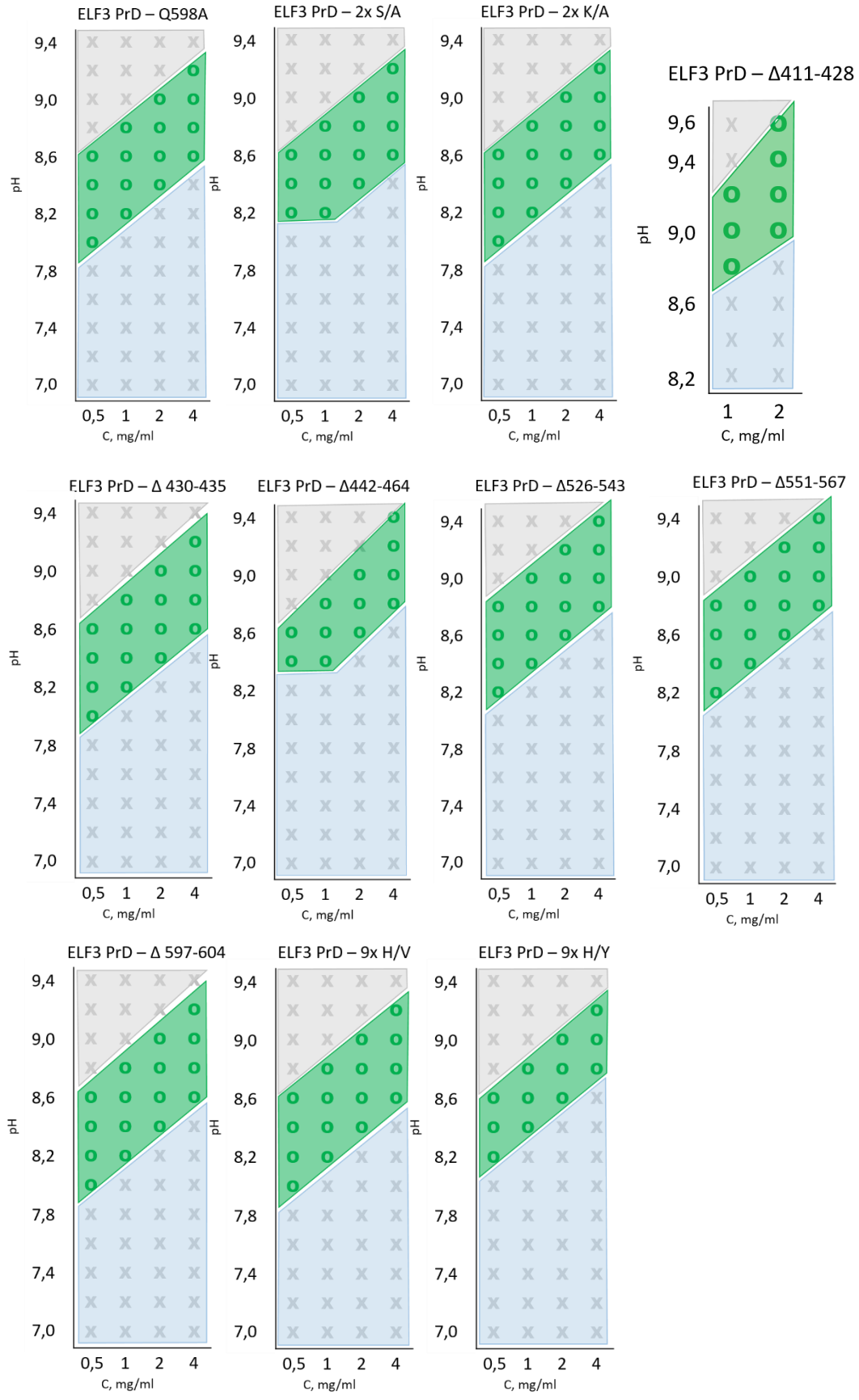

Figure 47. Phase diagrams of ELF3 mutants illustrate under which conditions a protein undergoes LLPS and gelation or precipitation. Examples of phase diagrams examining pH versus protein concentration.

Table 4. List of primers used in this project

Primers for genotyping	
Fwd_genotyp_R597A	GACATCCTGGAAATCTTCAGAACACC
Rev_genotyp_R597A	AATGGCCGAAAGGACTTGCTACC
Fwd_genotyp_YQ	AATCCAACTACATGCCTTTTGCAAACA
Rev_genotyp_YQ	ACAATATGGGTTCATTATGGTGGGCA
Fwd-35S_genotyping	CGTCTTCAAAGCAAGTGGATTGATGT
Rev-35S_genotyping	gccgaggaaacataggttccaatatc
Fwd-GFP_genotyping	AGCTCGTCCATGCCGAGAGT
Rev-GFP_genotyping	TCAAGGTGAACTTCAAGATCCGCC
Primers for clone *in vitro*	
Fwd-2x R/A	TATCCGGCAGCAGCAAAGAGCAGGCAAGGGAGCACAGG
Rev-2x R/A	CTCTTTGCTGCTGCCGGATAAGACTTTGTTGGCTGTTGCTG
Fwd-2x S/A	CCGCGAGCAAGAAAGGCCAGGCAAGGGAGCACAGGAAGC
Rev-2x S/A	CTGGCCTTTCTTGCTCGCGGATAAGCCTTTGTTGGCTGTTGC
Fwd-2x K/A	GCGTCTTATCCGCGAGCAAGAGCGAGCAGGCAAGGG
Rev-2x K/A	CTTGCTCGCGGATAAGACGCTGTTGGCTG
Fwd-Y484A	GACTGATAGCAAAGCCTCACCCAG
Rev-Y484A	GTGAGGCTTTGCTATCAGTCCTTCC
Fwd-M476A	TCCCTGTAGCATCTCCCTCGG
Rev-M476A	CGAGGGAGATGCTACAGGGATC
Fwd-P486A	GTAATGTCTGCATCGGAAGGACTG
Rev-P486A	CCTTCCGATGCAGACATTACAGG
Fwd-Q484Y	ggactgataTATaagcctcacccag
Rev-Q484Y	tgaggcttATAtatcagtccttccg
Fwd-Gibson assembly site	caatcgatagattgtcgcacctg
Rev-Gibson assembly site	gtgcgacaatctatcgattgtatggg
Fwd-Q432A	GTTGTCAAATGCAGGTCATCATCAAC
Rev-Q432A	GTTGATGATGACCTGCATTTGACAAC
Fwd-Q598A	AGAGCCGAGCAGGGAGC
Rev-Q598A	GCTCCCTGCTCGGCTCTT
Fwd-R597A	CAAGAAAGAGCGCACAAGGGAGC
Rev-R597A	GCTCCCTTGTGCGCTCTTTCTTG
Template for insertion of R592A, R594A, R597A	ACCCAACAACAACAACAGAGATCTGATAATGAACCTGCTCCA CAGCAACAGCAACAGCCAACAAAGTCTTATCCGGCAGCAGCAAAGAG CGCACAA
Fwd-template elongation	CATCCTGGAAATCTTCAGAACACCCAACAACAACAACAGAGA T
Rev- template elongation	CTTGGACTGCTTCCTGTGCTCCCTTGTGCGCTCTTTGCTGC
Fwd-vector	AGCACAGGAAGCAGTCCAAGTG
Rev-vector	TTCTGAAGATTTCCAGGATGTCCAAACT
Fwd-Y440Q	caatccaacCAAatgccttttgcaaac
Rev-Y440Q	aaaggcatTTGgttggattgttgatgatg
Fwd-Y456Q	ccaaatggaCAAtgctttcctcctcag
Rev-Y456Q	ggaaagcaTTGtccatttggagccg
Fwd-Y484Q	ggactgataCAAaagcctcacccag
Rev-Y484Q	tgaggcttTTGtatcagtccttccg
Fwd-Y496Q	cggggcatCAAggaggaCAAC
Rev-Y496Q	TTGtcctccTTGatgccccgtg

Fwd-Y499Q, Y500Q	tggaggaCAACAAggtcatCAAatgcc
Rev- Y499Q, Y500Q	GatgaccTTGTTGtcctccataatgccc
Fwd-Y503Q	tatggtcatcaaatgcctacaccaatgg
Rev-Y503Q	gtaggcatttgatgaccataatatcctccataatg
Fwd-Y513Q	atgcctcaaCAAcaccccgg
Rev-Y513Q	ccggggtgTTGttgaggcattac
Fwd-Y526Q, Y530Q	gtaatggcCAAttccctccaCAAggaatg
Rev- Y526Q, Y530Q	cattccTTGtggagggaaTTGgccattac
Fwd-Y540Q	atgaacccaCAAtgttcaagccaac
Rev-Y540Q	cttgaacaTTGtgggttcattatggtgg
Fwd-Y590Q	caaagtctCAAccgcgagcaag
Rev-Y590Q	tgctcgcggTTGagactttgttg
Fwd-Δ411-428	TTGTCAAATCAAGGTCATCATCAACAAT
Rev-Δ411-428	CGAGTCACCCCTTTGTTTGACGA
Fwd-Δ430-435	gccttttgcaaacaacccacc
Rev-Δ430-435	ctttccattttatgttggtcagtcttctc
Fwd-Δ442-464	TCAGGAAATCATCAGCAATGGTTGA
Rev-Δ442-464	CATGTAGTTGGATTGTTGATGATGACCTT
Fwd-Δ470-487	CCAGGTATGGCACACACGGG
Rev-Δ470-487	TTGCTGATGATTTCCTGAAGGAGG
Fwd-Δ490-525	TACTTCCCTCCATATGGAATGATGC
Rev-Δ490-525	TTGAGGCATTACCATTGGTGTAGG
Fwd-Δ526-543	CAACAACAACAACAACAACAACCC
Rev-Δ526-543	ATTACCAGGAGGTGGGAATCCC
Fwd-Δ551-567	CAACAACAACAACAGAGATCTGATAATGAACC
Rev-Δ551-567	TTGTTGTTGTTGTTGTTGTTGGCTTGAACA
Fwd-Δ586-596	AGGCAAGGGAGCACAGGAAG
Rev-Δ586-596	CTGTTGCTGTTGCTGTGGAGCA
Fwd-Δ597-604	cgagcaagaaagagcccaagtgggccacagggaatc
Rev-Δ597-604	ctgtggcccacttgggctctttcttgctcgcggataag
Primers for ELF3 full length codon-optimized cloning	
fwd_H1504-1510R	CGTCTGTCTAACCAGGGTCGTCGTCAGCAGT
rev_H1504-1510R	GTTAGACTGCTGACGACGACCCTGGTT
fwd_H1607-1609R	TCTGGTAACCGTCAGCAGTGGC
rev_H1607-1609R	CACTGCTGACGGTTACCAGACG
fwd_H1883-1885R	CAGTTCGGTCGTCCGGGTAAC
rev_H1883-1885R	TTACCCGGACGACCGAACTGGTT
Template for insertion with H/R 6 mutations	CCGCGTCCGGGTATGGCTCGTACCGGTCGTTACGGTGGTTAC TACGGTCGTTACATGCCGACCCCGATGGTTATGCCGCAGTACCGTCCG
Fwd-template elongation	CTCCGTCTGAAGGTCTGATCTACAAACCGCGTCCGGGTATGG CT
Rev-template elongation	GGCGGGAAACCCATACCCGGACGGTACTGCGGCAT
Fwd-vector	CGTCCGGGTATGGGTTTCCCGCCGCCG
Rev-vector	GATCAGACCTTCAGACGGAGACATAACCGGGATC
fwd_2x R/Amut	TTACCCGGCTGCTGCTAAATCT
rev_2x R/Amut	AGATTTAGCAGCAGCCGGGTAAG
fwd_3x R/A	CTAAATCTGCTCAGGGTTCTACC
rev_3x R/A	GGTAGAACCCTGAGCAGATTTAG

Template for insertion with Y/Q 5 mutations	CGGTTATGTCTCCGTCTGAAGGTCTGATCCAGAAACCGCACC CGGGTATGGCTCACACCGGTCACCAGGGTGGTCAGCAGGGTCACCAG ATGCCG
Fwd_Y513Q	TTATGCCGCAGCAGCACCCGGGTATG
Rev_Y513Q	ATACCCGGGTGCTGCTGCGGCATAACC
Fwd_Y526Q, Y530Q	GGTAACGGTCAGTTCCCGCCGCAGGGTATGA
Rev_Y526Q, Y530Q	TCATACCCTGCGGCGGGAACTGACCGTTACC
Fwd_Y540Q	ATGAACCCGCAGTGCTCTTCTCAG
Rev_Y540Q	GAGAAGAGCACTGCGGGTTCATGATGG
Fwd_Y590Q	ACCAAATCTCAGCCGCGTGCTCGT
Rev_Y590Q	GAGCACGCGGCTGAGATTTGGTCGG
Fwd-template elongation	CTGGTAACCACCAGCAGTGGCTGATCCCGGTTATGTCTCCGT CTGAAGG
Rev-template elongation	TGCGGCATAACCATCGGGGTCGGCATCTGGTGACCCTG
Fwd-vector	ACCCCGATGGTTATGCCGCAGTACCACCCGGGTATGGGTT
Rev-vector	CCACTGCTGGTGGTTACCAGACGGCGGCGGCTGCG
Fwd-Gibson assembly site	caatcgatagattgtcgcacctg
Rev-Gibson assembly site	gtgcgacaatctatcgattgtatggg
Primers for genomic plant constructs cloning	
Fwd_Fragment 1	CTGTCAAACACTGATAGTTTAAACCCGCGGCCGCCC
Rev_Fragment 1	cgtggactctttttgtcgttgtaataagaaactag
Fwd_Fragment 2	caacgacaaaaagagtccacgtcg
Rev_Fragment 2	CCGCTCTAGAACTAGTTAATTAATTACTTGTCGTCATCATCCT TGTAATCTTTATCATCG
Fwd_AscI-mGFP	CCTCTAAGCCTAAGGGTGGGCGCGCCAGTAAAGGAGAAGA ACttttcactggagttg
Rev_mGFP-AscI	GTACAAGAAAGCTGGGTCTGGCGCGCCTTTGTATAGTTCATC CATgccatgtgtaatcc
Fwd_PCR1 PrD in pFP - XhoI	gtatttgtttcttctcgagctgaaacaaacc
Rev_PCR1 PrD in pFP	AGAAATTCTGATGGAAGGAGCTTCTTCAC
Fwd_PCR3 PrD in pFP	CTCCTTCCATCAGAATTTCTGGTAAAGCC
Rev_PCR3 PrD in pFP	CCTCATCAACGGCTGCGAATG
Fwd_PCR2 PrD in pFP	ATTCGCAGCCGTTGATGAGG
Primers for CDNA plant constructs cloning	
fwd_Fragment2	GAGAAGATTAGCCTCTTCAATTTCAGA
Fwd_Fragment1	AGCTTGGAGCGAACGACCTACAC
fwd_Gene insertion	cattcgcagccgttgatgaggacagcaacatca
fwd_Fragment3	acataaaatggaaagctcagctgagaa
rev_Fragment1	TTGAAGAGGCTAATCTTCTCATTATCG
rev_Fragment3	TAGGTCGTTCGCTCCAAGCTGGG
rev_Fragment2	gctgagctttccattttatgttggtcagt
rev_PrD_pesprit	ctcatcaacggctgcgaatggccga
Fwd_ELF3_fl	GATTATGGATCCTatgaagagagggaaagatgaggagaag
Rev_ELF3_fl	cgcgctcgagaggcttagaggagtcatagcgt
Fwd_Terminator	cctctcgagcgcggccatgctagagtccg
Rev_Terminator	GTACCGGGCCCgacgtcgcatg

Table 5. List of ELF3 PrD constructs cloned and tested. The constructs are noted for LLPS behavior and observed conditions for liquid droplet appearance

Mutants name	Mutation positions	Characteristics	Observed LLPS	Conditions for LLPS
Δ411-428 mutant	Deletion of 411-YFPPYGMMPTIMNNPY-429	Evolutionarily conserved motif situated just before the predicted PrD region	Yes	Similar to WT
Δ430-435 mutant	Deletion of 430-SNQGHH-435	Predicted LARKS	Yes	Similar to WT
Δ442-464 mutant	Deletion of 441-YFPPYGMMPTIMNNPYCSS-464	A proline-rich motif	Yes	Similar to WT
Δ470-487 mutant	Deletion of 470-QWLIPVMSPSE GLIYKPH-487	A predicted β-hairpin motif	Yes	Undergoes LLPS at pH 9,6 – 9,0
Δ490-525 mutant	Deletion of 490-MAHTGHYGGYYGHYMPTPMVMPQYHPGMGFPPPGN G-525	An aromatic-rich motif	Yes	Undergoes LLPS at pH 9,6 – 9,0
Δ526-543 mutant	Deletion of 526-YFPPYGMMPTIMNNPYCSS-543	A conserved flanking region before polyglutamine stretch	Yes	Similar to WT
Δ551-567 mutant	Deletion of 551-PNEQMNQFGHPGNLQNT-567	Motif placed between two polyglutamine stretches	Yes	Similar to WT
Δ586-596 mutant	Deletion of 586-PTKSYPRARKS-596	A right-side flanking region of polyglutamine stretch	No	No observed LLPS
Δ597-604 mutant	Deletion of 597-RQGSTGSS-604	Seconds predicted LARKS	Yes	Similar to WT
Q432A mutant	Q432A	Replacement of glutamine to alanine in a first predicted LARKS region	Yes	Similar to WT

Q598A mutant	Q598A	Replacement of glutamine to alanine in a second predicted LARKS region	Yes	Similar to WT
R597A mutant	R597A	Replacement of arginine to alanine in a second predicted LARKS region	Yes	No observed LLPS under pH 9,4 – 7,0, at 200 mM – 100 mM salt LLPS was observed
2x K/A	K588A, K595A	Replacement of lysine to alanine	Yes	Similar to WT
2x S/A	S596A, S5989A	Replacement of lserine to alanine	Yes	Similar to WT
2x R/A	R592A, R594A	Replacement of arginine to alanine	No	No observed LLPS
3x R/A	R592A, R594A, R597A	Replacement of arginine to alanine	No	No observed LLPS
P486A mutant	P486A	Mutated proline in B-strand	Yes	Similar to WT
Y484A mutant	Y484A	Mutated aromatic residue in B-strand	Yes	Similar to WT
M476A mutant	M476A	Mutated aliphatic residue in B-strand	Yes	Similar to WT
12x Y/Q	Y440Q, Y456Q, Y484Q, Y496Q, Y497Q, Y500Q, Y503Q, Y513Q, Y526Q, Y530Q, Y540Q, Y590Q	Mutant with tyrosine replaced to glutamine	No	No observed LLPS
11x Y/Q	Y440Q, Y456Q, Y496Q, Y497Q, Y500Q, Y503Q, Y513Q, Y526Q, Y530Q, Y540Q, Y590Q	Mutant with tyrosine replaced to glutamine except one in the β-hairpin	No	No observed LLPS

11x Y/Q+Q484Y	Y440Q, Y456Q, Y496Q, Y497Q, Y500Q, Y503Q, Y513Q, Y526Q, Y530Q, Y540Q, Y590Q, Q484Y	Complementary mutant with tyrosine replaced to glutamine except one in the β-hairpin	No	No observed LLPS
10x Y/Q	Y440Q, Y456Q, Y484Q, Y496Q, Y497Q, Y500Q, Y503Q Y513Q, Y526Q, Y530Q	Mutant with tyrosine replaced to glutamine	No	No observed LLPS
8x Y/Q	Y440Q, Y456Q, Y484Q, Y496Q, Y499Q, Y500Q, Y503Q , Y513Q	Mutant with tyrosine replaced to glutamine	No	No observed LLPS
7x Y/Q	Y440Q, Y456Q, Y484Q, Y496Q, Y499Q, Y500Q, Y503Q	Mutant with tyrosine replaced to glutamine	Yes	Similar to WT
6x Y/Q	Y440Q, Y456Q, Y496Q, Y499Q, Y500Q, Y503Q	Mutant with tyrosine replaced to glutamine	Yes	Similar to WT
7x Y/Q - GFP	Y440Q, Y456Q, Y484Q, Y496Q, Y499Q, Y500Q, Y503Q	Mutant with tyrosine replaced to glutamine	No	No observed LLPS
9x H/R	H434R, H435R, H468R, H487R, H492R, H495R, H502R, H514R, H560R	Mutant with histidine replaced to arginine	Yes	Forms droplets at higher pH (for 4 mg/ml llps in range of pH 10,3-9,7
9x H/Y	H434Y, H435Y, H468Y, H487Y, H492Y, H495Y, H502Y, H514Y, H560Y	Mutant with histidine replaced to tyrosine	Yes	Similar to WT
9x H/V	H434V, H435V, H468V, H487V, H492V, H495V, H502V, H514V, H560V	Mutant with histidine replaced to valine	Yes	Similar to WT

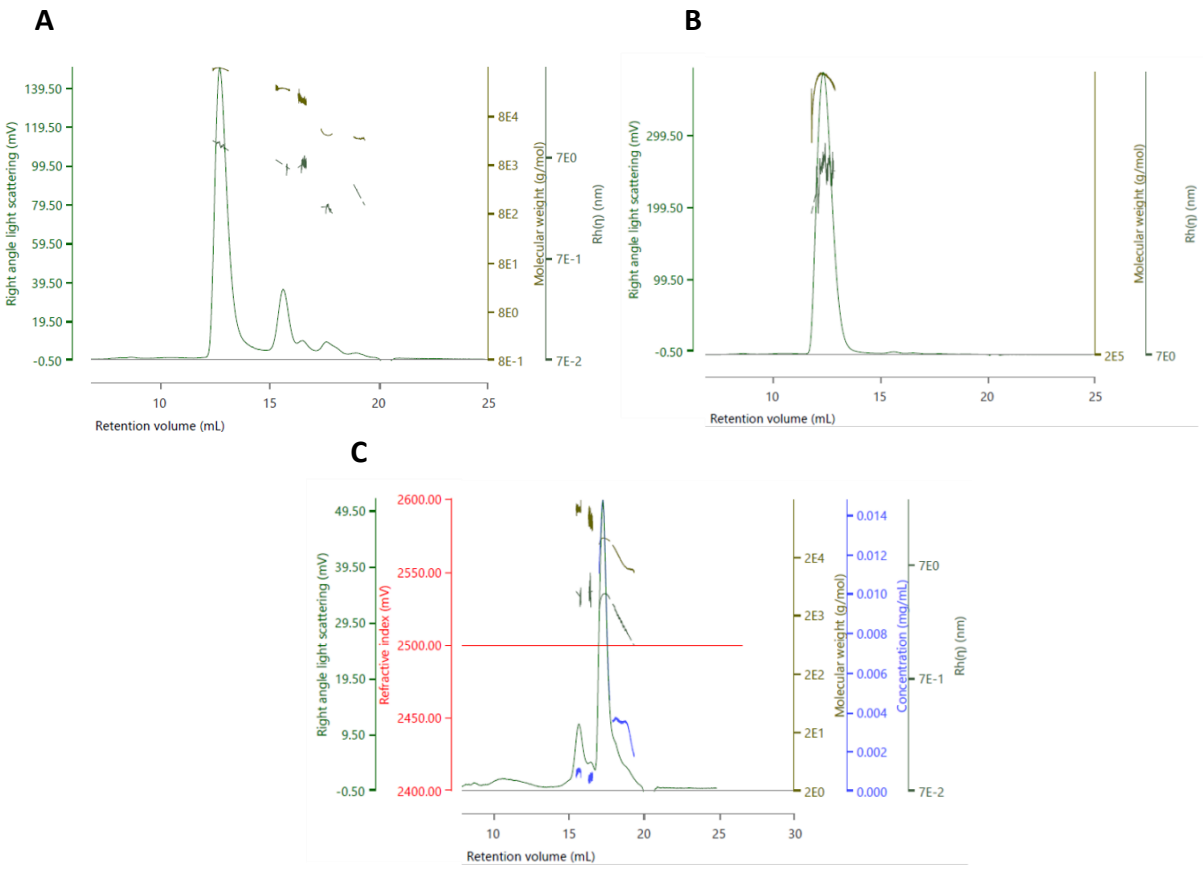

Figure 48. SEC-MALLS analyses of (A) ELF3^{PrDR597A}, (B) ELF3$^{PrD3xR/A}$ and (C) ELF3$^{PrDR12xY/Q}$. The molar masses of ELF3^{PrDR597A} and ELF3$^{PrD3xR/A}$ were ~ 800-900 kDa and ELF3$^{PrDR12xY/Q}$ was ~ 30 kDa**.**

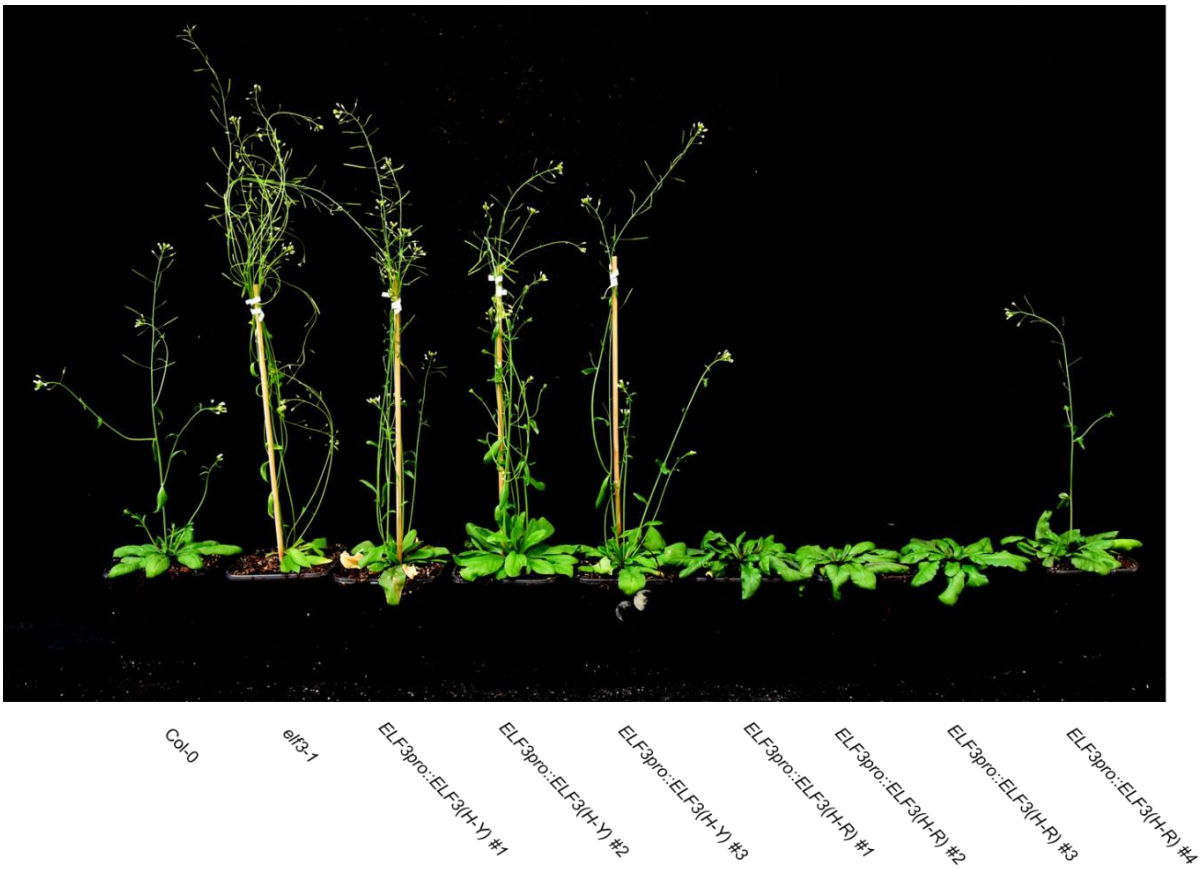

Figure 49. Plant phenotype of Col-0, *elf3-1*, ELF3*pro::ELF3 9x H/Y* and ELF3*pro::ELF3 9x H/R*. Plant were grown at 22° C under LD conditions. P. Wigge, unpublished.